Existence of Wormholes in Different Spacetimes under Einstein and $f(R)$ Gravity

A THESIS

submitted for the partial fulfilment of the requirements for the degree

M.Sc. in Applied Mathematics

by

SREYA SAHA

Enrollment No: 2322221002001

Registration No: 230020015261

Under the Guidance of

DR. MD SAYEEDUL ISLAM

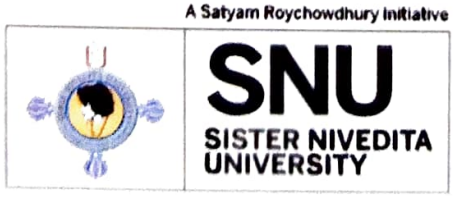

Department of Mathematics

Sister Nivedita University

Academic Year: 2023-2025

Existence of Wormholes in Different Spacetimes under Einstein and $f(R)$ Gravity

This project work is submitted in partial fulfillment of the requirements for the degree

M.Sc. in Applied Mathematics

by

SREYA SAHA

Enrollment No: 2322221002001
Registration No: 230020015261

A Satyam Roychowdhury Initiative

Department of Mathematics
Academic Year: 2023-2025

Forwarded by

Md. Sayeedul Islam
05/05/2025

(Supervisor)

Dr. Md Sayeedul Islam
Assistant Professor
Department of Mathematics
Sister Nivedita University

Approved by

Abhik Sur
05/05/2025

(Head of the Department)

Associate Professor and Head
Department of Mathematics
School of Natural Sciences
Sister Nivedita University
Block DG-1/2, Action Area 1
New Town, Kolkata-700 156

Dr. Abhik Sur
Associate Professor, HOD
Department of Mathematics
Sister Nivedita University

DECLARATION BY THE STUDENT

I hereby declare that the work which is being presented in this dissertation entitled "**Existence of Wormholes in Different Spacetimes under Einstein and $f(R)$ Gravity**" in partial fulfilment of the requirements for the award of the degree of **Masters of Science in Applied Mathematics** is an authentic record of my own work carried out during the period from **06 January 2025** to **05 May 2025** under the supervision of **Dr. Md Sayeedul Islam**, Department of Mathematics, Sister Nivedita University.

I acknowledge that I have read and understood the UGC regulations, 2018 (*Promotion of Academic integrity and Prevention of Plagiarism in Higher Educational Institutions*).

I confirm that this dissertation has been checked for plagiarism using the plagiarism checking software **Duplichecker**. At the end of the dissertation, a copy of the summary report demonstrating similarities in content and its potential source (if any), generated online using plagiarism checking software is enclosed. I herewith confirm that the dissertation has been less than 10% similarity according to the plagiarism checking software's report and meets the UGC Regulations as well as plagiarism rules of Sister Nivedita University.

I further declare that no portion of the dissertation or its data will be published without the Institute's or supervisor's permission. I have not previously applied for any other degree or award using the topics and findings described in my dissertations.

Sreya Saha 05/05/25

(Signature of the student with Date)

Name of the Student: Sreya Saha

Registration no.: 230020015261

Department: Mathematics

Acknowledgement

I would like to thank the Head of Department, Dr. Abhik Sur, for providing me the oppurtunity to undertake this project titled **"Existence of Wormholes in Different Spacetimes under Einstein and $f(R)$ Gravity"**. I want to thank my supervisor, Dr. Md Sayeedul Islam. Whenever I had doubts, he always helped me to solve them. With his guidance and help, I was able to successfully complete this thesis.

Date: 05/05/25

Place: Kolkata

Sreya Saha

Sreya Saha

Enrollment Number: 2322221002001

Registration No: 230020015261

email ID: sreyasaha4564@gmail.com

Department of Mathematics

Sister Nivedita University

Kolkata 700156, West Bengal

Abstract

In this study, we explore the possible existence of traversable wormholes within the ultra-diffuse galaxy Dragonfly 44 by employing the Morris-Thorne metric to derive the wormhole shape function $b(r)$. We analyze key conditions necessary for wormhole formation, including the flare-out condition at the throat and the violation of the null-energy condition (NEC). The study is conducted using three distinct galactic dark-matter density profiles: the Navarro-Frenk-White (NFW) profile, the Universal Rotation Curve (URC) profile, and the Ultra Diffuse Galaxy (UDG) King profile.

Ultra-Diffuse Galaxies (UDGs) are a highly unusual type of dwarf galaxy characterized by their extremely low stellar densities and luminosities, as well as their low surface brightness. Discovered in 2016, Dragonfly 44 is a remarkable UDG, with a mass similar to that of the Milky Way but emitting only about 1 percent of its light. These characteristics imply that Dragonfly 44 is mainly made up of dark matter, making it a prime candidate for investigating exotic gravitational phenomena such as wormholes.

We conduct our analysis in the context of both Einstein gravity and $f(R)$ theories of gravity. The results imply that dark-matter distributions conforming to the NFW and URC profiles within the ultra-diffuse galaxy Dragonfly 44 might support traversable wormholes, while the UDG King's model is less conducive to such structures.

Contents

Abstract **iv**

1 Introduction to Spacetime Geometry **1**
1.1 Newtonian Gravity 1
1.2 Relativity 2
1.3 Galilean Relativity 2
1.4 Special Theory of Relativity 3
1.5 General Theory of Relativity 8
1.5.1 Einstein Field Equations: 9
1.6 Energy Conditions 10
1.6.1 Null Energy Condition 11
1.6.2 Weak Energy Condition 11
1.6.3 Strong Energy condition 12
1.6.4 Dominant energy condition 12
1.7 Black Hole: A Solution of General Relativity 13
1.8 Modified theories of gravity: 14
1.8.1 $f(R)$ gravity 14
1.8.2 Lovelock Gravity Theory 15
1.8.3 Einstein Dilation Gauss–Bonnet (EdGB) Gravity 16
1.8.4 $f(T)$ gravity 16
1.8.5 $f(R,T)$ gravity 16
1.8.6 $f(Q)$ gravity 17

2 Wormhole Dynamics: Construction and Types **18**
2.1 Historical Overview of Wormholes 18
2.2 Construction of Wormholes 22
2.2.1 The Einstein-Rosen bridge: 23

2.2.2 Basic Terminologies 23
2.2.3 Setting up the Wormhole Spacetime: 24
2.2.4 Conditions for wormholes: 24
2.3 Different types of Wormholes: 25
2.3.1 Traversable Wormholes: 25
2.3.2 Non-Traversable Wormholes: 26
2.3.3 Kerr Wormholes (Rotating Wormholes): . . . 27
2.3.4 Wormholes in Higher Dimensions: 28

3 Wormhole solutions in UDGs using Einstein gravity 29
3.1 Christoffel Symbols: 30
3.2 Shape function: 35
3.3 Navarro-Frank-White(NFW) Density Profile 37
3.4 UDG King's Model 51
3.5 Universal Rotation Curve Density Profile 68
3.6 Stability Analysis 73
3.6.1 Tolman-Oppenheimer-Volkoff Balance Condition: 73
3.6.2 Test for Einstein Gravity 73

4 Formation of wormholes in UDGs by $f(R)$ gravity 77
4.1 Navarro-Frank-White(NFW) Density Profile 82
4.2 UDG King's Model 91
4.3 Universal Rotation Curve Density Profile 99
4.4 Stability Analysis 101

Concluding remarks 105

Future Scope 107

Bibliography 109

A Appendix: Python programs for generating graphs 114

List of Figures

1.1 Galilean Transformation 2
1.2 Lorentz Transformation - 1 4
1.3 Lorentz Transformation - 2 4
1.4 A 2-D diagram describing the warping of spacetime [3] 8

2.1 A general description of a wormhole [2] 22
2.2 A holographic wormhole traversed in a quantum computer [10] 25

3.1 $b(r)$ versus r plot 39
3.2 ($b(r) - r$) versus r plot 39
3.3 $\rho(r)$ versus r plot 39
3.4 Null energy Violation 39
3.5 $b(r)$ versus r plot 41
3.6 ($b(r) - r$) versus r plot 41
3.7 $\rho(r)$ versus r plot 41
3.8 Null energy Violation 41
3.9 $b(r)$ versus r plot 43
3.10 ($b(r) - r$) versus r plot 43
3.11 $\rho(r)$ versus r plot 43
3.12 Null energy Violation 43
3.13 $b(r)$ versus r plot 45
3.14 ($b(r) - r$) versus r plot 45
3.15 $\rho(r)$ versus r plot 45
3.16 Null energy Violation 45
3.17 $b(r)$ versus r plot 47
3.18 ($b(r) - r$) versus r plot 47
3.19 $\rho(r)$ versus r plot 47
3.20 Null energy Violation 47

3.21 $b(r)$ versus r plot 50
3.22 ($b(r) - r$) versus r plot 50
3.23 $\rho(r)$ versus r plot 50
3.24 Null energy Violation 50
3.25 $\frac{b(r)}{r}$ versus r plot 58
3.26 NEC Violation 58
3.27 $b(r)$ versus r plot 58
3.28 $b'(r)$ versus r plot 58
3.29 $b(r)$ versus r plot 61
3.30 $\frac{b(r)}{r}$ versus r plot 61
3.31 NEC Violation 61
3.32 $b'(r)$ versus r plot 61
3.33 $b(r)$ versus r plot 67
3.34 $\frac{b(r)}{r}$ versus r plot 67
3.35 NEC Violation 67
3.36 $b'(r)$ versus r plot 67
3.37 $b(r)$ versus r plot 72
3.38 $b'(r)$ versus r plot 72
3.39 $\rho(r)$ versus r plot 72
3.40 NEC violation 72
3.41 $(b(r) - r)$ versus r plot 72
3.42 A plot showing the behaviour of the three forces in the TOV equilibrium condition against r 75

4.1 $b'(r)$ versus r plot 85
4.2 $\rho(r)$ versus r plot 85
4.3 NEC Violation 85
4.4 ($b(r) - r$) versus r plot 85
4.5 $b'(r)$ versus r plot 88
4.6 $\rho(r)$ versus r plot 88
4.7 NEC Violation 88
4.8 ($b(r) - r$) versus r plot 88
4.9 $b'(r)$ versus r plot 90
4.10 $\rho(r)$ versus r plot 90
4.11 NEC Violation 90
4.12 ($b(r) - r$) versus r plot 90

4.13 $b'(r)$ versus r plot 93
4.14 $\rho(r)$ versus r plot 93
4.15 NEC Violation 93
4.16 ($b(r) - r$) versus r plot 93
4.17 $b'(r)$ versus r plot 98
4.18 $\rho(r)$ versus r plot 98
4.19 NEC Violation 98
4.20 ($b(r) - r$) versus r plot 98
4.21 $b'(r)$ versus r plot 100
4.22 Energy density 100
4.23 NEC Violation 100
4.24 $(b(r) - r)$ versus r plot 100
4.25 $\frac{b(r)}{r}$ versus r plot 100
4.26 A plot showing the behaviour of the three forces in the TOV equilibrium condition against r in $f(R)$ gravity 104

A.1 NFW CASE - 1: $\gamma = 1$ for Einstein Gravity 114
A.2 UDG King's CASE - 3: $\eta = -\frac{3}{2}$ for Einstein Gravity . 115
A.3 UDG King's CASE - 3: $\eta = -\frac{3}{2}$ for Einstein Gravity . 115
A.4 URC density profile for Einstein Gravity 116
A.5 URC density profile for Einstein Gravity 116
A.6 NFW CASE - 1: $\gamma = 1$ for $f(R)$ Gravity 117
A.7 NFW CASE - 1: $\gamma = 1$ for $f(R)$ Gravity 117
A.8 UDG King's CASE - 1: $\eta = -\frac{1}{2}$ for $f(R)$ Gravity . . 118
A.9 UDG King's CASE - 1: $\eta = -\frac{1}{2}$ for $f(R)$ Gravity . . 118
A.10 URC density profile for $f(R)$ Gravity 119
A.11 URC density profile for $f(R)$ Gravity 119
A.12 Stability Analysis of Einstein Gravity 120
A.13 Stability Analysis of $f(R)$ Gravity 120

Chapter 1

Introduction to Spacetime Geometry

1.1 Newtonian Gravity

In 1687, Sir Isaac Newton introduced the Universal Law of Gravitation [1]. The law states that every body in the universe attracts another body in such a manner that the force between them is directly proportional to the product of their masses and inversely proportional to the square of the distance between them [1].

Mathematically,

$$F = \frac{G\ m_1\ m_2}{r^2} \tag{1.1}$$

where,

$F \rightarrow$ Gravitational force between the bodies

m_1 and $m_2 \rightarrow$ Mass of the bodies

$G \rightarrow$ Constant of proportionality called the Universal Gravitational Constant

The universal law of gravitation helped to explain the motion of planetary orbits, as all objects exert gravitational influence on each other.

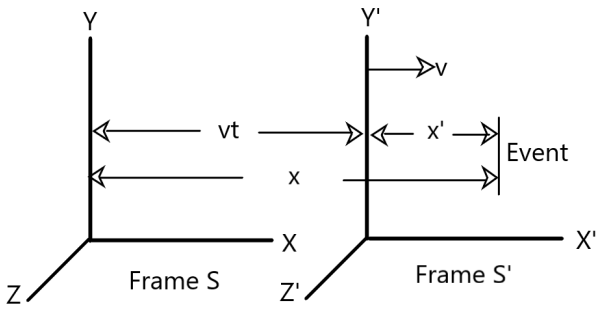

Figure 1.1: Galilean Transformation

1.2 Relativity

Relativity is a fundamental theory of physics that explains how motion, space, and time act, particularly when moving quickly or in environments with strong gravitational fields. [48] [19]

1.3 Galilean Relativity

In 1632, Galilean relativity stated that there is no change; the laws of motion are the same in every inertial frame.

Inertial Reference Frames: It is defined as a frame of reference with no acceleration, i.e., where an object either remains at rest or moves at a constant velocity, provided no external force acts upon it. These frames follow Newton's first law of motion (law of inertia).

Suppose that frame S is moving in the x-direction with velocity v, and there is no change in y and z. The frame S' is the new position of frame S after time t as shown in figure:1.1. So, the Galilean transformation equations are given as follows:

$$x' = x - vt \tag{1.2}$$

$$y' = y \tag{1.3}$$

$$z' = z \tag{1.4}$$

$$t' = t \tag{1.5}$$

For example, we have two people, namely J and K, travelling in two different trains. The trains are moving at the same speed and in the same direction. So, from the inertial reference frame of J, K appears to be stationary and vice versa.

Galileo assumed that time is absolute. This principle is used to understand the transformation of coordinates (equivalent quantities, such as position and velocity) between two different inertial reference frames. But it only works when the inertial frames move at a velocity very very small compared to the speed of light.

1.4 Special Theory of Relativity

The special theory of relativity [46]introduced by Albert Einstein in 1905, states the following postulates:

1. Despite being in different inertial reference frames [50], the laws of physics remain unchanged for everyone.
2. Regardless of the motion of the light source or the motion of the observer, the speed of light remains constant for all observers.

Lorentz Transformation:

It describes the transformation between two inertial reference frames when they move with constant velocity with respect to each other. Lorentzian transform works well when the velocity is close to the speed of light (i.e. $v < c$).

Suppose that, frame S is moving with velocity v to the right along the x-direction as shown in figure:1.2, with no change in y and z. The frame S' denotes the new position of the frame S after time t. [20]

Due to contraction in length [50] and dilation in time [15], we have,

$$x = \gamma(\ x' + vt'\ ) \tag{1.6}$$

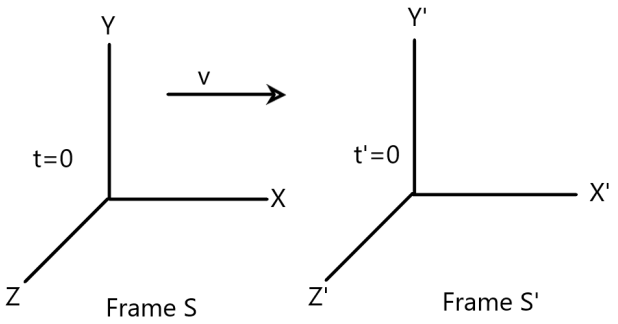

Figure 1.2: Lorentz Transformation - 1

$$y = y' \tag{1.7}$$

$$z = z' \tag{1.8}$$

Since, the motion is relative, we can also say that the frame S' is stationary while frame S moves to the left along the x-axis with velocity v as we can see in figure:1.3. So,

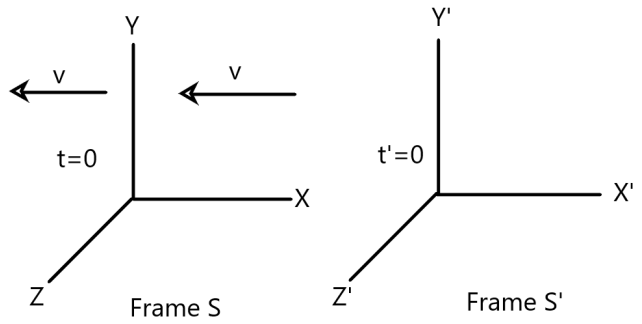

Figure 1.3: Lorentz Transformation - 2

$$x' = \gamma(\ x - vt\ ) \tag{1.9}$$

$$y' = y \tag{1.10}$$

$$z' = z \tag{1.11}$$

On substituting the value of x' from equation (1.9) to (1.6), we get,

$$x = \gamma(\ x' + vt'\ )$$

$$\Rightarrow\ x = \gamma[\ \gamma\ (\ x - vt\ )\ + vt'\ ]$$

$$\Rightarrow\ vt' = \frac{x}{\gamma}\ -\ \gamma x\ + \gamma vt \tag{1.12}$$

$$\Rightarrow\ t' = \gamma t - \left(\frac{\gamma\ x}{v}\right)\left(1 - \frac{1}{\gamma^2}\right) \tag{1.13}$$

Similarly,

$$t = \gamma t' - \left(\frac{\gamma x'}{v}\right)\left(1 - \frac{1}{\gamma^2}\right) \tag{1.14}$$

From the second postulate of the theory of relativity, we know that regardless of the motion of the light source or the motion of the observer, the speed of light remains constant for all observers.

Let a light signal be given at the origin O at time $t = 0$, $t' = 0$. After sometime, the signal travels with a speed of light, denoted as c, in both frames.

Its position from S is $x = ct$ and from S' is $x' = ct$. On substituting x and x' in equation (1.6), and (1.9) respectively, we get,

$$ct ='\ (c + v) \tag{1.15}$$

$$ct' = \gamma t\ (c - v) \tag{1.16}$$

$$t' = \gamma t\ \left(\frac{c - v}{c}\right) \tag{1.17}$$

Now putting t' in equation (1.15),

$$ct = \gamma^2 t\ \left(\frac{c - v}{c}\right)\ (c + v)$$

$$\Rightarrow \ c^2 = \gamma^2(c^2 - v^2)$$

$$\Rightarrow \ \gamma^2 = \left(\frac{c^2}{c^2 - v^2}\right)$$

$$\Rightarrow \ \gamma = \left(\frac{1}{\sqrt{1 - \left(\frac{v}{c}\right)^2}}\right) \tag{1.18}$$

Now, by putting the value of γ in equations (1.6) and (1.9),we get,

$$x = \left(\frac{1}{\sqrt{1 - \left(\frac{v}{c}\right)^2}}\right) (\ x' + vt' \ ) \tag{1.19}$$

$$x' = \left(\frac{1}{\sqrt{1 - \left(\frac{v}{c}\right)^2}}\right) (\ x - vt \ ) \tag{1.20}$$

Now, putting $\left(1 - \frac{1}{\gamma^2}\right) = \frac{v^2}{c^2}$ in equation (1.13) and (1.14),

$$t' = \gamma t - \left(\frac{\gamma x}{v}\right)\left(1 - \frac{1}{\gamma^2}\right)$$

$$\Rightarrow \ t' = \gamma t - \left(\frac{\gamma x}{v}\right)\left(\frac{v^2}{c^2}\right)$$

$$\Rightarrow \ t' = \gamma t - \left(\frac{\gamma x v}{c^2}\right)$$

$$\Rightarrow \ t' = \gamma \left[t - \left(\frac{xv}{c^2}\right)\right]$$

$$\Rightarrow \ t' = \left(\frac{t - \frac{xv}{c^2}}{\sqrt{1 - \left(\frac{v}{c}\right)^2}}\right) \tag{1.21}$$

Similarly, we get,

$$t = \left(\frac{t' + \frac{x'v}{c^2}}{\sqrt{1 - \left(\frac{v}{c}\right)^2}} \right) \tag{1.22}$$

Therefore, the Lorentz transformation equations are as follows:

$$x' = \left(\frac{x - vt}{\sqrt{1 - \left(\frac{v}{c}\right)^2}} \right) \tag{1.23}$$

$$y' = y \tag{1.24}$$

$$z' = z \tag{1.25}$$

$$t' = \left(\frac{t - \frac{xv}{c^2}}{\sqrt{1 - \left(\frac{v}{c}\right)^2}} \right) \tag{1.26}$$

The Lorentzian transformation equations reduce to the classical Galilean transformation equations when the velocity is very small compared to the speed of light (i.e. $v << c$).

The special theory of relativity provided a new direction to the existing notions in the study of gravity. [20]

1. Time and space are relative.
2. Mass and energy are equivalent and influence spacetime.

$$E = mc^2 \tag{1.27}$$

1.5 General Theory of Relativity

In 1915, Albert Einstein extended the theory of relativity to study non-inertial frames. In this theory, gravity is explained as the warping of spacetime (due to mass and energy) rather than as just a force, as previously considered by Newton. [25]

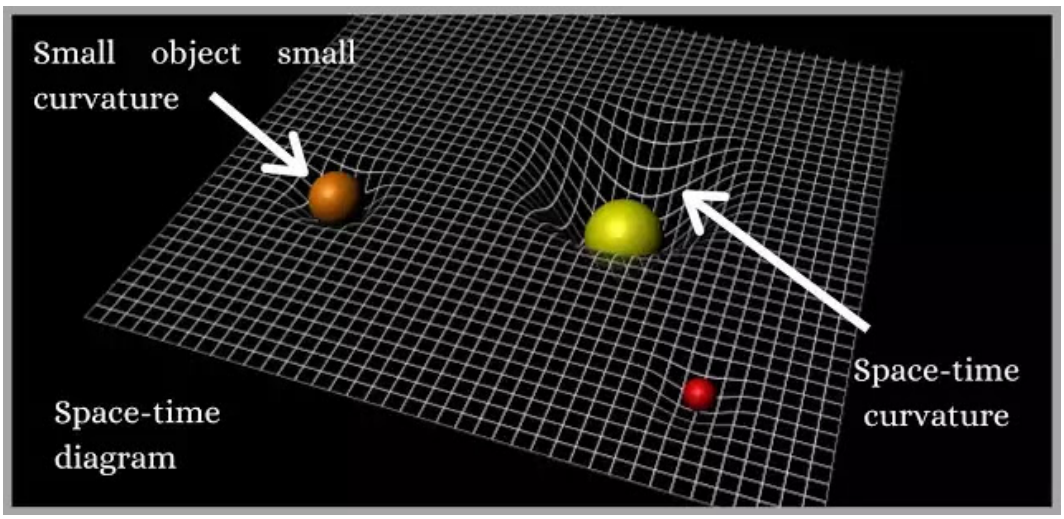

Figure 1.4: A 2-D diagram describing the warping of spacetime [3]

The general theory of relativity introduces spacetime as a 4-D fabric: consisting of the three dimensions of space (length, width and height) along with time as the fourth dimension.

For example, I have decided to watch a movie with my friends in the movie theatre. To ensure that we meet for the same show slot, we have to decide on a specific location, date, and time to meet at the movie theatre. Thus, the location and time together make it possible that my friend and I don't miss each other and can watch the movie together.

Similarly, space and time are interwoven in a fabric called spacetime [15]. Mass and energy curve spacetime, creating what we perceive as gravity. Figure:1.4 describes the warping of spacetime due to mass and energy. Suppose that, we have a thin piece of fabric, and put a heavier mass on it. What will happen then? The fabric wraps

around the object. We get the same result by putting another object on the fabric, which is slightly lighter than the first object. The fabric will also wrap around the second object. But the curvature caused by both objects will differ because of the difference in their mass. We will observe that the lighter object tends to move towards the bigger object (as the heavier or bigger the object causes deeper curvature in the fabric). Exactly this is depicted in Figure-4. This explains gravity, how smaller bodies are attracted to bodies with a larger mass, like the planets orbit the Sun.

1.5.1 Einstein Field Equations:

It describes the relationship between spacetime curvature and energy-matter within it [16].

$$\boldsymbol{G_{\mu\nu} = \left(\frac{8\pi G}{c^4}\right) T_{\mu\nu}} \tag{1.28}$$

where,

$G_{\mu\nu}$ $\rightarrow$ Einstein tensor (describes spacetime curvature)

$T_{\mu\nu}$ $\rightarrow$ Stress-energy tensor (describes matter and energy distribution)

By adding the cosmological constant, the Einstein field equation can also be written as follows:

$$\boldsymbol{G_{\mu\nu} + \Lambda\, g_{\mu\nu} = \kappa\, T_{\mu\nu}} \tag{1.29}$$

where,

$G_{\mu\nu} = R_{\mu\nu} - \frac{1}{2}\, R\, g_{\mu\nu}$, is the Einstein tensor

$R_{\mu\nu} \rightarrow$ Ricci curvature tensor

$R \rightarrow$ Ricci scalar curvature

$g_{\mu\nu} \rightarrow$ metric tensor

$\Lambda \rightarrow$ Cosmological constant (it is said to be positive as the Universe is expanding)

$\kappa = \frac{8\pi G}{c^4} \approx 2.07665 \times 10^{-43} \ N^{-1}$, is the Einstein's Gravitational constant

$G \rightarrow$ Newton's Gravitational constant

$c \rightarrow$ Speed of light

$T_{\mu\nu} \rightarrow$ Stress-energy tensor

The Einstein field equation can also be written as:

$$\boldsymbol{R_{\mu\nu} - \frac{1}{2} R\, g_{\mu\nu} + \Lambda\, g_{\mu\nu} = \left(\frac{8\pi G}{c^4}\right) T_{\mu\nu}} \tag{1.30}$$

1.6 Energy Conditions

For an isotropic distribution matter,

$$T_{\mu\nu} = (\rho + p_t)U_\mu U_\nu \ + \ p_t \ g_{\mu\nu} \ + \ (p_r - p_t)X_\mu X_\nu \tag{1.31}$$

where,

$\rho(r) \rightarrow$ Energy density

$p_t(r) \rightarrow$ Transverse pressure (measured orthogonal to X^μ direction)

$p_r(r) \rightarrow$ Radial pressure (measured in the X^μ direction)

$U_\mu \rightarrow$ Fourth velocity

$X^\mu \rightarrow$ Unit space-like vector in the radial direction

$$T_{\mu\nu} = \begin{bmatrix} -\rho(r) & 0 & 0 & 0 \\ 0 & p_r(r) & 0 & 0 \\ 0 & 0 & p_t(r) & 0 \\ 0 & 0 & 0 & p_t(r) \end{bmatrix} \tag{1.32}$$

Earlier, we read that spacetime is a 4-D fabric connecting space and time. The path an object takes through the spacetime is depicted

by the spacetime interval [**?**, 54] :

$$ds^2 = -c^2dt^2 + dx^2 + dy^2 + dz^2 \qquad \text{(in flat spacetime)} \qquad (1.33)$$

This interval tells us the nature of the path an object or signal follows through spacetime.

1. **Time-like Observer:** Objects that move slower than the speed of light are said to follow a time-like path.
   For these observers, $\boldsymbol{ds^2 < 0}$

2. **Light-like or Null Observer:** An object that moves at the speed of light is said to follow a null or light-like path.
   For these observers, $\boldsymbol{ds^2 = 0}$

3. **Spacelike Observer:** Objects that move faster than the speed of light or are physically unrecognizable by an observer are said to follow a spacelike path.
   For these observers, $\boldsymbol{ds^2 > 0}$

1.6.1 Null Energy Condition

The energy density measured by any null (light-like) observer is non-negative.

$$NEC \;\Leftrightarrow\; T_{\mu\nu}k^\mu k^\nu \geq 0 \qquad (1.34)$$

And in terms of principal pressures,

$$NEC \;\Leftrightarrow\; \forall j, \rho + p_j \geq 0 \qquad (1.35)$$

1.6.2 Weak Energy Condition

The energy density measured by any timelike observer is non-negative.

$$WEC \;\Leftrightarrow\; T_{\mu\nu}V^\mu V^\nu \geq 0 \qquad (1.36)$$

If this is true for any timelike vector, it will also (by continuity) imply the null energy condition. The physical significance of this condition

is that it forces the local energy density as measured by any timelike observer to be positive. In terms of the principal pressures

$$WEC \;\Leftrightarrow\; \rho \geq 0, \forall j, \rho + p_j \geq 0 \tag{1.37}$$

1.6.3 Strong Energy condition

The trace of the tidal gravitational field is non-negative for all timelike observers.

$$SEC \Leftrightarrow \left(T_{\mu\nu} - \frac{T}{2} g_{\mu\nu}\right) V^\mu V^\nu \geq 0 \tag{1.38}$$

where $T \rightarrow$ the trace of the stress-energy tensor is denoted as $T = T_{\mu\nu}$.
In terms of principal pressures,

$$T = -\rho + \sum_j p_j \;\; and, \;\; SEC \;\Leftrightarrow, \forall j, \rho + p_j \geq 0 \;\; and \;\; \rho + \sum_j p_j \geq 0 \tag{1.39}$$

$$\sum_{j=1}^{n} = An \tag{1.40}$$

From the SEC, we can interpret that gravity is always attractive in nature. SEC is used in singularity theorems (e.g., Hawking-Penrose).

1.6.4 Dominant energy condition

Energy flux is causal (i.e., not faster than light), and energy density is non-negative.

$$DEC \;\Leftrightarrow\; T_{\mu\nu} V^\mu V^\nu \geq 0 \quad \text{and} \quad T_{\mu\nu} V^\nu \quad \text{is not spacelike} \tag{1.41}$$

Thus, energy flows at or below the speed of light. DEC implies WEC and NEC.
In terms of principal pressures,

$$DEC \;\Leftrightarrow\; \rho \geq 0, \quad and \quad \forall j, p_j \in [-\rho, +\rho\,] \tag{1.42}$$

1.7 Black Hole: A Solution of General Relativity

A black hole is a region of spacetime where gravity is so intense that no electromagnetic wave or particle can escape from its boundary (event horizon). It is like a trapdoor; once you enter, the door closes with no way out. [18]

A Schwarzschild black hole is static with neither electric charge nor angular momentum (non-rotating). Its event horizon is a perfect sphere at radius, $r_s = \frac{2GM}{c^2}$ (Schwarzschild radius).

Any non-rotating and non-charged mass that is smaller than its Schwarzschild radius forms a black hole. The Schwarzschild metric describes the geometry of spacetime around a non-rotating, uncharged black hole. It is the simplest solution to Einstein's field equations in a vacuum($T_{\mu\nu} = 0$). [44]

$$ds^2 = -\left(1 - \frac{2GM}{r}\right) \mathrm{d}t^2 + \left(1 - \frac{2GM}{r}\right)^{-1} \mathrm{d}r^2 + r^2(\mathrm{d}\theta^2 + \sin^2\theta \mathrm{d}\phi^2) \tag{1.43}$$

where,

$ds^2 \rightarrow$ Spacetime interval (determines how distance and time behave)

$G \rightarrow$ Gravitational constant

$M \rightarrow$ Mass of the black hole

$c \rightarrow$ Speed of light

$r \rightarrow$ Radial distance from the center

$t \rightarrow$ Time coordinate

$\Omega \rightarrow$ A point on the two sphere S^2

θ : Co-altitude coordinate

ϕ: Longitude coordinate

θ and ϕ are angular coordinates (spherical symmetry)

1.8 Modified theories of gravity:

The study of modified theories of gravity aims to minimize the need for exotic matter by introducing higher-order curvature terms, different type of scalars or functions, and checking how they affect the energy conditions. [42]

The Einstein field equations for general theory (Einstein gravity) can be derived from the Hilbert-Einstein action principle:

$$S = \frac{1}{2\kappa} \int \sqrt{-g}\ R\ d^4x \tag{1.44}$$

where,

g Determinant of the metric tensor ($g_{\mu\nu}$)

$R \rightarrow$ Ricci scalar

$\kappa = \frac{8\pi G}{c^4} \rightarrow$ Einstein gravitational constant

1.8.1 $f(R)$ gravity

The Ricci scalar R in Einstein gravity is replaced by a function of R denoted by $f(R)$, for example, $f(R) = R+\alpha R^n$, where α is a constant the Hilbert-Einstein action principle for $f(R)$ gravity [42] is given as follows:

$$S = \frac{1}{2\kappa} \int \sqrt{-g} \;\; f(R) \; d^4x + S_M(g^{\mu\nu}, \psi) \tag{1.45}$$

where,

$g = det(g_{\mu\nu}) \rightarrow$ Determinant of the metric tensor $(g_{\mu\nu})$

$\kappa = \frac{8\pi G}{c^4} \rightarrow$ is the Einstein gravitational constant

$S_M(g^{\mu\nu}, \psi) = \int \sqrt{-g} \; \mathcal{L}_m(g_{\mu\nu}, \psi) \; d^4x$

here,

$S_M \rightarrow$ Matter action

$\mathcal{L}_m \rightarrow$ Lagrangian density of the matter

$\psi \rightarrow$ Matter field

1.8.2 Lovelock Gravity Theory

The Ricci scalar R in Einstein gravity is replaced by the Lagrangian function of the metric and the Riemann tensor.
The Hilbert-Einstein action principle for Lovelock gravity [42] is given as follows:

$$S = \int \sqrt{-g} \;\; \mathcal{L}[\; g^{\mu\nu}, \; R^{\mu}_{\nu\rho\delta} \;] \; d^Dx \; + \; S_m \tag{1.46}$$

where,

g Determinant of the metric tensor $(g_{\mu\nu})$

$S_m \rightarrow$ Matter action

$\mathcal{L} \rightarrow$ Lagrangian density of the matter

1.8.3 Einstein Dilation Gauss–Bonnet (EdGB) Gravity

EdGB gravity is a modified gravity theory that includes a scalar curvature term R, a quadratic Gauss–Bonnet curvature term $L^{(2)}$(second-order term from Lovelock gravity), and a scalar field term known as the dilation field ϕ. The Hilbert-Einstein action principle for EdGB [42] is given as follows:

$$S = \frac{1}{16\pi} \int \; d^4x\sqrt{-g} \left(R - \frac{1}{2} \; \partial_\mu \; \phi \; \partial^\mu \phi \; + \; \alpha \; e^{-\gamma\phi} \;\; L^{(2)} \right) \quad (1.47)$$

where,

$\phi \rightarrow$ Dilation field

$R \rightarrow$ Ricci scalar curvature

$L^{(2)} \rightarrow$ Gauss-Bonnet curvature

1.8.4 $f(T)$ gravity

In $f(T)$ gravity, the Ricci scalar R is replaced by the Torsion scalar T. T incorporates twisting and non-metricity of spacetime.

The Hilbert-Einstein action principle for Lovelock gravity [42] is given as follows:

$$S = \int f(T) \; \sqrt{-g} \;\; d^4x \quad (1.48)$$

1.8.5 $f(R,T)$ gravity

This modified gravity theory has implications in cosmology and gravitational lensing. For example, $f(R,T) = R + \alpha R^2 + \lambda T$

$$S = \int d^4x \, \sqrt{-g} \left[\frac{f(R,T)}{2\kappa^2} \right] \tag{1.49}$$

where, T is the torsion scalar , α and γ are constants

1.8.6 $f(Q)$ gravity

$f(Q)$ models are used to describe phenomena without using concepts like dark matter and dark energy.

$$S = \int \left[\left(\frac{-1}{16\pi G} \right) f(Q) \; + \; \mathcal{L}_m \right] \; \sqrt{-g} \; d^4x \tag{1.50}$$

where,

g Determinant of the metric tensor ($g_{\mu\nu}$)

$\mathcal{L}_m \rightarrow$ Lagrangian density of the matter

Chapter 2

Wormhole Dynamics: Construction and Types

2.1 Historical Overview of Wormholes

In 1916, Flamm contributed to the early theoretical work related to the Einsteinian theory of gravitation. Then, Einstein and Rosen discussed the Einstein-Rosen bridge [21] in 1935.

In 1957, Misner and Wheeler presented classical physics concepts such as gravitation, electromagnetism, unquantized charge, and mass as geometric properties of curved empty space [7, 22, 23, 37]. Their paper skirted the idea of "space-time foam" [28], proposing that the geometry and topology of space oscillate constantly, giving rise to the creation of wormholes at the microscopic level. [34]

Bronnikov wrote about scalar-tensor theory and scalar charge in the year 1973 [42]. In 1979, Ellis introduced the evolving, non-gravitating particle model of the flowless drain hole in general relativity [7,22,23,37]. In the year 1988, Morris and Thorne investigated the feasibility of wormholes in for interstellar travel [54]. They emphasized the importance of exotic matter (consisting negative energy density) that aids in wormhole traversability [34] and talked about the weak energy condition [34]. Their paper is regarded as a milestone in the study of wormhole physics.

Morris, Thorne, and Yurtsever's study of wormholes in 1988 fur-

ther confirmed the importance of exotic matter [7, 22, 23]. Visser studied wormholes (traversable) in 1989, from the surgically modified Schwarzschild spacetimes and supported the previous findings of Morris and Thorne's work [53]. In 1994, Hayward suggested a unified general theory of wormhole and black hole dynamics. He characterized wormhole mouths in terms of temporal outer-trapping horizons. [28]

In 1997, Hochberg and Visser discussed about the wormhole throat in their work "Generic Wormhole Throats" [27]. Contemporaneously, Hayward also arrived at the same conclusion. They characterized the wormhole throat by a flare-out condition and energy conditions. Their research also investigated the throat structure static traversable wormhole, and dynamic wormholes. [29]

Anchordoqui et al. began to search for natural wormholes in 1998. They also investigated the geometry for dynamic [27] wormholes. In 1998, Hochberg and Visser went on to further study the null energy condition for dynamic wormholes in depth. They also presented additional analysis visualizing wormhole throats as anti-trapped surfaces. They generalized Morris and Thorne's null energy condition violation for all traversable wormholes, including time-dependent contexts in which there may be two throats. [30]

In the year 1999, Hayward defined the wormhole throat in terms of trapping horizons, hypersurfaces foliated by marginal surfaces and extremal surfaces in a null hypersurface [27]. In 2001, Ferrari, Pauri, and Piazza worked on perturbation theory [9], which can be further applied to the stability of wormholes. In 2002, Hayward, Kim, and Lee discovered that the HKL wormhole was analytically dynamically stable. They also worked on the construction of a dilatonic wormholes [28]. Numerically, Shinkai and Hayward discovered the first Morris-Thorne wormhole to be dynamically unstable [28].

In 2003, Visser, Dadhich, and Kar demonstrated that it is possible to have traversable wormholes with arbitrarily small energy condi-

tion violations. Visser and Barceló further discussed the violation of energy condition [47]. Traversable wormhole energy condition violations were measured by Kar, Dadhich, and Visser in 2004. [30]

Lobo presented a review of traversable wormholes in the year 2006 [**?**, 29]. Kar and Sengupta gave a brief review of the Raychaudhuri equations in 2007 [30]. Shatskiy, Novikov, and Kardashev gave new analytic traversable wormhole models in 2008 [8]. In the year 2009, Lobo and Oliveira together investigated wormhole geometries within the modified $f(R)$ gravity theories [51]. Richarte and Simeone investigated Einstein-Born-Infeld wormholes, investigating the exotic matter content and mechanical stability. [47]

Harko and Lobo introduced $f(R, L_m)$ gravity in 2010[60]. In 2013, Rahaman et al. explored the existence of traversable wormholes in the galactic halo region [45]. In the year 2015, Mehdizadeh, Zangeneh, and Lobo explored Einstein-Gauss-Bonnet traversable wormholes that meet the weak energy condition [42]. In 2016, Bronnikov and Skvortsova talked about wormholes that connect to extra dimensions [8]. Capozziello, De Laurentis, and Odintsov investigated the neutron star mass-radius relation in $f(R)$ gravity. [49]

In 2016, Lobo gave a compact historical overview of wormhole physics, from the Flamm-Einstein-Rosen bridge to contemporary investigation. The review briefly mentioned stimulation of research on energy condition breaches, closed time-like structures, and faster than light travel via wormholes [19, 52]. In 2017, Bronnikov, Baleevskikh, and Skvortsova introduced wormholes with fluid sources and further investigated wormholes and black universes mediated by extra dimensions. [35]

In the year 2018, Sayeedul Islam, Farook Rahaman, Ali Ovgun, and Mustafa Halilsoy discussed the formation of wormholes in the galaxy Dragonfly 44 based on the Ultra Diffuse Galaxies (UDGs) and Navarro-Frank-White (NFW) dark-matter profiles. They indicated that Dragonfly 44's generalized NFW dark matter profile may sup-

port a wormhole. [51]

Xu et al. proposed f(Q,T) gravity in 2019 [42]. And, in 2020, Capozziello et al. spoke on extended gravity description for a supermassive neutron star [49]. Kashargin and Sushkov researched collapsing wormholes supported by dust-like matter [44]. Bronnikov, Kashargin, and Sushkov researched magnetized dusty black holes and wormholes in 2021 [8, 42]. Capozziello et al. researched traversable wormholes with vanishing sound speed in $f(R)$ gravity [45]. Mishra et al. discussed traversable wormhole models in $f(R)$ gravity in the year 2022. [42]

In 2023, Khyllep et al. performed a cosmological analysis of unified dynamical systems in $f(Q)$ gravity [42]. Solanki et al. investigated wormhole solutions in $f(R, Lm)$ gravity [51]. Rao et al. examined the thermodynamics of the $f(Q)$ universe in 2024. [42]

This study showcases the notable advancement in wormhole physics since the earlier works on spacetime geometries. The study of traversable wormholes was led by Morris and Thorne's discovery of the importance of presence of exotic matter that breaks the null energy condition (NEC) within General Relativity (GR). On the other hand, the investigation of modified theories of gravity, including $f(R)$ gravity, scalar-tensor theories, and brane-world models, has provided new avenues where wormhole solutions could be supported by modifications to the gravitational field equations, possibly enabling normal matter to meet standard energy conditions. The definition and dynamics of wormholes, such as the generalization of the throat concept to non-static spacetime using trapping horizons, have been a major concern. The stability of such exotic geometries continues to be a key question, with analyses depending on the particular exotic matter model or the nature of the modified gravity theory.

In addition, the possibility of creating traversable wormholes from general black hole solutions by adding conditions for exotic matter, and their possible evolution to black holes or inflationary universes,

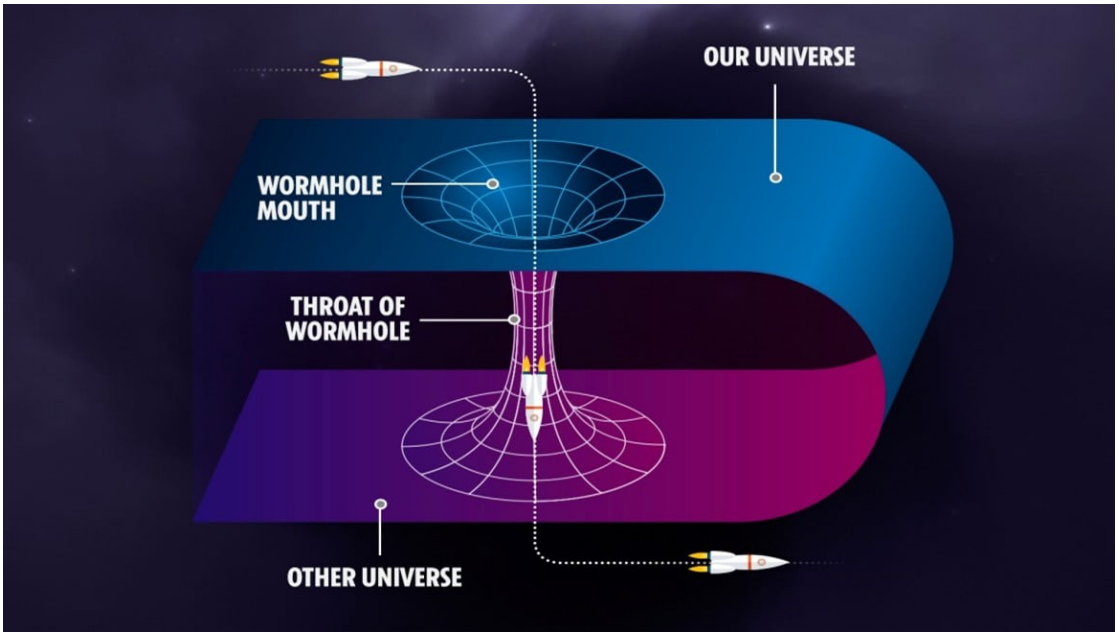

Figure 2.1: A general description of a wormhole [2]

highlights the rich dynamics involved with such theoretical objects. Recent studies have also shown potential occurrence of wormholes in astrophysical environments, like galactic halos, through the study of dark matter density profiles and galactic rotation curves.

2.2 Construction of Wormholes

A wormhole [21, 25, 36, 52, 54] connects different large or infinite regions of spacetime or even different universes, creating a "shortcut" between them [54]. In theory, it allows faster travel than light or instant travel between two locations, bypassing the conventional limitations of space-time. Wormholes [12–14, 17, 26, 31, 32, 39, 41](also known as Lorentzian wormholes) are often depicted in science fiction as portals or tunnels that could allow space travelers to move through vast distances in the same space-time or different space-times in an instant [21]. Wormholes are also called 'Einstein-Rosen bridges'. Though the idea of wormholes is fascinating, they remain speculative and unproven by any experimental evidence at present.

2.2.1 The Einstein-Rosen bridge:

Wormhole physics can be traced back to 1916 [11], when Flamm analyzed the Schwarzschild solution. Then, in 1935, Einstein and Rosen constructed an elementary particle model with two identical sheets connected by a 'bridge.' This mathematical representation of the physical spaces connected using a wormhole-type solution was referred to as an 'ER bridge'. [21]

2.2.2 Basic Terminologies

1. **Throat:** The throat of a wormhole is the narrowest region that connects two regions of spacetime. [21, 54]

2. **Mouth:** The entry and exit points of the wormhole. These can be located in the same universe (a traversable wormhole) or in different universes (Einstein-Rosen bridge). [21, 54]

3. **Shape Function** $b(r)$**:** This function determines the radius of the throat of the wormhole and its curvature. [21, 54]

4. **Redshift Function** $f(r)$: Describes the gravitational time dilation inside the wormhole. It should be finite everywhere to avoid event,i.e., allow passage through a wormhole. [21, 54]

5. **Flare-Out Condition:** It ensures that the wormhole remains open and does not collapse. Exotic matter (negative energy density) is essential to prevent the wormhole from collapsing. [21, 54]

6. **Exotic Matter:** A type of matter with negative energy density, it violates the null energy condition (NEC). It is required to prevent the wormhole from collapsing under gravity. Exotic matter don't interact with any kind of electromagnetic waves. [54]

2.2.3 Setting up the Wormhole Spacetime:

The general form of the wormhole spacetime is defined using the Morris-Thorne line element [43]:

$$ds^2 = -e^{2f(r)}dt^2 + \left(1 - \frac{b(r)}{r}\right)^{-1} dr^2 + r^2(\ d\theta^2 + \sin^2\theta\ d\phi^2\ ) \quad (2.1)$$

where,

$f(r)$: Redshift function, which must be finite to avoid an event horizon.

$b(r)$: Shape function that determines the geometry of the wormhole

r: Radial coordinate

r_0 : Throat of the wormhole where $b(r_0) = r_0$.

θ : Co-altitude coordinate

ϕ: Longitude coordinate

2.2.4 Conditions for wormholes:

1. **No Event Horizon:** Ensure that $f(r)$ is finite everywhere.
2. **Flare-Out Condition:** Verify that $b'(r_0) < 1$ at the throat r_0.
3. **Shape Function Condition:** Check that $\frac{b(r)}{r} < 1$ for $r > r_0$.
4. **Null Energy Condition:** Confirm the violation of NEC, i.e., $\rho + p_r < 0$, for the wormhole to be traversable.

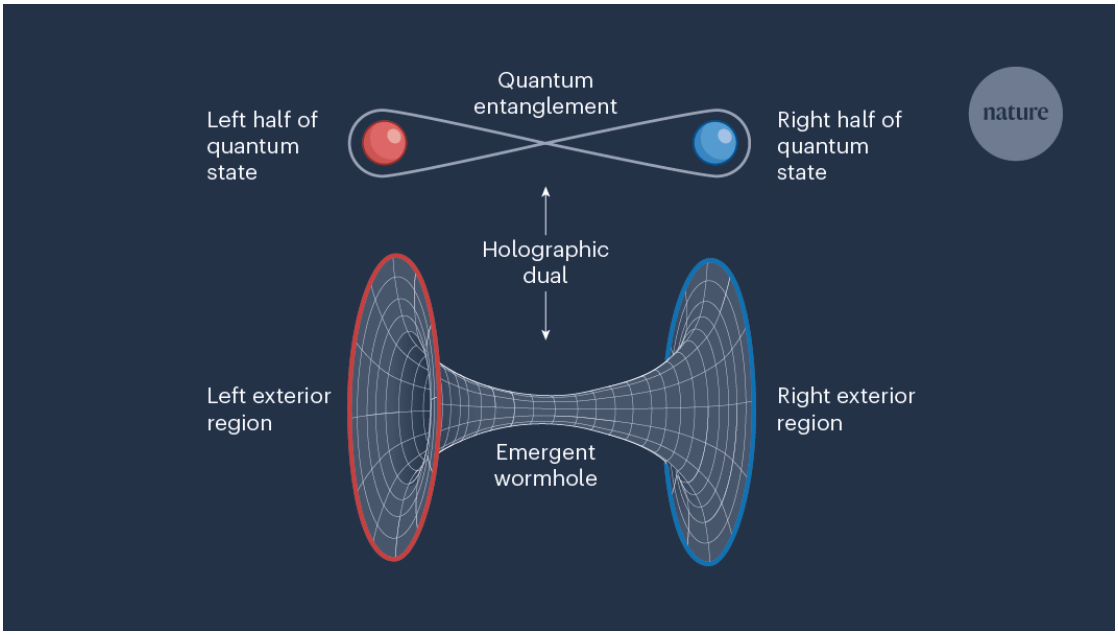

Figure 2.2: A holographic wormhole traversed in a quantum computer [10]

2.3 Different types of Wormholes:

2.3.1 Traversable Wormholes:

This type of wormhole is often depicted in science fiction as capable of allowing matter (such as humans or spaceships) to pass through it.

It has two mouths (entrances) connected by a tunnel called the "throat" of the wormhole. A traversable wormhole [12–14, 17, 26, 31, 32, 39, 41] will allow objects to move through it without collapsing (i.e. they should be stable). In order to form wormholes, we require exotic matter. The Morris-Thorne metric is a spherically symmetric solution to Einstein's equations:

$$ds^2 = e^{-2f(r)}dt^2 + \left(1 - \frac{b(r)}{r}\right)^{-1} dr^2 + r^2(\ d\theta^2 + sin^2\theta\ d\phi^2\ ) \quad (2.2)$$

where,

$r \rightarrow$ Radial coordinate

θ : Co-altitude coordinate

ϕ: Longitude coordinate

$b(r) \rightarrow$ Shape function (describes the structure of the wormhole)

$ds^2 \rightarrow$ Spacetime interval

2.3.2 Non-Traversable Wormholes:

These are theoretical solutions to the equations of general relativity, often referred to as 'Einstein-Rosen bridges' [21, 52]. They connect two distant regions of spacetime but are not traversable by any object or information.

They can be thought of as more of a mathematical concept than a physical phenomenon. These types of wormholes do not have the necessary structure to allow safe passage through them, as they collapse immediately as one tries to pass through the wormhole.

The **Schwarzchild metric** describes a non-traversable wormhole, also known as an Einstein-Rosen bridge:

$$ds^2 = -\left(1 - \frac{2GM}{r}\right) c^2\, dt^2 + \left(1 - \frac{2GM}{r}\right)^{-1} dr^2 + r^2(\, d\theta^2 + sin^2\theta\, d\phi^2\,) \tag{2.3}$$

where,

$r \rightarrow$ Radial coordinate

$ds^2 \rightarrow$ Spacetime interval

$G \rightarrow$ Gravitational constant

$c \rightarrow$ Speed of light

$M \rightarrow$ Mass of the black hole.

This solution describes a wormhole that collapses too quickly and hence is unfit for travel.

2.3.3 Kerr Wormholes (Rotating Wormholes):

The Kerr wormhole is a solution based on the rotating black hole model, derived from the Kerr metric. Theoretically, these are special types of traversable wormholes with a rotating black hole at each mouth. [36, 54]

The rotation of the wormhole can add to its stability, but the presence of exotic matter is essential for the throat to remain open. A rotating black hole could theoretically allow time travel, though this is purely speculative.

The Kerr metric in terms of coordinates (t, r, θ, ϕ) is given by the line element:

$$ds^2 = -N^2\ dt^2 + \left(1 - \frac{b(r)}{r}\right)^{-1} dr^2 + r^2K^2(\ d\theta^2 + sin^2\theta\ (d\psi - \omega\ dt^2)) \tag{2.4}$$

Here,

$N = \sqrt{1 - \frac{2M}{r}}$, is the redshift function

$b(r) = \frac{r_0^2\ +\ 2M(r-r_0)}{r}$, is the shape function

$r \rightarrow$ Radial coordinate

$\theta \rightarrow$ Polar angle

$\phi \rightarrow$ Azimuthal angle

$\omega \rightarrow$ Angular momentum

2.3.4 Wormholes in Higher Dimensions:

Some theories, such as string theory or brane theory, propose that wormholes could exist in dimensions higher than and beyond the familiar three spatial dimensions and time. These types of wormholes might connect different universes or different regions within a higher-dimensional space [42].

EdGB gravity is a modified gravity theory that includes a scalar curvature term R, a quadratic Gauss–Bonnet curvature term $L^{(2)}$(second-order term from Lovelock gravity), and a scalar field term known as the dilation field ϕ.

$$S = \frac{1}{16\pi} \int \; d^4x\sqrt{-g} \left(R - \frac{1}{2} \; \partial_\mu \; \phi \; \partial^\mu \phi \; + \; \alpha \; e^{-\gamma\phi} \;\; L^{(2)} \right) \qquad (2.5)$$

where,

$\phi \rightarrow$ Dilation field

$R \rightarrow$ Ricci scalar curvature

$L^{(2)} \rightarrow$ Gauss-Bonnet curvature

Chapter 3

Wormhole solutions in UDGs using Einstein gravity

Ultra-Diffuse Galaxies (UDGs) are an extreme case of low-surface brightness galaxies [5]. They are defined as dwarf galaxies with low luminosity. UDGs were first detected in large numbers in the Coma Cluster and have since been found in galaxy groups and clusters [5]. Studying UDGs is important because their extreme properties challenge our understanding of galaxy formation and evolution [40]. They can provide insights into galaxy formation mechanisms and evolutionary paths, probe the nature of dark matter, and test different cosmological models. The formation of UDGs remains an area of active research.

Dragonfly 44 [38] a galaxy discovered in 2016 in the Coma Cluster, is an ultra-diffuse galaxy (UDG). Observations of its rotational speed indicate that its mass is nearly identical to the Milky Way. However, what makes Dragonfly 44 particularly interesting is that it emits only about 1 percent of the light produced by the Milky Way. This significant discrepancy led astronomers to suggest that Dragonfly 44 might be composed almost entirely of dark matter [6, 24]. Studies have observed around 90 percent globular clusters associated with Dragonfly 44. We try to explore the possibility of wormhole formation by dark matter present in the galaxy Dragonfly 44.

3.1 Christoffel Symbols:

The metric for wormhole geometry (traversable) in spherical coordinate (t, r, θ, ϕ) is given as:

$$ds^2 = -e^{2f(r)}dt^2 + \left(1 - \frac{b(r)}{r}\right)^{-1} dr^2 + r^2(\ d\theta^2 + sin^2\theta\ d\phi^2) \quad (3.1)$$

where,

$f(r) \rightarrow$ Redshift function

$b(r) \rightarrow$ Shape function

$r \rightarrow$ Radial coordinate

Writing the above equation in matrix form:

$$g_{ab} = \begin{bmatrix} -e^{2f(r)} & 0 & 0 & 0 \\ 0 & \left(1 - \frac{b(r)}{r}\right)^{-1} & 0 & 0 \\ 0 & 0 & r^2 & 0 \\ 0 & 0 & 0 & r^2 sin^2\theta \end{bmatrix} \quad (3.2)$$

The non-zero components of the metric tensor are:

$$g_{11} = g_{tt} = -e^{2f(r)} \quad (3.3)$$

$$g_{22} = g_{rr} = \left(1 - \frac{b(r)}{r}\right)^{-1} \quad (3.4)$$

$$g_{33} = g_{\theta\theta} = r^2 \quad (3.5)$$

$$g_{44} = g_{\phi\phi} = r^2 sin^2\theta \quad (3.6)$$

As the matrix is a diagonal matrix, just inverting the diagonal terms will give us the inverse matrix:

$$g^{ab} = \begin{bmatrix} \frac{1}{-e^{2f(r)}} & 0 & 0 & 0 \\ 0 & \left(1 - \frac{b(r)}{r}\right) & 0 & 0 \\ 0 & 0 & \frac{1}{r^2} & 0 \\ 0 & 0 & 0 & \frac{1}{r^2 sin^2\theta} \end{bmatrix} \tag{3.7}$$

Similarly, the non-zero components:

$$g^{11} = g^{tt} = \frac{1}{-e^{2f(r)}} \tag{3.8}$$

$$g^{22} = g^{rr} = \left(1 - \frac{b(r)}{r}\right) \tag{3.9}$$

$$g^{33} = g^{\theta\theta} = \frac{1}{r^2} \tag{3.10}$$

$$g^{44} = g^{\phi\phi} = \frac{1}{r^2 sin^2\theta} \tag{3.11}$$

The non-zero Christoffel symbols we will get are as follows:

$$\Gamma^2_{11}, \quad \Gamma^1_{21} = \Gamma^1_{12}, \quad \Gamma^2_{22}, \quad \Gamma^2_{33}, \quad \Gamma^3_{23} = \Gamma^3_{32}, \quad \Gamma^2_{44},$$
$$\Gamma^4_{24} = \Gamma^4_{42}, \quad \Gamma^3_{44}, \quad and \quad \Gamma^4_{34} = \Gamma^4_{43} \quad [\ \Gamma_{ij} = \Gamma_{ji} \text{ symmetry }] \tag{3.12}$$

We know,

$$\Gamma^i_{jk} = \frac{1}{2} g^{il} \left(g_{jl,k} + g_{lk,j} - g_{jk,l}\right) \tag{3.13}$$

$$\Gamma^2_{11} = \frac{1}{2} g^{2l} (g_{1l,1} + g_{l1,1} - g_{11,l})$$

$$= \frac{1}{2}[g^{21}(g_{11,1} + g_{11,1} - g_{11,1}) \ + \ g^{22}(g_{12,1} + g_{21,1} - g_{11,2})$$
$$+ \ g^{23}(g_{13,1} + g_{31,1} - g_{11,3}) \ + \ g^{24}(g_{14,1} + g_{41,1} - g_{11,4})] \tag{3.14}$$

Since g^{21}, g^{23} and g^{24} are equal to zero, we have,

$$\Gamma^2_{11} = \frac{1}{2} g^{22} (g_{12,1} + g_{21,1} - g_{11,2})$$

$$= \frac{1}{2}\left(1 - \frac{b(r)}{r}\right)\left[0 + 0 - \frac{\partial}{\partial r}(-e^{2f(r)})\right]$$

$$= \frac{1}{2}\left(1 - \frac{b(r)}{r}\right)[-2e^{2f(r)}f'(r)]$$

$$\Rightarrow \ \boldsymbol{\Gamma^2_{11} = e^{2f(r)}f'(r)\left(1 - \frac{b(r)}{r}\right)} \tag{3.15}$$

Similarly, we calculate the other Christofell symbols.
As $\Gamma^1_{21} = \Gamma^1_{12}$

$$\Gamma^1_{12} = \frac{1}{2}g^{1l}(g_{1l,2} + g_{l2,1} - g_{12,l})$$

$$= \frac{1}{2}[g^{11}(g_{11,2} + g_{12,1} - g_{12,1}) + 0 + 0 + 0]$$

$$= \frac{1}{2}(-e^{2f(r)})\left[\frac{\partial}{\partial r}(-e^{2f(r)})\right]$$

$$\Rightarrow \ \boldsymbol{\Gamma^1_{12} = \frac{1}{2}\frac{1}{(-e^{2f(r)})}(-e^{2f(r)})[2f'(r)] = f'(r)} \tag{3.16}$$

Then,

$$\Gamma^2_{22} = \frac{1}{2}g^{2l}(g_{2l,2} + g_{l2,2} - g_{22,l})$$

$$= \frac{1}{2}[g^{22}(g_{22,2} + g_{22,2} - g_{22,2}) + 0 + 0 + 0]$$

$$= \frac{1}{2}g^{22}(g_{22,2})$$

$$= \frac{1}{2}\left(1 - \frac{b(r)}{r}\right)\left[\frac{\partial}{\partial r}\left(1 - \frac{b(r)}{r}\right)^{-1}\right]$$

$$\frac{1}{2}\left(1-\frac{b(r)}{r}\right)\left[(-1)\left(1-\frac{b(r)}{r}\right)^{-2}\left(\frac{-rb'(r)-b(r)}{r^2}\right)\right]$$

$$=\frac{1}{2}\left(1-\frac{b(r)}{r}\right)^{-1}\left(\frac{rb'(r)+b(r)}{r^2}\right)$$

$$=\left(\frac{rb'(r)+b(r)}{2r^2}\right)\left(1-\frac{b(r)}{r}\right)^{-1} \tag{3.17}$$

Again,

$$\Gamma^2_{33}=\frac{1}{2}g^{2l}(g_{3l,3}+g_{l3,3}-g_{33,l})$$

$$=\frac{1}{2}[g^{22}(g_{32,2}+g_{23,3}-g_{33,2})+0+0+0]$$

$$=\frac{1}{2}g^{22}(-g_{33,2})$$

$$=-\frac{1}{2}\left(1-\frac{b(r)}{r}\right)\left[\frac{\partial}{\partial r}(r^2)\right]$$

$$=-r\left(1-\frac{b(r)}{r}\right)$$

$$\Rightarrow\ \boldsymbol{\Gamma^2_{33}}\ =\ \boldsymbol{b(r)-r} \tag{3.18}$$

As $\Gamma^3_{23}=\Gamma^3_{32}$,

$$\Gamma^3_{23}=\frac{1}{2}g^{3l}(g_{2l,3}+g_{l3,2}-g_{23,l})$$

$$=\frac{1}{2}[g^{33}(g_{23,3}+g_{33,2}-g_{23,3})+0+0+0]$$

$$= \frac{1}{2} g^{33}(g_{33,2})$$

$$= -\frac{1}{2}\left(\frac{1}{r^2}\right)\left[\frac{\partial}{\partial r}\left(\frac{1}{r^2}\right)\right]$$

$$\Rightarrow \boldsymbol{\Gamma^3_{23} = \frac{-1}{r^5}} \tag{3.19}$$

As $\Gamma^4_{24} = \Gamma^4_{42}$

$$\Gamma^4_{24} = \frac{1}{2} g^{4l}(g_{2l,4} + g_{l4,2} - g_{24,l})$$

$$= \frac{1}{2}[g^{44}(g_{24,4} + g_{44,2} - g_{24,4}) + 0 + 0 + 0]$$

$$= \frac{1}{2} g^{44}(g_{44,2})$$

$$= \frac{1}{2}\left(\frac{1}{r^2 sin^2\theta}\right)\left[\frac{\partial}{\partial r}(r^2 sin^2\theta)\right]$$

$$\Rightarrow \boldsymbol{\Gamma^4_{24} = \frac{1}{r}} \tag{3.20}$$

Then,

$$\Gamma^3_{44} = \frac{1}{2} g^{3l}(g_{4l,4} + g_{l4,4} - g_{44,l})$$

$$= \frac{1}{2}[g^{33}(g_{43,4} + g_{34,4} - g_{44,3}) + 0 + 0 + 0]$$

$$= \frac{1}{2} g^{33}(-g_{44,3})$$

$$= -\frac{1}{2}\left(\frac{1}{r^2}\right)\left[\frac{\partial}{\partial r}(r^2 sin^2\theta)\right]$$

$$= \ -sin\theta cos\theta$$

$$\Rightarrow \boldsymbol{\Gamma^3_{44} = \ -\frac{sin2\theta}{2}} \tag{3.21}$$

Also,

$$\Gamma^4_{34} = \frac{1}{2}g^{4l}(g_{3l,4} + g_{l4,3} - g_{34,l})$$

$$= \frac{1}{2}[g^{44}(g_{34,4} + g_{44,3} - g_{34,4}) + 0 + 0 + 0]$$

$$= \frac{1}{2}g^{44}(g_{44,2})$$

$$= \frac{1}{2}\left(\frac{1}{r^2 sin^2\theta}\right)\left[\frac{\partial}{\partial\theta}(r^2 sin^2\theta)\right]$$

$$\Rightarrow \boldsymbol{\Gamma^4_{34} = \frac{sin2\theta}{2}} \tag{3.22}$$

3.2 Shape function:

The metric for the geometry of the traversable wormhole in spherical coordinates (t, r, θ, ϕ) is given as:

$$ds^2 = -e^{2f(r)}dt^2 + \left(1 - \frac{b(r)}{r}\right)^{-1} dr^2 + r^2(d\theta^2 + sin^2\theta d\phi^2) \tag{3.23}$$

In the earlier section, we calculated the Christoffel symbol:

$$\Gamma^r_{tt} = f'(r)e^{2f(r)}\left(1 - \frac{b(r)}{r}\right) \tag{3.24}$$

Ricci tensor:

$$R_{tt} = f''(r) + [f'(r)]^2 - f'(r)\left[\frac{rb'(r) - b(r)}{2r(r - b(r)}\right] \tag{3.25}$$

Trace of the Ricci tensor, Ricci scalar:

$$R = g^{\mu\nu} R_{\mu\nu} \tag{3.26}$$

Now, using the Einstein tensor, $G_{\mu\nu} = R_{\mu\nu} - \frac{1}{2} g_{\mu\nu} R$ and the Einstein field equation, $G_{\mu\nu} = 8\pi T_{\mu\nu}$, we have,

$$G_t^t = \frac{b'(r)}{r^2} \quad \Rightarrow \quad 8\pi T_t^t = \frac{b'(r)}{r^2} \quad \Rightarrow \quad T_t^t = \frac{b'(r)}{8\pi r^2} \tag{3.27}$$

The non-zero components of the stress-energy tensor are as follows:

1. **Energy Density** $(-\rho)$**:**

$$T_t^t = -\rho \quad \Rightarrow \quad \frac{b'(r)}{8\pi r^2} = -\rho \tag{3.28}$$

2. **Radial pressure** (p_r) **:**

$$T_r^r = p_r = \frac{1}{8\pi} \left[\frac{-b(r)}{r^3} + 2 \left(1 - \frac{b(r)}{r} \frac{f'(r)}{r} \right) \right] \tag{3.29}$$

3. **Tangential pressure** (p_t):

$$T_\theta^\theta = T_\phi^\phi = p_t \tag{3.30}$$

$$p_t = \frac{1}{8\pi} \left(1 - \frac{b(r)}{r} \right) \left[f''(r) + f'(r)^2 + \left(\frac{f'(r)}{r} \right) \right]$$

$$- \frac{1}{8\pi} \left(1 - \frac{b(r)}{r} \right) \left[\left(\frac{1}{r} + f'(r) \right) \left(\frac{r b'(r) - b(r)}{2r(r - b(r))} \right) \right] \tag{3.31}$$

From the expression of energy density, we have,

$$b'(r) = 8\pi r^2 \rho(r) \Rightarrow \qquad \boldsymbol{b(r) = \int 8\pi r^2 \rho(r) dr} \tag{3.32}$$

3.3 Navarro-Frank-White(NFW) Density Profile

The NFW profile is a model used to describe how dark matter spreads in galaxies. It shows that the density is highest at the center and decreases with distance from the center. The density profile for the dark matter distribution is as follows [4]:

$$\rho(r) = \frac{\rho_0}{r^{\gamma}\left(1+\frac{r}{r_0}\right)^{3-\gamma}} \tag{3.33}$$

where,

$\rho(r) \rightarrow$ represents the dark matter density at a radius r

$\gamma \rightarrow$ inner slope of the profile

$r_0 \rightarrow$ scale radius

CASE-1: $\gamma = 1$

$$\rho(r) = \frac{\rho_0}{r\left(1+\frac{r}{r_0}\right)^{2}} \tag{3.34}$$

$$b(r) = \int 8\pi r^2 \rho(r) dr \tag{3.35}$$

Now, by substituting the value of $\rho(r)$, we obtain,

$$b(r) = 8\pi\rho_0 \int \frac{r^2}{r\left(1+\frac{r}{r_0}\right)^{2}}\ dr \ = \ 8\pi\rho_0 \int \frac{r}{\left(1+\frac{r}{r_0}\right)^{2}}\ dr$$

$$\text{Let,}\ \ u = \left(1+\frac{r}{r_0}\right)$$

By differentiating both sides with respect to r, we get,

$$du = \left(\frac{1}{r_0}\right) dr$$

Also, using the substitution, we can write,

$$u = \left(\frac{r + r_0}{r_0}\right) \quad \Rightarrow \; u\, r_0 = r + r_0 \quad \Rightarrow \; r = r_0(u-1)$$

Therefore,

$$b(r) = 8\pi\rho_0 \int \frac{r_0^2(u-1)}{u^2} du$$

$$= 8\pi\rho_0 r_0^2 \quad \left[\int \frac{du}{u} - \int \frac{du}{u^2} \right]$$

$$= 8\pi\rho_0 r_0^2 \quad \left[ln(u) + \frac{1}{u} + C \right]$$

$$\Rightarrow \; \boldsymbol{b(r) = 8\pi\rho_0 r_0^2} \quad \left[\boldsymbol{ln\left(1 + \frac{r}{r_0}\right) + \frac{1}{\left(1 + \frac{r}{r_0}\right)} + C} \right] \tag{3.36}$$

Using the boundary condition : $b(r_0) = r_0$, we have,

$$r_0 = 8\pi\rho_0 r_0^2 \left[ln(2) + \frac{1}{2} + C \right]$$

Hence,

$$\boldsymbol{C = \frac{1}{8\pi\rho_0 r_0^2} - ln(2) - \frac{1}{2}} \tag{3.37}$$

In Figure: 3.1, the graph shows asymptotic behavior. Here, as r

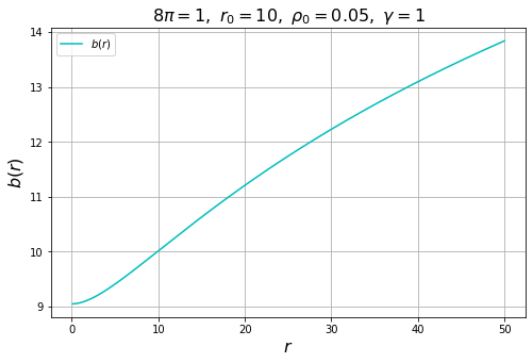

Figure 3.1: $b(r)$ versus r plot

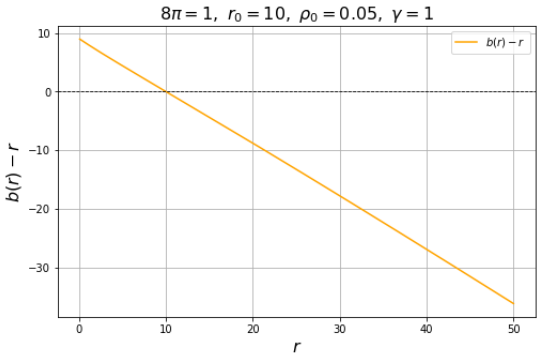

Figure 3.2: ($b(r) - r$) versus r plot

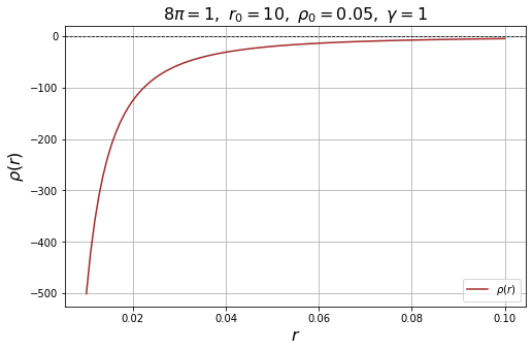

Figure 3.3: $\rho(r)$ versus r plot

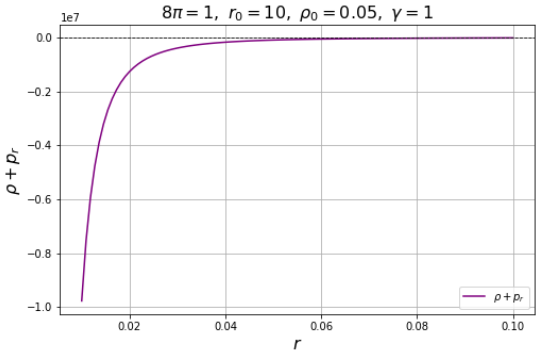

Figure 3.4: Null energy Violation

increases, $b(r)$ increases, but after some point there is a decline in the rate of increase of $b(r)$. As we move away from the throat of the wormhole, $b(r)$ almost tends to become linear with r, indicating an asymptotically flat wormhole. Figure: 3.2, shows that, $b(r) - r$ is negative; it confirms that the flare-out condition $b(r) < r$ is met. Thus, ensuring that the wormhole is traversable.

In Figure: 3.3, we observe that $\rho(r)$ is negative everywhere, and the curve approaches zero asymptotically. Figure: 3.4$\rho(r) + p_r$ is also negative everywhere, violating the NEC, i.e., $(\rho(r) + p_r) < 0$ which means that exotic matter is present and is highly concentrated at the throat (due to large values at the throat) of the wormhole. The rapid approach to zero in both the curves signifies that the exotic matter has an influence over only a significantly small region around the throat.

CASE-2: $\gamma = 2$

$$\rho(r) = \frac{\rho_0}{r^2\left(1+\frac{r}{r_0}\right)} \tag{3.38}$$

$$b(r) = \int 8\pi r^2 \rho(r) dr$$

Thus, we have,

$$b(r) = 8\pi\rho_0 \int \frac{r^2}{r^2\left(1+\frac{r}{r_0}\right)} dr \;=\; 8\pi\rho_0 \int \frac{dr}{\left(1+\frac{r}{r_0}\right)}$$

$$\text{Let,} \quad u = \left(1+\frac{r}{r_0}\right)$$

By differentiating both sides with respect to r, we get,

$$du = \left(\frac{1}{r_0}\right) dr$$

Also, using the substitution, we can write,

$$u = \left(\frac{r+r_0}{r_0}\right) \;\Rightarrow\; u\; r_0 = r + r_0 \;\Rightarrow\; r = r_0\;(u-1)$$

Therefore,

$$b(r) = 8\pi\rho_0 \int \left(\frac{r_0}{u}\right) du$$

$$= 8\pi\rho_0 r_0\; ln(u) + C$$

$$= 8\pi\rho_0 r_0 \;\; ln\left(1+\frac{r}{r_0}\right) + C \tag{3.39}$$

Using the boundary condition : $b(r_0) = r_0$, we have,

$$r_0 = 8\pi\rho_0 r_0 \; ln(2) + C$$

$$\Rightarrow \boldsymbol{C = r_0(1 - 8\pi\rho_0 \; ln(2))} \tag{3.40}$$

In Figure: 3.5, $b(r)$ is positive and monotonically increases as r increases. In the graph $b(r)$ v/s r for CASE-1, the change in $b(r)$ was sharper than in this case. This graph shows a more gradual decrease in the rate of increase of the shape function. Figure: 3.6, shows that $b(r) - r$ is negative; it confirms that the flare-out condition $b(r) < r$ is met, thus ensuring that the wormhole is traversable. Figure: 3.7 shows that energy density is negative everywhere. In Figure: 3.8, we observe a violation of NEC, i.e.,$(\rho(r) + p_r) < 0$.

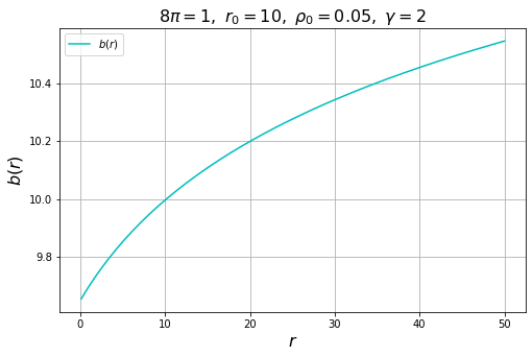

Figure 3.5: $b(r)$ versus r plot

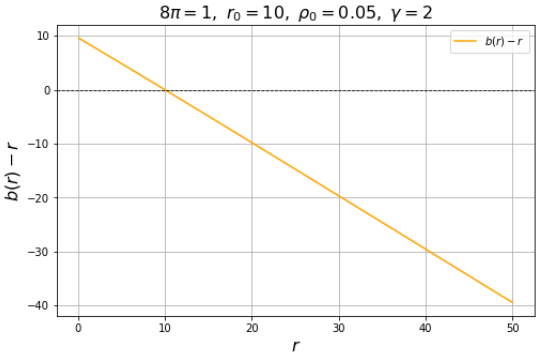

Figure 3.6: ($b(r) - r$) versus r plot

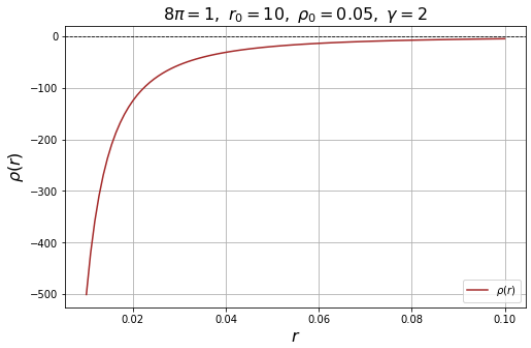

Figure 3.7: $\rho(r)$ versus r plot

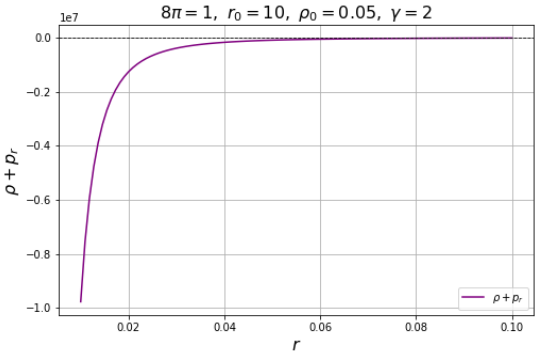

Figure 3.8: Null energy Violation

CASE-3 : $\gamma = 3$

$$\rho(r) = \frac{\rho_0}{r^3} \tag{3.41}$$

Thus, we get,

$$b(r) = \int 8\pi r^2 \rho(r) dr$$

$$= \int 8\pi r^2 \left(\frac{\rho_0}{r^3}\right) dr$$

$$= 8\pi\rho_0 \int \frac{dr}{r}$$

$$\Rightarrow \boldsymbol{b(r) = 8\pi\rho_0 \, [\, ln(r) + C \,]} \tag{3.42}$$

Using the boundary condition : $b(r_0) = r_0$, we have,

$$r_0 = 8\pi\rho_0 [\, ln(r_0) + C \,]$$

$$\Rightarrow \boldsymbol{C = \frac{r_0}{8\pi\rho_0} - ln(r_0)} \tag{3.43}$$

In Figure: 3.9, $b(r)$ shows logarithmic growth. This suggests that the throat of the wormhole expands as r increases. In Figure: 3.10, we can clearly see that $b(r) - r$ is negative, confirming the flare-out condition, $b(r) < r$ which ensures that the wormhole is traversable. We can see that $\rho(r)$ is negative everywhere in Figure: 3.11. Figure: 3.12, depicts the violation of NEC, i.e.,$(\rho(r) + p_r) < 0$.

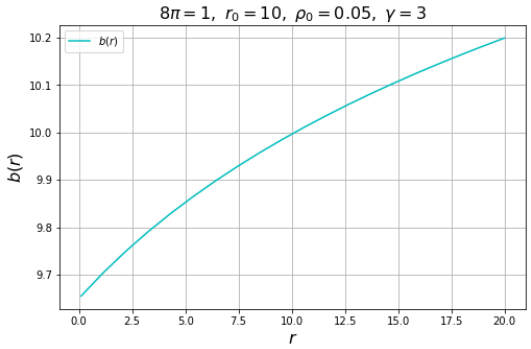

Figure 3.9: $b(r)$ versus r plot

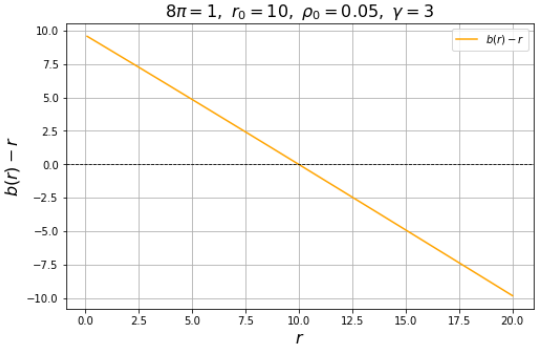

Figure 3.10: ($b(r) - r$) versus r plot

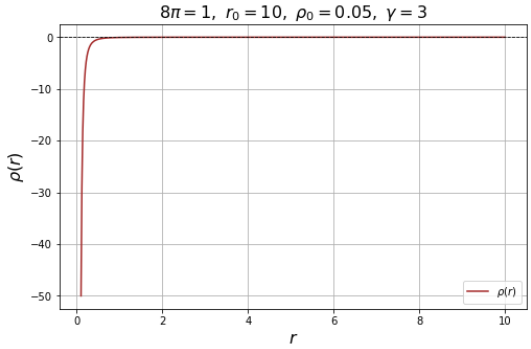

Figure 3.11: $\rho(r)$ versus r plot

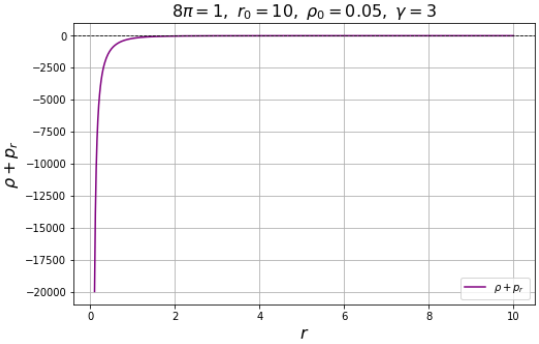

Figure 3.12: Null energy Violation

CASE-4 : $\gamma = 4$

$$\rho(r) = \frac{\rho_0}{r^4\left(1+\frac{r}{r_0}\right)^{-1}} \tag{3.44}$$

Thus, we get,

$$b(r) = \int 8\pi r^2 \rho(r) dr$$

$$= \int 8\pi r^2 \left[\frac{\rho_0}{r^4\left(1+\frac{r}{r_0}\right)^{-1}} \right] dr$$

$$= 8\pi\rho_0 \int \frac{1}{r^2}\left(1+\frac{r}{r_0}\right) dr$$

$$= 8\pi\rho_0 \left[\int \frac{dr}{r^2} + \left(\frac{1}{r_0}\right)\int \frac{dr}{r} \right]$$

$$\Rightarrow \boldsymbol{b(r) = 8\pi\rho_0 \left[\frac{-1}{r} + \frac{1}{r_0} ln(r) + C \right]} \tag{3.45}$$

Using the boundary condition : $b(r_0) = r_0$, we have,

$$r_0 = 8\pi\rho_0 \left[-\frac{1}{r_0} + \left(\frac{1}{r_0}\right) ln(r_0) + C \right]$$

$$\Rightarrow \boldsymbol{C = \frac{r_0}{8\pi\rho_0} + \frac{1}{r_0} - \left(\frac{1}{r_0}\right) ln(r_0)} \tag{3.46}$$

In Figure: 3.13, $b(r)$ increases with an increase in r. This suggests that the throat of the wormhole expands as r increases. In

Figure: 3.14 we can clearly see that $b(r) - r$ is negative, confirming the flare-out condition, $b(r) < r$ which ensures that the wormhole is traversable. Just like the previous cases, Figure: 3.15 shows negative energy density. Figure: 3.16 shows a similar nature to 3.11. The NEC is violated, i.e.,$(\rho(r) + p_r) < 0$.

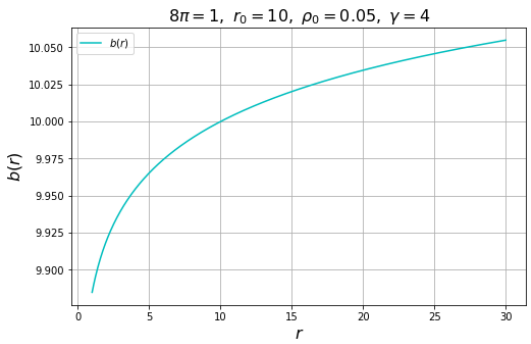

Figure 3.13: $b(r)$ versus r plot

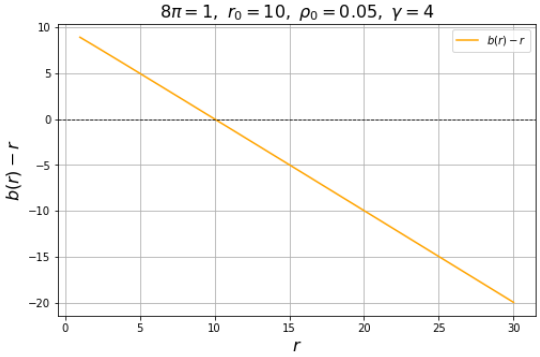

Figure 3.14: ($b(r) - r$) versus r plot

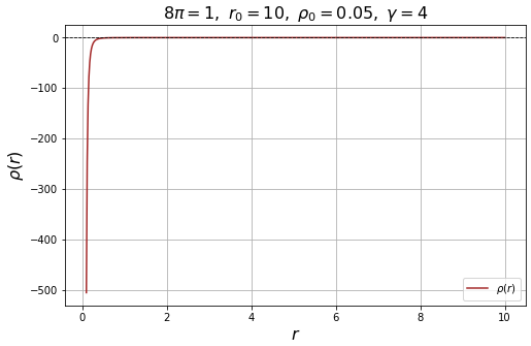

Figure 3.15: $\rho(r)$ versus r plot

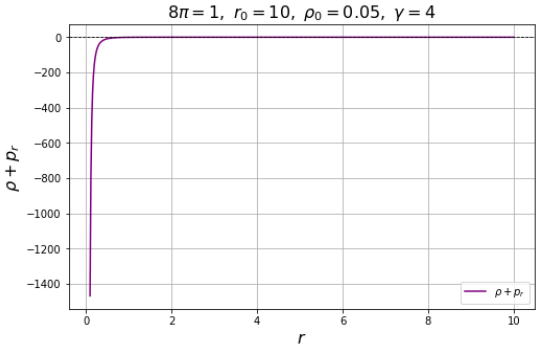

Figure 3.16: Null energy Violation

CASE-5 : $\gamma = 5$

$$\rho(r) = \frac{\rho_0}{r^5 \left(1 + \frac{r}{r_0}\right)^{-2}} \tag{3.47}$$

Thus, we have,

$$b(r) = \int 8\pi r^2 \rho(r) dr$$

$$= \int 8\pi r^2 \left[\frac{\rho_0}{r^5 \left(1 + \frac{r}{r_0}\right)^2} \right] dr$$

$$= 8\pi\rho_0 \int \frac{1}{r^3} \left(1 + \frac{r}{r_0}\right)^2 dr$$

$$= 8\pi\rho_0 \left[\int \frac{dr}{r^3} + \int \frac{dr}{r r_0^2} + 2 \int \frac{dr}{r^2 r_0} \right]$$

$$\Rightarrow \boldsymbol{b(r) = 8\pi\rho_0 \left[\frac{-1}{2r^2} + \frac{ln(r)}{r_0^2} + \left(\frac{-2}{r r_0}\right) + C \right]} \tag{3.48}$$

Using the boundary condition : $b(r_0) = r_0$, we have,

$$r_0 = 8\pi\rho_0 \left[\frac{-1}{2r_0^2} + \frac{ln(r_0)}{r_0^2} + \left(\frac{-2}{r_0^2}\right) + C \right]$$

$$\Rightarrow \boldsymbol{C = \frac{r_0}{8\pi\rho_0} + \frac{1}{2r_0^2} - \frac{ln(r_0)}{r_0^2} + \frac{2}{r_0^2}} \tag{3.49}$$

In Figure: 3.17, $b(r)$ is positive and increases with r, but the curve

becomes almost flat as r increases. This graph shows a rapid convergence compared to the previous cases. For larger values of r, $b(r)$ becomes almost constant, whereas in all the previous cases $b(r)$ kept on increasing with a decrease in the rate of increase of the shape function.

In Figure: 3.18 we can clearly see that $b(r)-r$ is negative, confirming the flare-out condition $b(r) < r$ which ensures that the wormhole is traversable. Figure: 3.19 and Figure: 3.20 show a similar nature to all previous cases, with $\rho(r)$ being negative and violating the NEC, i.e.,$(\rho(r) + p_r) < 0$.

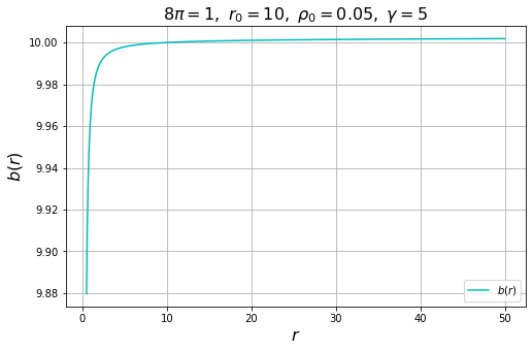

Figure 3.17: $b(r)$ versus r plot

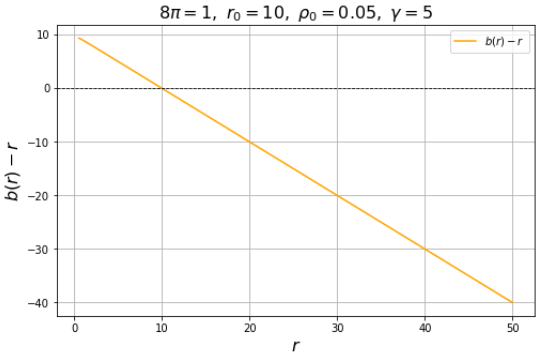

Figure 3.18: ($b(r) - r$) versus r plot

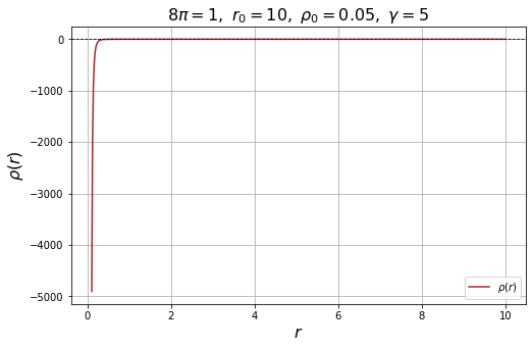

Figure 3.19: $\rho(r)$ versus r plot

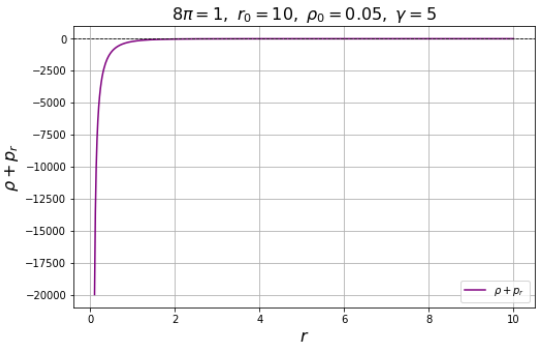

Figure 3.20: Null energy Violation

CASE-6: $\gamma = 6$

$$\rho(r) = \frac{\rho_0}{r^6 \left(1 + \frac{r}{r_0}\right)^{-3}} \tag{3.50}$$

Thus, we have,

$$b(r) = \int 8\pi r^2 \rho(r) dr$$

$$= \int 8\pi r^2 [\frac{\rho_0}{r^6 \left(1 + \frac{r}{r_0}\right)^3}] dr$$

$$\text{Let, } \; u = \left(1 + \frac{r}{r_0}\right)$$

By differentiating both sides with respect to r, we get,

$$du = \left(\frac{1}{r_0}\right) dr$$

Also, using the substitution, we can write,

$$u = \left(\frac{r + r_0}{r_0}\right) \Rightarrow \; u\, r_0 = r + r_0 \; \Rightarrow \; r = r_0\, (u - 1)$$

Hence,

$$b(r) = 8\pi\rho_0 \int \frac{u^3 r_0}{r_0^4 (u-1)^4} du \quad = \quad \frac{8\pi\rho_0}{r_0^3} \int \frac{u^3}{(u-1)^4}$$

$$\text{Again let,} \quad v = (u - 1)$$

By differentiating both sides with respect to u, we get,

$$dv = du$$

Using the substitution, we have $u = v + 1$,

Now, by substituting all the values in the expression of $b(r)$, we obtain,

$$b(r) = \frac{8\pi\rho_0}{r_0^3}\left[\ \int \frac{(v+1)^3}{v^4}\ \ dv\ \right]$$

$$= \frac{8\pi\rho_0}{r_0^3}\int\left(\frac{v^3+3v^2+3v+1}{v^4}\right)\ dv$$

$$= \frac{8\pi\rho_0}{r_0^3}\left[\int\frac{dv}{v} + \ 3\int\frac{dv}{v^2} + \ 3\int\frac{dv}{v^3} + \ \int\frac{dv}{v^4}\ \right]$$

$$= \frac{8\pi\rho_0}{r_0^3}\left[\ ln(v)\ -\ \frac{3}{v}\ -\ \frac{3}{2v^2}\ -\ \frac{1}{3v^3}\ +\ C\right]$$

$$= \frac{8\pi\rho_0}{r_0^3}\left[\ ln(u-1) - \ \frac{3}{u-1} - \ \frac{3}{2(u-1)^2} - \ \frac{1}{3(u-1)^3}\ +\ C\ \right]$$

$$\Rightarrow \boldsymbol{b(r) = \frac{8\pi\rho_0}{r_0^3}\left[\ \frac{ln(r)}{r_0^3} - \frac{3}{rr_0^2} - \frac{3}{2r^2r_0} - \frac{1}{3r^2} + C\ \right]} \quad (3.51)$$

Using the boundary condition : $b(r_0) = r_0$, we get,

$$r_0 = \frac{8\pi\rho_0}{r_0^3}\left[\frac{ln(r_0)}{r_0^3} - \frac{3}{r_0^3} - \frac{3}{2r_0^3} - \frac{1}{3r_0^2} + C\right]$$

$$\Rightarrow \boldsymbol{C = \frac{r_0}{8\pi\rho_0} + \frac{1}{3r_0^3} + \frac{3}{2r_0^3} + \frac{3}{r_0^3} - \frac{ln(r_0)}{r_0^3}} \quad (3.52)$$

In Figure: 3.21, $b(r)$ is positive and increases with r, but the curve becomes almost flat as r increases. This graph shows a rapid convergence similar to CASE-5. For larger values of r, $b(r)$ becomes almost constant. In Figure: 3.22 we can clearly see that $b(r) - r$ is negative, confirming the flare-out condition $b(r) < r$ which ensures that the wormhole is traversable. Figure: 3.23 shows negative energy density, i.e., the presence of exotic matter. In Figure: 3.24 we observe a violation of NEC, i.e.,$(\rho(r) + p_r) < 0$.

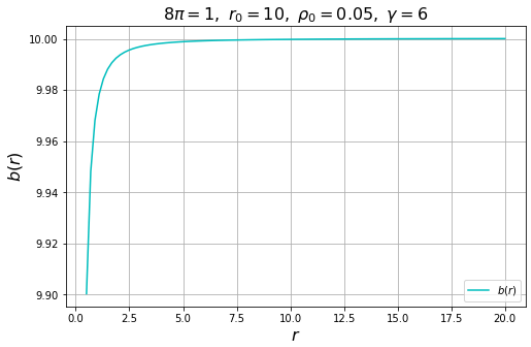

Figure 3.21: $b(r)$ versus r plot

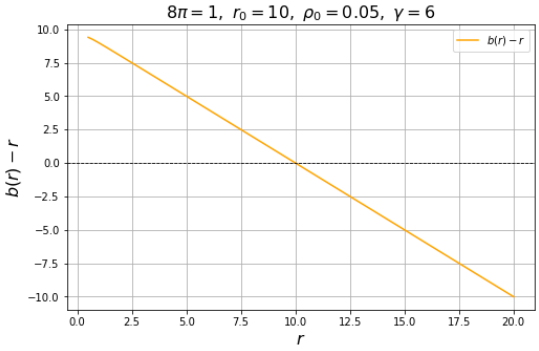

Figure 3.22: ($b(r) - r$) versus r plot

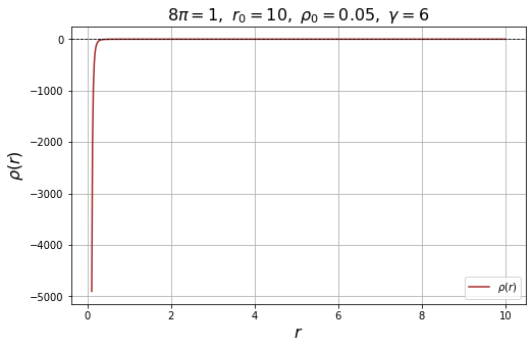

Figure 3.23: $\rho(r)$ versus r plot

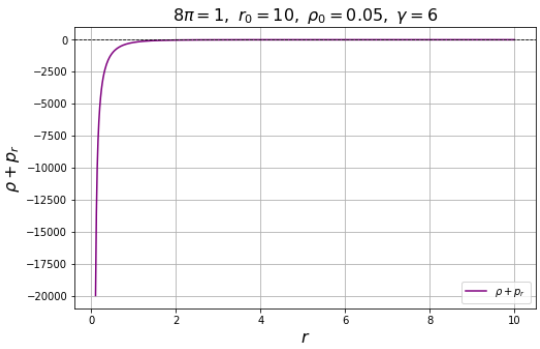

Figure 3.24: Null energy Violation

3.4 UDG King's Model

This model is tailored to describe the dark matter distribution in Ultra Diffuse Galaxies (UDGs). It uses a modified King density profile for dark matter distribution as follows: [14, 32]

$$\rho(r) = \kappa \left[\left(\frac{r}{r_0} \right)^2 + \lambda \right]^{\eta} \tag{3.53}$$

where, η, κ and λ are parameters

Velocity dispersion [14, 32] in the cluster is given as:

$$v^{\phi} = \alpha r e^{-k_1 r} + \beta[\ 1 - e^{-k_2 r}\ ] \tag{3.54}$$

$$v^{\phi} = \sqrt{r f'(r)} \quad \Rightarrow \quad f'(r) = \frac{(v^{\phi})^2}{r} \tag{3.55}$$

So, we have,

$$f'(r) = \frac{(\alpha r e^{-k_1 r} + \beta[\ 1 - e^{-k_2 r}\ ])^2}{r}$$

$$= \frac{\alpha^2 r^2 e^{-2k_1 r} + 2\alpha r e^{-k_1 r}\beta[\ 1 - e^{-k_2 r}\ ] + \beta^2[\ 1 - e^{-k_2 r}\ ]^2}{r}$$

$$= \alpha^2 r e^{-2k_1 r} + 2\alpha\beta e^{-k_1 r} - 2\alpha\beta e^{-(k_1+k_2)r} + \frac{\beta^2}{r} - \frac{2\beta^2}{r} e^{-k_2 r} + \frac{\beta^2}{r} e^{-2k_2 r}$$

$$\text{Let, } A = \alpha^2 r e^{-2k_1 r}\ ,\ B = \frac{2\beta^2}{r} e^{-k_2 r} \text{ and } D = \frac{\beta^2}{r} e^{-2k_2 r} \tag{3.56}$$

By integrating both sides with respect to r , we get ,

$$A = \int \alpha^2 r e^{-2k_1 r} dr$$

$$\text{Let , } u = r \ \ and$$

Now, by differentiating both sides with respect to r, we obtain,

$$du = dr$$

$$\text{Also let, } dv = e^{-2k_1 r} dr$$

Again, by integrating both sides with respect to r, we get,

$$\Rightarrow \ v = -\frac{e^{-2k_1 r}}{2k_1}$$

Using integration by parts, we have,

$$\int u dv = uv - \int v du$$

$$= \frac{-r}{2k_1} e^{-2k_1 r} + \int \left(\frac{e^{-2k_1 r}}{2k_1} \right) dr$$

$$= \left(\frac{-r}{2k_1} \right) e^{-2k_1 r} - \frac{e^{-2k_1 r}}{4k_1^2} + C$$

$$\Rightarrow A = -\alpha^2 e^{-2k_1 r} \left(\frac{-r}{2k_1} - \frac{-1}{4k_1^2} \right)$$

$$B \ = 2\beta^2 \int \left(\frac{1}{r} \right) e^{-k_2 r} dr \ = \ -2\beta^2 E_1(k_2 r) \quad \left[\text{Since, } \int \frac{e^{-\lambda x}}{x} = -E_1(\lambda x) \right]$$

Similarly,

$$D = \int \frac{\beta^2}{r} e^{-2k_2 r} = -\beta^2 E_1(2k_2 r)$$

Hence,

$$f(r) = -\alpha^2 e^{-2k_1 r} \left(\frac{r}{2k_1} + \frac{1}{4k_1^2} \right) + 2\alpha\beta \left(\frac{e^{-k_1 r}}{-k_1} \right) + \frac{2\alpha\beta e^{-(k_1+k_2)r}}{(k_1+k_2)}$$

$$+\beta^2 \ ln(r) + 2\beta^2 E_1(k_2 r) - \beta^2 E_1(2k_2 r) + C$$

$$\Rightarrow f(r) = \frac{-\alpha^2 r}{2k_1 e^{2k_1 r}} - \frac{\alpha^2}{4k_1^2 e^{2k_1 r}} - \frac{2\alpha\beta}{k_1 e^{k_1 r}} + \frac{2\alpha\beta}{(k_1+k_2)e^{-(k_1+k_2)r}}$$

$$+\beta^2\ ln(r) + 2\beta^2 E_1(k_2 r) - \beta^2 E_1(2k_2 r) + C \tag{3.57}$$

where,

$C \rightarrow$ integral constant

$E_1 \rightarrow$ exponential integral function $[E_i(x)]$

CASE-1 : $\boldsymbol{\kappa = 1,\ \lambda = 1}$ and $\boldsymbol{\eta = -\frac{1}{2}}$

$$\rho(r) = \left[\left(\frac{r}{r_0}\right)^2 + 1\right]^{-\frac{1}{2}} \tag{3.58}$$

We know,

$$b(r) = \int r^2 \rho(r) dr \tag{3.59}$$

Substitute the value of $\rho(r)$ in (3.58), we obtaion,

$$\Rightarrow \quad b(r) = \int r^2 \left[\left(\frac{r}{r_0}\right)^2 + 1\right]^{-\frac{1}{2}} dr$$

$$\text{Let,}\ \ u = \frac{r}{r_0}$$

By differentiating both sides with respect to r, we get,

$$du = \frac{1}{r_0} dr$$

Also, using the substitution, we can write,

$$u = \frac{r}{r_0} \quad \Rightarrow \quad r = \ u\ r_0$$

Thus, we have,

$$b(r) = \int u^2 \; r_0^2 \; (u^2+1)^{-\frac{1}{2}} \;\; r_0 \; du$$

$$= \int u^2 \; r_0^3 \; (u^2+1)^{-\frac{1}{2}} \; du$$

$$= r_0^3 \int \frac{u^2}{\sqrt{(u^2+1)}} \; du$$

$$= r_0^3 \int \frac{(u^2+1)-1}{\sqrt{(u^2+1)}} \; du$$

$$\Rightarrow \boldsymbol{b(r) = r_0^3 \left[\int \sqrt{(u^2+1)} \; du - \int \frac{du}{\sqrt{(u^2+1)}} \right]} \qquad (3.60)$$

Now, we will separately solve the two integral terms in the expression of $b(r)$.

First term:

$$\int \sqrt{(u^2+1)} \; du$$

$$\text{Let, } u = sinh(t)$$

Now, by applying sine inverse on both sides, we get,

$$t = sinh^{-1}(u)$$

$$\text{Also let, } \; du = cosh(t) \; dt$$

Therefore,

$$\int \sqrt{(u^2+1)} \; du = \int \sqrt{(sinh(t)^2+1)} \; cosh(t) \; dt$$

$$= \int \sqrt{(cosh(t))^2}\ cosh(t)\ dt \qquad [\text{ Since, } cosh^2(t) - sinh^2(t) = 1\ ]$$

$$= \int cosh^2(t) dt$$

$$= \frac{1}{2} \int [\ 1 + cosh(2t)\ ]\ dt$$

$$= \frac{1}{2} \left[\int dt + \int cosh(2t)\ dt \right]$$

$$= \frac{1}{2} \left[t + \frac{sinh(2t)}{2} \right]$$

$$= \frac{1}{2} \left[t + \frac{1}{2}(2\ sinh(t)\ cosh(t)) \right] \quad [\text{Since, } sinh(2t) = 2\ sinh(t)\ cosh(t)\ ]$$

$$= \frac{1}{2} [\ t + sinh(t)\ cosh(t)\ ]$$

$$= \frac{1}{2} \left[sinh^{-1}(u) + u\sqrt{u^2+1}) \right] \quad \left[\text{Since, } cosh(t) = \sqrt{1 + sinh^2(t)}\ \right]$$

$$= \frac{ln(u + \sqrt{u^2+1})}{2} + \frac{u\sqrt{u^2+1}}{2} \quad \left[\text{ Since, } sinh^{-1}(x) = ln(x + \sqrt{x^2+1})\right] \tag{3.61}$$

Second term:

$$\int \frac{du}{\sqrt{u^2+1}}$$

$$\text{Let, } u = tan\theta$$

By differentiating both sides with respect to θ, we get,

$$du \ = \ sec^2\theta\ d\theta$$

Also, we know that, $(1 + tan^2\theta) = sec^2\theta \Rightarrow sec\theta = \sqrt{u^2+1}$
Thus,

$$\int \frac{du}{\sqrt{u^2+1}} = \int \frac{sec^2\theta}{\sqrt{tan^2\theta+1}}\ d\theta$$

$$= \int sec\theta\ \ d\theta \qquad [\text{Since, } (1 + tan^2\theta) = sec^2\theta]$$

$$= ln(\ sec\theta + tan\theta\ )$$

Hence,

$$\int \frac{du}{\sqrt{u^2+1}} = ln(\sqrt{1+u^2} + u) \tag{3.62}$$

Now, by putting equations (3.61) and (3.62) in (3.60), we obtain,

$$b(r) = r_0^3 \left[\frac{1}{2}\ ln(u + \sqrt{u^2+1}) + \frac{1}{2}\ (u\sqrt{u^2+1}) - \ ln(\sqrt{1+u^2}) + \ C_1 \right]$$

$$= \left(\frac{r_0^3}{2}\right) \left[\ u\sqrt{u^2+1} - \ ln(u + \sqrt{1+u^2}) + \ C \right]$$

Thus, we finally get,

$$\boldsymbol{b(r) = \frac{r_0^3}{2} \left[\left(\frac{r}{r_0}\right) \sqrt{1 + \left(\frac{r}{r_0}\right)^2} - ln \left(\left(\frac{r}{r_0}\right) + \sqrt{1 + \left(\frac{r}{r_0}\right)^2} \right) + C \right]} \tag{3.63}$$

Using the boundary condition: $b(r_0) = r_0$,we have,

$$r_0 = \left(\frac{r_0^3}{2}\right) \left[\ \sqrt{2} - ln(1 + \sqrt{2}) + C \ \right]$$

$$\Rightarrow \frac{2}{r_0^2} = 0.533 + C$$

Thus, we have,

$$\boldsymbol{C = \left(\frac{2}{r_0^2}\right) - 0.533} \tag{3.64}$$

Flare-out condition : $(b'(r) < 1)$

$$b(r) = \frac{r_0^3}{2}\left[\left(\frac{r}{r_0}\right)\sqrt{1+\left(\frac{r}{r_0}\right)^2} - ln\left(\left(\frac{r}{r_0}\right)+\sqrt{1+\left(\frac{r}{r_0}\right)^2}\right) + C\right]$$

By differentiating both sides with respect to r , we get,

$$b'(r) = \left(\frac{r_0^3}{2}\right)\left[\left(\frac{\left(\frac{r^2}{r_0^3}\right)}{\sqrt{1+\left(\frac{r}{r_0}\right)^2}}\right) + \left(\frac{\sqrt{1+\left(\frac{r}{r_0}\right)}}{r_0}\right)\right]$$

$$- \left(\frac{r_0^3}{2}\right)\left[\left(\frac{1}{\left(\frac{r}{r_0}\right) + \sqrt{1+\left(\frac{r}{r_0}\right)^2}}\right)\left(\left(\frac{1}{r_0}\right) + \frac{\left(\frac{r}{r_0^2}\right)}{\sqrt{1+\left(\frac{r}{r_0}\right)^2}}\right)\right]$$

Now, by assigning $r_0 = 1$, the expression becomes,

$$b'(r) = \frac{1}{2}\left[\frac{r^2}{\sqrt{1+r^2}} + \sqrt{1+r^2} - \left(\frac{1}{r+\sqrt{1+r^2}}\right)\left(1+\frac{r}{\sqrt{1+r^2}}\right)\right]$$

$$= \frac{1}{2}\left[\frac{r^2}{\sqrt{1+r^2}} + \sqrt{1+r^2} - \frac{1}{\sqrt{1+r^2}}\right]$$

$$= \frac{1}{2}\left[\frac{r^2 - 1}{\sqrt{1+r^2}} + \sqrt{1+r^2}\right]$$

$$= \frac{1}{2}\left[\frac{1+r^2+r^2-1}{\sqrt{1+r^2}}\right] = \frac{r^2}{\sqrt{1+r^2}}$$

Hence,

$$b'(r) = \frac{r^2}{\sqrt{1+r^2}} \quad \text{, at} \quad r_0 = 1,\ \kappa = 1,\ \lambda = 1,\ \text{and}\ \eta = -\frac{1}{2}$$

In Figure : 3.25, the condition $\frac{b(r)}{r} < 1$ is not satisfied. Thus, a wormhole will not exist in this case. Figure : 3.26 depicts a strong violation of NEC, $\rho + p_r < 0$ at the throat of the wormhole. In Figure : 3.27, $b(r)$ increases rapidly, suggesting a non-asymptotically flat spacetime. Here, $b(r) >> r$, so asymptotic flatness is violated. This suggests the presence of a wormhole in a dynamic and curved universe (like cosmological spacetime, which is expanding). In Figure : 3.28, $b'(r)$ is increasing but stays well below 1, i.e., the flare-out condition $b'(r_0) < 1$ is satisfied, which guarantees a wormhole.

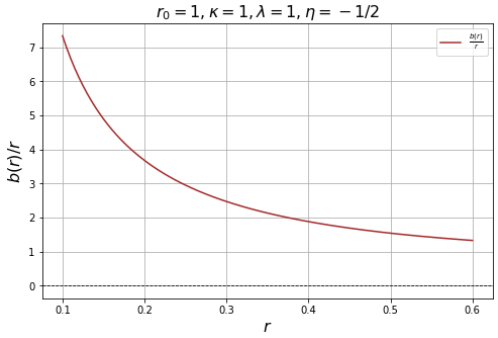

Figure 3.25: $\frac{b(r)}{r}$ versus r plot

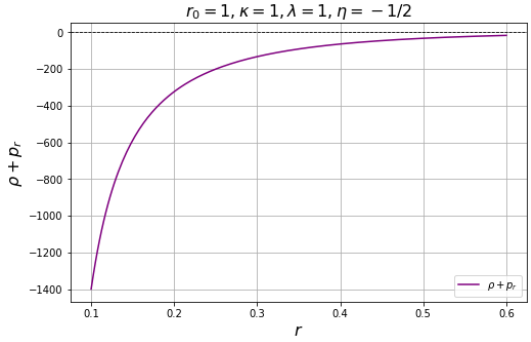

Figure 3.26: NEC Violation

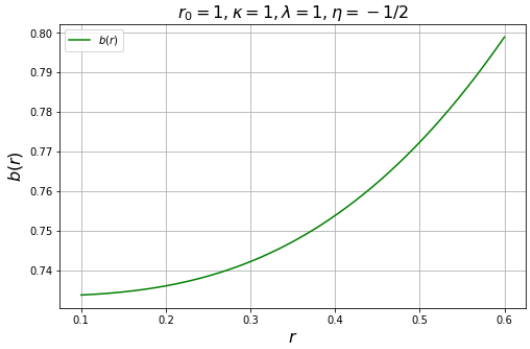

Figure 3.27: $b(r)$ versus r plot

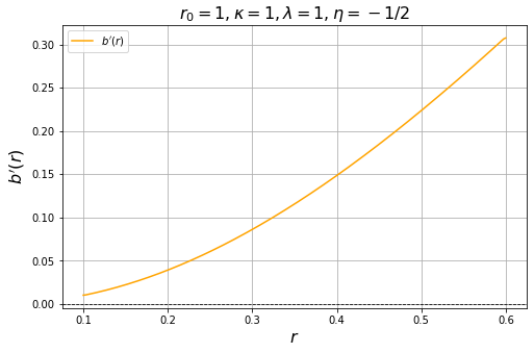

Figure 3.28: $b'(r)$ versus r plot

CASE-2: $\kappa = 1,\ \lambda = 1$ and $\eta = -1$

$$\rho(r) = \left[\left(\frac{r}{r_0}\right)^2 + 1 \right]^{-1}$$

$$\text{Let,} u = \left(\frac{r}{r_0}\right)^2$$

By differentiating both sides with respect to r, we get,

$$du = \left(\frac{2\ r}{r_0^2}\right)\ dr$$

Thus,

$$b(r) = \int \left(\frac{r^2}{u+1}\right)\left(\frac{r_0^2}{2\ r}\right)\ du$$

$$= \left(\frac{r_0^3}{2}\right)\int\ \left(\frac{\sqrt{u}}{u+1}\right) du$$

$$\text{Let, } v = \sqrt{u}$$

By differentiating both sides with respect to u, we get,

$$dv = \frac{1}{2\sqrt{u}}\ du$$

Thus,

$$b(r) = \left(\frac{r_0^3}{2}\right)\int\ \left(\frac{v}{v^2\ +\ 1}\right)\ 2v\ dv$$

$$= r_0^3 \int \left(\ \frac{v^2}{v^2+1}\ \right) dv$$

$$= r_0^3 \int \left(\frac{(v^2+1)-1}{v^2+1} \right) dv$$

$$= r_0^3 \left[\int dv \; - \; \int \frac{dv}{v^2+1} \right]$$

$$= r_0^3 \; [\; v \; - \; tan^{-1}(v) \; + \; C \;]$$

$$= r_0^3 \; [\; \sqrt{u} \; - \; tan^{-1}(\sqrt{u}) \; + \; C \;]$$

Finally, we obtain,

$$b(r) = \; r_0^3 \; \left[\left(\frac{r}{r_0} \right) \; - \; tan^{-1} \left(\frac{r}{r_0} \right) \; + \; C \right] \tag{3.65}$$

By differentiating both sides with respect to r, we have,

$$b'(r) = \; r_0^3 \; \left[\left(\frac{1}{r_0} \right) \; - \; \left(\frac{1}{1 + \left(\frac{r}{r_0} \right)^2} \right) \right] \tag{3.66}$$

Now, using the boundary condition: $b(r_0) = r_0$ in the expression of $b(r)$ that we obtained earlier, we get,

$$r_0 = \; r_0^3 \; \left[\left(\frac{r}{r_0} \right) \; - \; tan^{-1}(1) \; + \; C \right]$$

Hence,

$$\boldsymbol{C = \left(\frac{1}{r_0^2} \right) \; - \; 1 \; + \; \frac{\pi}{4}} \tag{3.67}$$

In Figure: 3.29, $b(r)$ increases rapidly at first, then saturates to a constant value. This plot shows signs of asymptotic flatness as the shape of the wormhole flattens out at larger values of r. This supports the presence of a wormhole in flat spacetime. In Figure: 3.30, $\frac{b(r)}{r} > 1$, thus a wormhole does not exist in this case. Figure:3.31 depicts the violation of NEC, $\rho + p_r < 0$ at the throat of the wormhole. In Figure: 3.32, the flare-out conditionis satisfied as $b'(r_0) < 1$ everywhere.

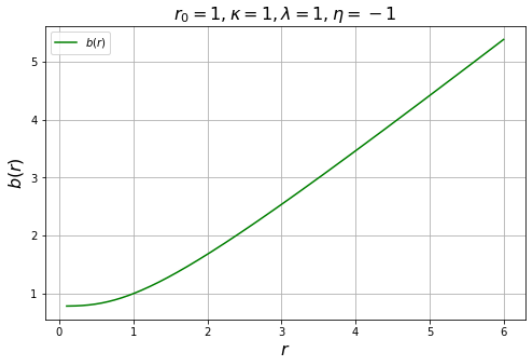

Figure 3.29: $b(r)$ versus r plot

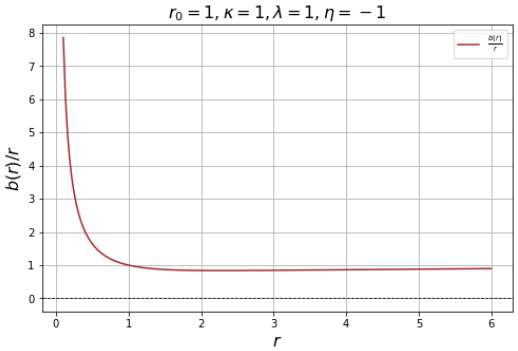

Figure 3.30: $\frac{b(r)}{r}$ versus r plot

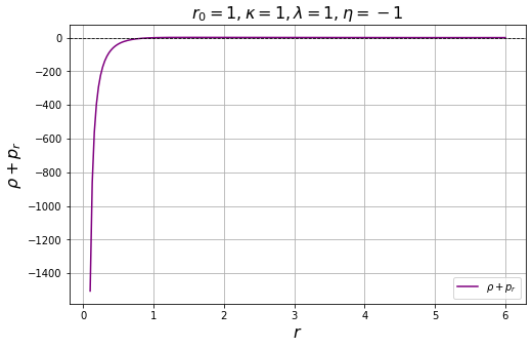

Figure 3.31: NEC Violation

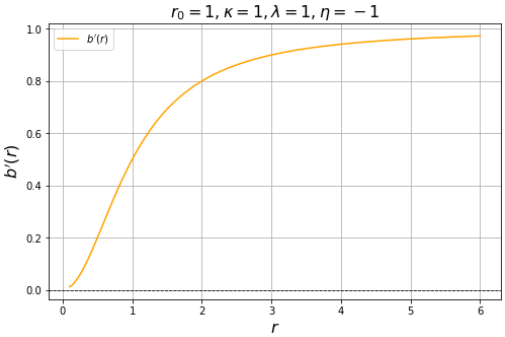

Figure 3.32: $b'(r)$ versus r plot

CASE-3 : $\kappa = 1,\ \lambda = 1$ and $\eta = -\frac{3}{2}$

$$\rho(r) = \left[\left(\frac{r}{r_0}\right)^2 + 1\right]^{-\frac{3}{2}} \tag{3.68}$$

We know,

$$b(r) = \int r^2 \rho(r) dr$$

$$\Rightarrow \quad b(r) = \int r^2 \left[\left(\frac{r}{r_0}\right)^2 + 1\right]^{-\frac{3}{2}} dr$$

$$\text{Let,} u = \left(\frac{r}{r_0}\right)^2$$

By differentiating both sides with respect to r, we get,

$$du = \left(\frac{2\ r}{r_0^2}\right)\ dr$$

Using the above substitution, we can write,

$$u\ r_0^2\ =\ r^2 \quad \Rightarrow \quad r =\ r_0\ \sqrt{u}$$

Thus,

$$b(r)\ =\ r_0^3 \int\ \left(\frac{\sqrt{u}}{(u+1)^{3/2}}\right)\ du$$

$$\text{Let, } v = \sqrt{u}$$

By differentiating both sides with respect to u, we get,

$$dv = \frac{1}{2\sqrt{u}}\ du$$

Thus, we have,

$$b(r) = r_0^3 \int \frac{v}{(v^2 + 1)^{3/2}}\, dv$$

$$= 2\ r_0^3 \int \left(\frac{(v^2+1)-1}{(v^2+1)^{3/2}} \right) dv$$

$$= 2\ r_0^3 \left[\int \frac{dv}{\sqrt{v^2+1}} - \int \frac{dv}{(v^2+1)^{3/2}} \right] \tag{3.69}$$

We will now separately solve the two integral terms in the expression of $b(r)$.

First term:

$$\int \frac{dv}{\sqrt{v^2+1}}$$

$$\text{Let } v = tan\theta$$

By differentiating both sides with respect to θ, we get,

$$dv \ = \ sec^2\theta\ d\theta$$

Also, using the substitution, we can write,

$$sec\theta \ = \ \sqrt{1 + tan^2\theta} = \sqrt{1+v^2}$$

So, we have,

$$\int \frac{dv}{\sqrt{v^2+1}} \ = \ \int \left(\frac{sec^2\theta}{tan^2\theta + 1} \right)\ d\theta$$

$$= \int sec\theta\ d\theta$$

$$= ln(\ sec\theta + tan\theta\ )$$

Hence,

$$\int \frac{\boldsymbol{dv}}{\sqrt{\boldsymbol{v^2+1}}} = \boldsymbol{ln(\ \sqrt{1+v^2}\ +\ v\ )} \tag{3.70}$$

Second term:

$$\int \frac{dv}{(v^2+1)^{3/2}}$$

Let, $v = tan\theta$

By differentiating both sides with respect to θ, we get,

$$dv\ =\ sec^2\theta\ d\theta$$

Also, using the substitution, we can also write,

$$\theta = tan^{-1}(v)$$

Thus,

$$\int \frac{dv}{(v^2+1)^{3/2}}\ =\ \int \left(\frac{1}{(1+tan^2\theta)^{3/2}}\right)\ \ sec^2\theta\ d\theta$$

$$= \int \frac{sec^2\theta}{(sec^2\theta)^{3/2}}\ \ d\theta$$

$$= \int \frac{d\theta}{\sqrt{sec^2\theta}}$$

$$= \int \frac{d\theta}{\sqrt{sec\theta}}$$

$$= \int cos\theta\ \ d\theta\ =\ sin\theta$$

Hence,

$$\int \frac{dv}{(v^2+1)^{3/2}} \;=\; sin(tan^{-1}(v))$$

$$\text{Let, } a \;=\; tan^{-1}(v) \quad \Rightarrow \quad v = tan(a)$$

We know,

$$seca \;=\; \sqrt{1+tan^2 a} = \sqrt{1+v^2}$$

$$\text{So,} \quad cosa \;=\; \frac{1}{\sqrt{1+v^2}}$$

$$\text{Also,} \quad sina \;=\; \sqrt{1-cos^2 a}$$

$$= \sqrt{1-\left(\frac{1}{1+v^2}\right)^2}$$

$$= \sqrt{\frac{v^2+1-1}{1+v^2}}$$

$$= \sqrt{\frac{v^2}{1+v^2}}$$

Thus,

$$sin(tan^{-1}(v)) \;=\; \sqrt{\frac{v^2}{1+v^2}}$$

Therefore,

$$\int \frac{\boldsymbol{dv}}{\boldsymbol{(v^2+1)^{3/2}}} \;=\; \sqrt{\frac{\boldsymbol{v^2}}{\boldsymbol{1+v^2}}} \tag{3.71}$$

Now by substituting equations (3.70) and (3.71) in (3.69), we get,

$$b(r) = 2\ r_0^3\ \left[\ \int \frac{dv}{\sqrt{v^2+1}}\ -\ \int \frac{dv}{(v^2+1)^{3/2}}\ \right]$$

$$= 2\ r_0^3\ \left[\ v\ +\ ln(\ \sqrt{1+v^2}\ )\ -\ \sqrt{\frac{v^2}{1+v^2}}\ +\ C\ \right]$$

$$= 2\ r_0^3\ \left[\ \sqrt{u}\ +\ ln(\ \sqrt{1+u}\ )\ -\ \sqrt{\frac{u}{1+u}}\ +\ C\ \right]$$

Hence,

$$b(r) = 2\ r_0^3 \left[\ \left(\frac{r}{r_0}\right)^2 + ln\left(\sqrt{1+\left(\frac{r}{r_0}\right)^2}\right)\right]$$

$$-2\ r_0^3 \left[\ \sqrt{\frac{\left(\frac{r}{r_0}\right)^2}{1+\left(\frac{r}{r_0}\right)^2}}\ +\ C\ \right] \tag{3.72}$$

Now, using the boundary condition: $b(r_0) = r_0$, we get,

$$r_0 =\ 2r_0^3\ \left[\ ln(1+\sqrt{2})\ -\ \left(\frac{1}{\sqrt{2}}\right)\ +\ C\ \right]$$

Hence,

$$\boldsymbol{C = \left(\ \frac{1}{2\ r_0^2}\ \right)\ -\ 0.174} \tag{3.73}$$

In Figure: 3.33, similar to the nature of Figure:25, $b(r)$ increases rapidly, suggesting a non-asymptotically flat spacetime. Here, $b(r) >> r$, so asymptotic flatness is violated. This suggests the presence of a wormhole in a dynamic and curved universe (like cosmological spacetime, which is expanding). Figure: 3.34,shows that $\frac{b(r)}{r} > 1$ hence a wormhole will not exist in this case. In Figure: 3.35,the flare-out condition $b'(r_0) < 1$ is satisfied, so a wormhole may exist. In Figure: 3.36, NEC is violated ,i.e, $\rho + p_r < 0$ at the throat of the wormhole.

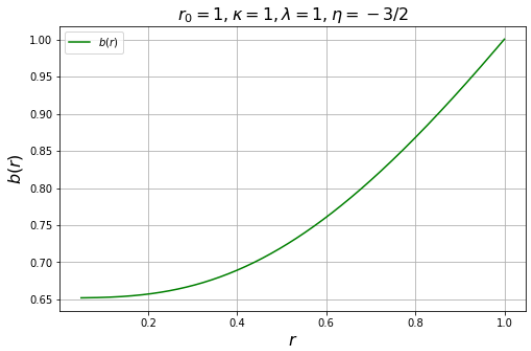

Figure 3.33: $b(r)$ versus r plot

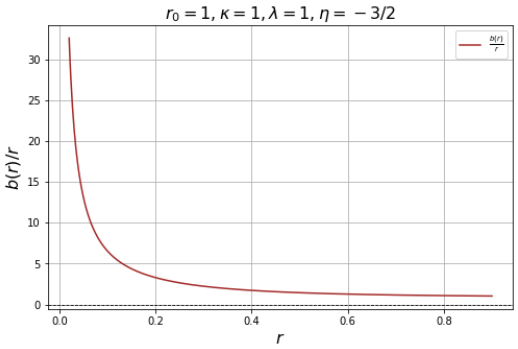

Figure 3.34: $\frac{b(r)}{r}$ versus r plot

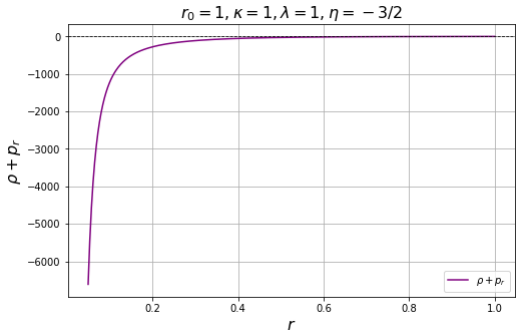

Figure 3.35: NEC Violation

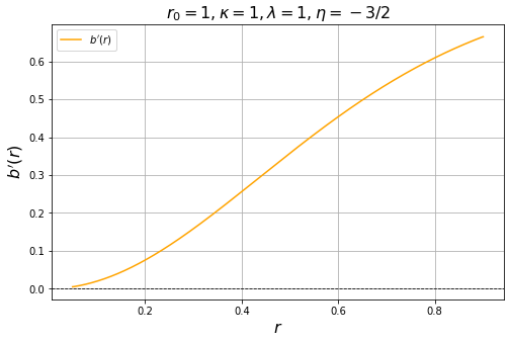

Figure 3.36: $b'(r)$ versus r plot

3.5 Universal Rotation Curve Density Profile

The URC profile models the mass distribution in spiral galaxies by fitting observed galactic rotation curves. It combines contributions from both dark matter and baryons, typically using empirical fits to match a wide range of galaxy types, especially in low-luminosity galaxies. The density profile for the dark matter distribution [45] is as follows:

$$\rho(r) = \frac{\rho_0 r^3}{(r + r_0)(r^2 + r_0^2)} \tag{3.74}$$

We know that,

$$\rho_r = -\frac{b'(r)}{r^3}$$

$$\Rightarrow b(r) = \int 8\pi r^2 \rho_r dr$$

$$= \int 8\pi r^2 \left[\frac{\rho_0 r^3}{(r + r_0)(r^2 + r_0^2)}\right] dr$$

$$= 8\pi\rho r_0^3 \int \left[\frac{r^2}{(r + r_0)(r^2 + r_0^2)}\right] dr \tag{3.75}$$

Using partial fraction decomposition, we have,

$$\left[\frac{r^2}{(r + r_0)(r^2 + r_0^2)}\right] = \frac{A}{(r + r_0)} + \frac{Br + C}{(r^2 + r_0^2)} \tag{3.76}$$

$$\Rightarrow r^2 = A(r^2 + r_0^2) + (Br + C)(r + r_0)$$

$$\Rightarrow r^2 = Ar^2 + Ar_0^2 + Br^2 + Brr_0 + Cr + Cr_0$$

$$\Rightarrow r^2 = r^2(A + B) + r(Br_0 + C) + r_0(Ar_0 + C)$$

By comparing both sides, we get,

$$A + B = 1 \quad \Rightarrow \quad B = 1 - A \tag{3.77}$$

$$Br_0 + C = 0$$

$$\Rightarrow \quad C = -Br_0 \tag{3.78}$$

$$\Rightarrow \quad C = -(1 - A)r_0 \tag{3.79}$$

$$Ar_0 + C = 0$$

$$\Rightarrow \quad C = -Ar_0 \tag{3.80}$$

Now, by equating the two values of C with respect to A and B, we obtain,

$$Ar_0 = Br_0 \quad \Rightarrow \quad A = 1 - A \quad \Rightarrow \quad A = \frac{1}{2}$$

By putting the value of A in the relation: $B = 1 - A$. we get,

$$B = \left(1 - \frac{1}{2}\right) \quad \Rightarrow \quad B = \frac{1}{2}$$

By substituting the value of A in the relation $\quad C = -Ar_0$, we get,

$$C = -\left(\frac{r_0}{2}\right)$$

Therefore, by substituting the values of A, B and C in equation (3.74), we have,

$$\int \left(\frac{r^2}{(r + r_0)(r^2 + r_0^2)}\right) dr = \int \left[\frac{\left(\frac{1}{2}\right)}{(r + r_0)} + \left(\frac{\left(\frac{r}{2} + \left(\frac{-r_0}{2}\right)\right)}{r^2 + r_0^2}\right)\right] dr$$

$$= \frac{1}{2}\left[\int \frac{dr}{(r + r_0)} + \int \left(\frac{r - r_0}{r^2 + r_0^2}\right) dr\right]$$

$$= \frac{1}{2}\left[\int \frac{dr}{(r+r_0)} + \int \left(\frac{r}{r^2+r_0^2}\right) + \frac{r_0}{2}\int \frac{dr}{(r^2+r_0^2)}\right]$$

$$\text{Let,} \quad u = (r+r_0)$$

By differentiating both sides with respect to r, we get,

$$du = dr$$

$$\text{Also let, } v = (r^2+r_0^2)$$

Again, by differentiating both sides with respect to r, we get,

$$dv = 2rdr \quad \Rightarrow \quad \frac{dv}{2} = rdr$$

Hence,

$$\int \left(\frac{r^2}{(r+r_0)(r^2+r_0^2)}\right) dr \;=\; \frac{1}{2}\left[\int \frac{du}{u} + \int \frac{1}{2}\left(\frac{dv}{v}\right) - \frac{r_0}{2}\int \frac{dr}{(r^2+r_0^2)}\right]$$

$$= \frac{ln(u)}{2} + \frac{ln(v)}{4} - \frac{1}{2}\tan^{-1}\left(\frac{r}{r_0}\right) + C_1 \quad \left[Since, \int \frac{1}{a^2+x^2} = \frac{1}{a}tan^{-1}\left(\frac{x}{a}\right)\right]$$

$$= \frac{1}{2}\, ln(r+r_0) + \frac{1}{4}\, ln(r^2+r_0^2) - \left(\frac{1}{2}\right)\tan^{-1}\left(\frac{r}{r_0}\right) + C_1 \qquad (3.81)$$

Finally, we have,

$$\boldsymbol{b(r) = 4\pi\rho_0 r_0^3\left[ln(r+r_0) + \frac{ln(r^2+r_0^2)}{2} - \tan^{-1}\left(\frac{r}{r_0}\right) + C\right]} \qquad (3.82)$$

Using the boundary condition $b(r_0) = r_0$, we get,

$$r_0 = 4\pi\rho_0 r_0^3\left[ln(2r_0) + \frac{1}{2}\, ln(2r_0^2) - \tan^{-1}(1) + C\right]$$

$$\Rightarrow \; r_0 = 4\pi\rho_0 r_0^3\left[ln(2) + ln(r_0) + \frac{ln(2) + 2ln(r_0)}{2} - \tan^{-1}\left(tan\frac{\pi}{4}\right) + C\right]$$

$$\Rightarrow \frac{1}{4\pi\rho_0 r_0^2} = ln(2) + \frac{1}{2}\, ln(2) + 2ln(r_0) - \frac{\pi}{4} + C$$

$$\Rightarrow C = \frac{1}{4\pi\rho_0 r_0^2} - \frac{3}{2}ln(2) - 2ln(r_0) + \frac{\pi}{4}$$

$$\boldsymbol{\Rightarrow C = \frac{1}{4\pi\rho_0 r_0^2} - 2\, ln(r_0) - 0.254} \tag{3.83}$$

Figure: 3.37 shows that $b(r)$ is positive and increases with an increase in r. It begins with a positive value and then rises monotonically. As we can see in Figure: 3.38, $b'(r)$ is positive and relatively small; thus, it satisfies the flare-out condition $b'(r) < 1$ at the throat $r = r_0$.

In Figure: 3.39 we observe that ρ is negative everywhere; thus, we can say that exotic matter is present. Figure: 3.40 shows that at the throat, $\rho + p_r$ has a large negative value. From this we can infer that the concentration of the exotic matter is higher at the throat, i.e., it ensures that the wormhole does not collapse. As r increases, both ρ and $\rho + p_r$ approach zero, i.e., the spacetime becomes asymptotically flat.

In Figure: 3.41 we can clearly see that $b(r) - r$ is negative, confirming the flare-out condition: $b(r) < r$ which ensures that the wormhole is traversable.

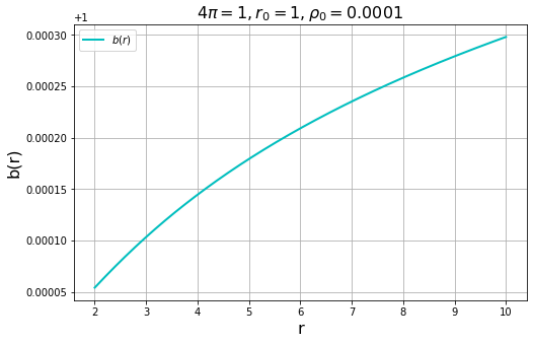

Figure 3.37: $b(r)$ versus r plot

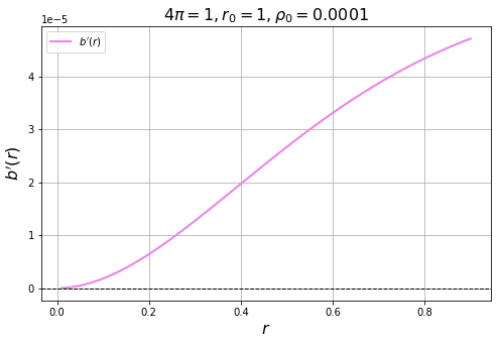

Figure 3.38: $b'(r)$ versus r plot

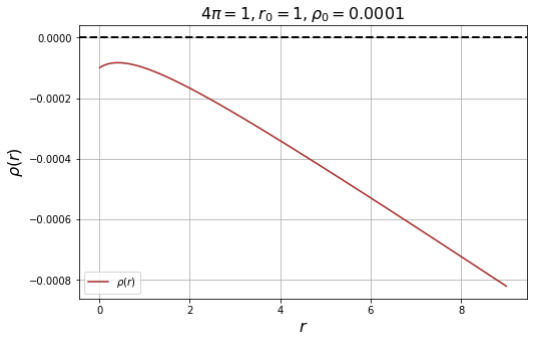

Figure 3.39: $\rho(r)$ versus r plot

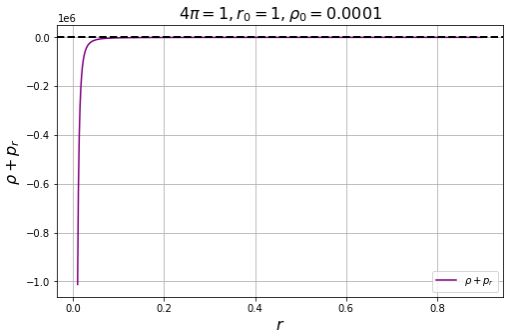

Figure 3.40: NEC violation

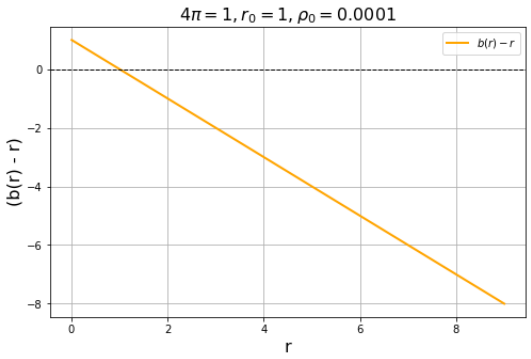

Figure 3.41: $(b(r) - r)$ versus r plot

3.6 Stability Analysis

3.6.1 Tolman-Oppenheimer-Volkoff Balance Condition:

A wormhole is stable if the force due to gravity, pressure gradient, and anisotropic stresses balance each other [33]:

$$\boldsymbol{F_g + F_h + F_a = 0} \tag{3.84}$$

where,

Gravitational force, $F_g = -(\rho + p_r)\Phi'(r)$

Hydrostatic force, $F_h = -\frac{dp_r}{dr}$

Anisotropic force, $F_a = -\frac{2}{r}(p_r - p_t)$

Here,

$\Phi(r) \rightarrow$ Redshift function

$\rho \rightarrow$ Energy density

$p_r \rightarrow$ Radial pressure

$p_t \rightarrow$ Tangential pressure

3.6.2 Test for Einstein Gravity

In the Einstein gravity, we have denoted the redshift function as $f(r)$.

Now, from equations (3.28), (3.28),(3.29), and (3.30), we know that,

$$\rho = -\frac{b'(r)}{8\pi r^2}$$

$$p_r = \frac{1}{8\pi}\left[\frac{-b(r)}{r^3} + 2\left(1 - \frac{b(r)}{r}\frac{f'(r)}{r}\right)\right]$$

$$p_t = \frac{1}{8\pi}\left(1 - \frac{b(r)}{r}\right)\left[f''(r) + f'(r)^2 + \left(\frac{f'(r)}{r}\right)\right]$$
$$- \left(1 - \frac{b(r)}{r}\right)\left(\frac{1}{r} + f'(r)\right)\left(\frac{rb'(r) - b(r)}{2r(r - b(r))}\right)$$

On large scales, $e^{2f(r)} = B_0 r^{(4v^\phi)}$. If v^ϕ tends to a constant value (flat rotation curve), then $2f(r) \sim ln(r)$, and $f'(r) \sim \frac{1}{r}$, which also tends to 0 as $r \to \infty$. So, we get, (also taking $8\pi = 1$)

$$\rho = -\frac{b'(r)}{r^2} \tag{3.85}$$

$$p_r = \frac{-b(r)}{r^3} \tag{3.86}$$

$$p_t = -\left(\frac{rb'(r) - b(r)}{2r^3}\right) \tag{3.87}$$

So, we have,

$$\boldsymbol{F_g = -(\rho + p_r) f'(r) = 0} \tag{3.88}$$

Then,

$$F_h = -\frac{dp_r}{dr}$$

$$= -\frac{d}{dr}\left[\frac{-b(r)}{r^3}\right]$$

$$= \left[\frac{r^3 b'(r) - b(r).3r^2}{(r^3)^2}\right]$$

$$\Rightarrow \quad \boldsymbol{F_h = \left(\frac{rb'(r) - 3b(r)}{r^4}\right)} \tag{3.89}$$

And,

$$F_a = -\frac{2}{r}(p_r - p_t)$$

$$= -\frac{2}{r}\left[\frac{-b(r)}{r^3} + \left(\frac{rb'(r) - b(r)}{2r^3}\right)\right]$$

$$= -\frac{2}{r^4}\left[\frac{-2b(r) + rb'(r) - b(r)}{2}\right]$$

$$\Rightarrow \quad \boldsymbol{F_a = -\left(\frac{rb'(r) - 3b(r)}{r^4}\right) = -F_h} \tag{3.90}$$

Therefore, we get,

$$F_g + F_h + F_a = (\ 0 + F_h - F_h\ ) = 0$$

Hence, the equilibrium condition is satisfied; thus, the wormhole is stable.

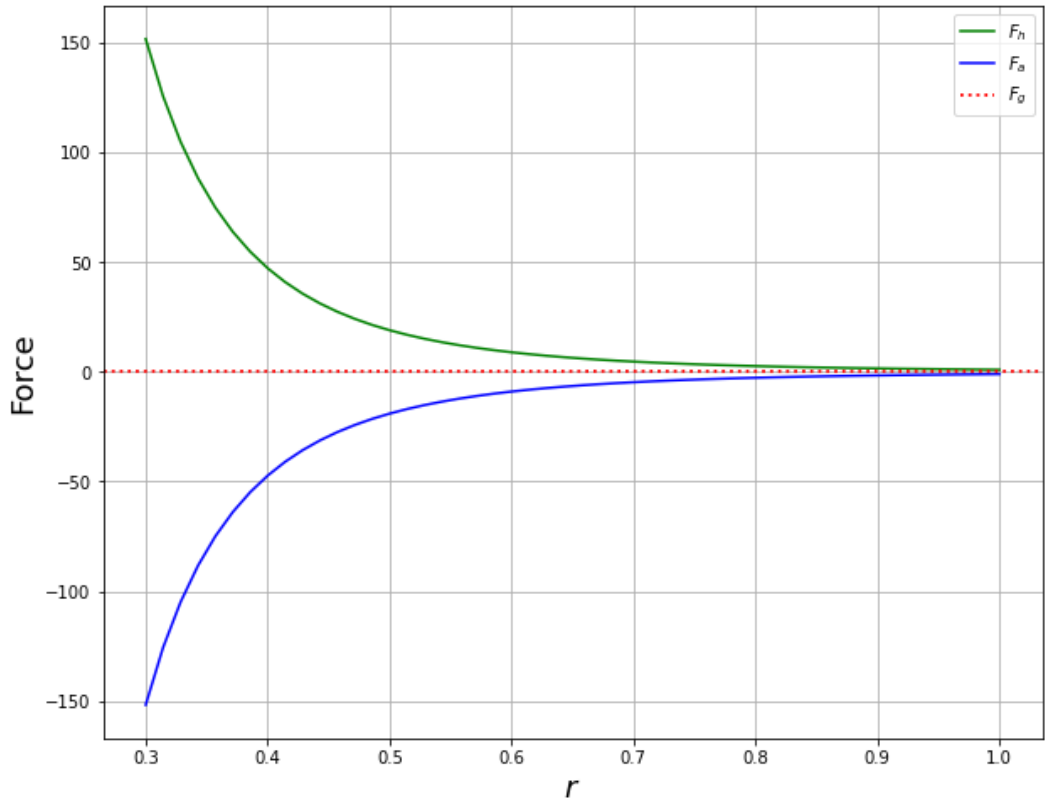

Figure 3.42: A plot showing the behaviour of the three forces in the TOV equilibrium condition against r

In the Figure: 3.42, the hydrostatic force F_h (represented by the green line) begins with a positive large value for small r and then rapidly decreases as the value of r increases. From this we can conclude that, at the throat of the wormhole, F_h is strong. But it decreases and eventually diminishes (approaching zero) as we move away from the throat.

In contrast to the nature of F_h, the anisotropic force F_a (represented by the blue line) begins at a large negative value at small r, and then increases with an increase in r, eventually approaching zero. From this behaviour, we can observe that F_a initially it contracts at the throat and then becomes less significant as we move away from the throat.

We had considered while solving the TOV equations that $f'(r) \sim \frac{1}{r}$, i.e., $f'(r) \to 0$ as $r \to \infty$. Therefore, the value of the gravitational force F_g (represented by the red dotted line) is too small, as shown in the graph.

Chapter 4

Formation of wormholes in UDGs by $f(R)$ gravity

The Einstein field equations for the general theory of relativity can be derived from the Hilbert-Einstein action principle:

$$S = \frac{1}{2\kappa} \int \sqrt{-g}\ R\ d^4x \tag{4.1}$$

where,

$g = det(g_{\mu\nu}) \rightarrow$ Determinant of the metric tensor $(g_{\mu\nu})$

$R \rightarrow$ Ricci scalar

$\kappa = \frac{8\pi G}{c^4} \rightarrow$ Einstein gravitational constant

The Ricci scalar R of general relativity is replaced by $f(R)$ in the $f(R)$ gravity.

Now, the Hilbert-Einstein action principle for $f(R)$ gravity is given as follows:

$$S = \frac{1}{2\kappa} \int \sqrt{-g}\ \ f(R)\ d^4x + S_M(g^{\mu\nu}, \psi) \tag{4.2}$$

where,

$g = det(g_{\mu\nu}) \rightarrow$ Determinant of the metric tensor $(g_{\mu\nu})$

$\kappa = \frac{8\pi G}{c^4} \rightarrow$ Einstein gravitational constant

$S_M(g^{\mu\nu}, \psi) = \int \sqrt{-g}\ \mathcal{L}_m(g_{\mu\nu}, \psi)\ d^4x$

here,

$S_M \rightarrow$ Matter action

$\mathcal{L}_m \rightarrow$Lagrangian density of the matter

$\psi \rightarrow$ Matter field

The Einstein field equation for general relativity:

$$R_{\mu\nu} - \frac{1}{2}Rg_{\mu\nu} + \Lambda g_{\mu\nu} = \left(\ \frac{8\pi G}{c^4}\ \right) T_{\mu\nu} \tag{4.3}$$

The Einstein field equation for $f(R)$ gravity :

$$FR_{\mu\nu} - \frac{1}{2}f(R)g_{\mu\nu} - \nabla_\mu\nabla_\nu F + g_{\mu\nu}\Box F = T^m_{\mu\nu} \tag{4.4}$$

where,

$F = \frac{df(R)}{dR}$

$R_{\mu\nu} \rightarrow$Ricci curvature tensor

$g_{\mu\nu} \rightarrow$ Metric tensor

∇_μ and $\nabla_\nu \rightarrow$ Covariant derivative

$\Box F = \ \nabla^\mu\nabla_\mu\ = \frac{1}{\sqrt{-g}}\ \partial_\mu(\sqrt{-g}\ \ g^{\mu\nu}\ \ \partial_\nu\ F)$

$T^m_{\mu\nu} \rightarrow$ Energy momentum tensor for matter fields in $f(R)$ gravity

The Einstein field equation for $f(R)$ gravity can be further reduced as follows:

$$FR - 2f(R) + 3\Box F = T \tag{4.5}$$

where,

$T = T^\mu_\mu$, is the trace of stress-energy tensor

We take the Morris-Thorne metric for traversable wormhole geometry

$$ds^2 = -e^{2\Phi(r)}dt^2 + \left(1 - \frac{b(r)}{r}\right)^{-1} dr^2 + r^2(d\theta^2 + \sin^2\theta d\phi^2)) \tag{4.6}$$

where,

$\Phi(r)$: redshift function, it must be finite to avoid an event horizon.

$b(r)$: shape function that determines the geometry of the wormhole
r : Radial coordinate

Here, r is non-monotonic, i.e., it decreases from ∞ to r_0 , where r_0 : throat of the wormhole [$b(r_0) = r_0$].

$\Phi(r)$ is finite everywhere. This prevents event horizon. Thus, $\Phi(r) \equiv 0$, which implies that $\Phi'(r) \equiv 0$. By further simplifying the above equation, we have,

$$G_{\mu\nu} \equiv R_{\mu\nu} - \frac{1}{2} R g_{\mu\nu} \;=\; T_{\mu\nu}^{eff} \tag{4.7}$$

where,

$$T_{\mu\nu}^{eff} = T_{\mu\nu}^{c_1} + T_{\mu\nu}^{c_2} \tag{4.8}$$

$$T_{\mu\nu}^{c_1} = \frac{1}{F}\left[\; \nabla_\mu \nabla_\nu F \;\; - \;\; \frac{1}{4} g_{\mu\nu}\; (RF + \Box F + T)\right] \tag{4.9}$$

$$T_{\mu\nu}^{c_2} = \left(\; \frac{T_{\mu\nu}^{m}}{F} \;\right) \tag{4.10}$$

Also, $\nabla^\mu G_{\mu\nu} = 0$ (Bianchi identity)

Thus, $\nabla^\mu T_{\mu\nu}^{m} = 0$ (Using field equations)

Hence, we get the following law of conservation:

$$\nabla^\mu T_{\mu\nu}^{c} = \left(\frac{1}{F^2}\right)\; T_{\mu\nu}^{m}\; \nabla^\mu F \tag{4.11}$$

For an isotropic matter distribution,

$$T_{\mu\nu} = (\rho + p_t) U_\mu U_\nu \;+\; p_t\; g_{\mu\nu} \;+\; (p_r - p_t) X_\mu X_\nu \tag{4.12}$$

where,

$\rho(r) \rightarrow$ Energy density

$p_t(r) \rightarrow$ Transverse pressure (measured orthogonal to X^μ direction)

$p_r(r) \rightarrow$ Radial pressure (measured in the X^μ direction)

$U_\mu \rightarrow$ Fourth velocity

$X^\mu \rightarrow$ Unit space-like vector in the radial direction

$$T_{\mu\nu} = \begin{bmatrix} -\rho(r) & 0 & 0 & 0 \\ 0 & p_r(r) & 0 & 0 \\ 0 & 0 & p_t(r) & 0 \\ 0 & 0 & 0 & p_t(r) \end{bmatrix} \tag{4.13}$$

Thus, we obtain,

$$\frac{b'(r)}{r^2} = \frac{\rho}{F} + \frac{H}{F}$$

$$\Rightarrow \rho + H = F\left(\frac{b'(r)}{r^2}\right)$$

$$\Rightarrow \rho = F\left(\frac{b'(r)}{r^2}\right) - H \tag{4.14}$$

And,

$$-\frac{b(r)}{r^3} = \frac{p_r}{F} + \frac{1}{F}\left[\left(1 - \frac{b(r)}{r}\right)\left(F'' - F'\left(\frac{rb'(r) - b(r)}{2r^2\left(1 - \frac{b(r)}{r}\right)}\right)\right) - H\right]$$

$$\Rightarrow p_r = F\left(\frac{b(r)}{r^3}\right) - \left(1 - \frac{b(r)}{r}\right)\left[F'' - F'\left(\frac{rb'(r) - b(r)}{2r^2\left(1 - \frac{b(r)}{r}\right)}\right)\right] + H \tag{4.15}$$

Also,

$$\left(\frac{-b'(r) - b(r)}{2r^3}\right) = \frac{p_t}{F} + \frac{1}{F}\left[\frac{F'}{r}\left(1 - \frac{b(r)}{r}\right) - H\right]$$

$$\Rightarrow p_t = F\left(\frac{b'(r)+b(r)}{2r^3}\right) - \frac{F'}{r}\left(1-\frac{b(r)}{r}\right) + H \tag{4.16}$$

Here,

$$H = H(r) = \frac{1}{4}(FR + \Box F + T) \tag{4.17}$$

where,

$$R = \frac{2b'(r)}{r^2} \tag{4.18}$$

$$\Box F = \left(1-\frac{b(r)}{r}\right)\left[F'' - F'\left(\frac{rb'(r)-b(r)}{2r^2\left(1-\frac{b(r)}{r}\right)}\right) + \frac{2F'}{r}\right] \tag{4.19}$$

Now, by reorganizing and simplifying, we obtain

$$\boldsymbol{\rho = F\left(\frac{b'(r)}{r^2}\right)} \tag{4.20}$$

$$\boldsymbol{p_r = -F\left(\frac{b(r)}{r^3}\right) + F'\left(\frac{b'(r)-b(r)}{2r^2}\right) - F''\left(1-\frac{b(r)}{r}\right)} \tag{4.21}$$

$$\boldsymbol{p_t = -\frac{F'}{r}\left(1-\frac{b(r)}{r}\right) + F\left(\frac{b(r)-b'(r)}{2r^3}\right)} \tag{4.22}$$

Here, we have taken,

$$\boldsymbol{f(R) = \alpha R^2} \tag{4.23}$$

We know,

$$F = \frac{d}{dR}(\ f(R)\ ) = \frac{d}{dR}(\alpha R^2) = 2\alpha R \quad \text{, where, } R = \frac{2b'(r)}{r^2} \tag{4.24}$$

By differentiating both sides with respect to R, we have,

$$\boldsymbol{F' = 2\alpha} = \text{constant} \tag{4.25}$$

Again, by differentiating both sides with respect to R, we get,

$$\boldsymbol{F'' = 0} \tag{4.26}$$

Thus, we can write,

$$\boldsymbol{F = 2\alpha R = 4\alpha \left(\frac{b'(r)}{r^2}\right)} \qquad \text{where, } \boldsymbol{R = \frac{2b'(r)}{r^2}} \tag{4.27}$$

4.1 Navarro-Frank-White(NFW) Density Profile

$$\rho(r) = \frac{\rho_0}{r^{\gamma}\left(1+\frac{r}{r_0}\right)^{3-\gamma}} \tag{4.28}$$

where,

$\rho(r) \rightarrow$ represents the dark matter density at a radius r

$\gamma \rightarrow$ inner slope of the profile

$r_0 \rightarrow$ scale radius

CASE-1: $\gamma = 1$

$$\rho(r) = \frac{\rho_0}{r\left(1+\frac{r}{r_0}\right)^{2}} \tag{4.29}$$

Now, we know,

$$b'(r) = \left(\frac{r^2}{2}\right)\sqrt{\frac{\rho}{\alpha}}$$

$$\Rightarrow b'(r) = \left(\frac{1}{2\sqrt{\alpha}}\right) r^2 \sqrt{\frac{\rho_0}{r\left(1+\frac{r}{r_0}\right)^{2}}}$$

$$\Rightarrow b(r) = \frac{1}{2}\sqrt{\frac{\rho_0}{\alpha}} \quad \int r^2 \sqrt{\frac{1}{r\left(1+\frac{r}{r_0}\right)^{2}}}\ dr$$

$$\text{Let, } \; u = \left(1 + \frac{r}{r_0}\right)$$

By differentiating both sides with respect to r, we get,

$$du = \left(\frac{1}{r_0}\right) dr$$

Also, using the substitution, we can write,

$$u = \left(\frac{r + r_0}{r_0}\right) \quad \Rightarrow \; u\, r_0 = r + r_0 \quad \Rightarrow \; r = r_0(u-1)$$

Therefore,

$$b(r) = \frac{1}{2}\sqrt{\frac{\rho_0}{\alpha}} \quad \int \left[r_0^3 (u-1)^2 \sqrt{\frac{1}{u^2\, r_0(u-1)}} \; \right] \quad du$$

$$b(r) = \frac{r_0^3}{2}\sqrt{\frac{\rho_0}{\alpha r_0}} \quad \int \left(\frac{(u-1)^2}{u\sqrt{u-1}} \right) \, du$$

$$\text{Let, } \; v^2 = u - 1$$

By differentiating both sides with respect to r, we get,

$$vdv = du$$

Also, using the substitution, we can write,

$$u = v^2 + 1$$

Hence,

$$b(r) = r_0^3 \sqrt{\frac{\rho_0}{\alpha r_0}} \quad \int \left(\frac{v^4}{v^2+1} \right) \, dv$$

$$= r_0^3\sqrt{\frac{\rho_0}{\alpha r_0}} \quad \int \left(\frac{(v^4-1)+1}{v^2+1}\right)\, dv$$

$$= r_0^3\sqrt{\frac{\rho_0}{\alpha r_0}} \quad \int \left(\frac{(v^2+1)(v^2-1)+1}{v^2+1}\right)\, dv$$

$$= r_0^3\sqrt{\frac{\rho_0}{\alpha r_0}} \quad \left[\, \int (v^2-1)\, dv + \int \frac{dv}{(v^2+1)} \,\right]$$

$$= r_0^3\sqrt{\frac{\rho_0}{\alpha r_0}} \quad \left[\, \int v^2\, dv - \int dv \; + \int \frac{dv}{(v^2+1)} \,\right]$$

$$= r_0^3\sqrt{\frac{\rho_0}{\alpha r_0}} \quad \left[\, \frac{v^3}{3} - v \; + tan^{-1}(v) \; + C \,\right]$$

$$= r_0^3\sqrt{\frac{\rho_0}{\alpha r_0}} \quad \left[\, \frac{(u-1)^3}{3} - \sqrt{u-1} \; + tan^{-1}(\sqrt{u-1}) \; + C \,\right]$$

Therefore,

$$\boldsymbol{b(r) = r_0^3\sqrt{\frac{\rho_0}{\alpha r_0}} \quad \left[\, \left(\frac{r}{r_0}\right)^{\frac{3}{2}} - \sqrt{\frac{r}{r_0}} \; + tan^{-1}\left(\sqrt{\frac{r}{r_0}}\right) \; + C \,\right]} \tag{4.30}$$

Now, applying the boundary condition: $b(r_0) = r_0$

$$r_0 = r_0^3\sqrt{\frac{\rho_0}{\alpha r_0}} \quad \left[\, \frac{1}{3} - 1 + tan^{-1}(1) + C \,\right]$$

$$\Rightarrow \sqrt{\frac{\alpha r_0}{\rho_0}}\left(\frac{1}{r_0^2}\right) = \left[\, -\frac{2}{3} + \frac{\pi}{4} + C \,\right]$$

Figure: 4.1 shows a steep negative slope near the origin, which indicates that the shape function $b(r)$ decreases rapidly in this region. $b'(r)$ starts with a rapid decrease for small negative r, then it gradually increases with a decreasing rate, eventually asymptotically

reaching zero for large r.

Figure: 4.2 indicates that the energy density is negative. Figure: 4.3 satisfies the violation of NEC, i.e., $\rho + p_r < 0$. In Figure: 4.4 we see that $b(r) - r$ decreases monotonically, and the curve appears to approach a horizontal asymptote as $r \to \infty$.

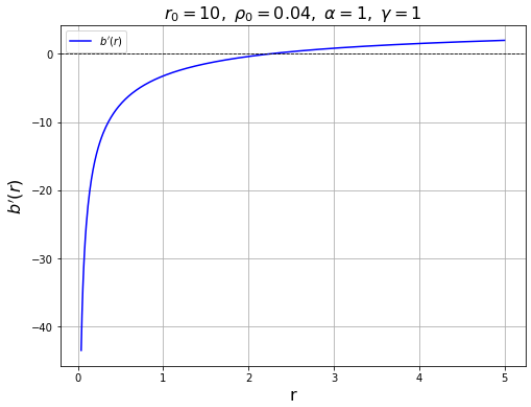

Figure 4.1: $b'(r)$ versus r plot

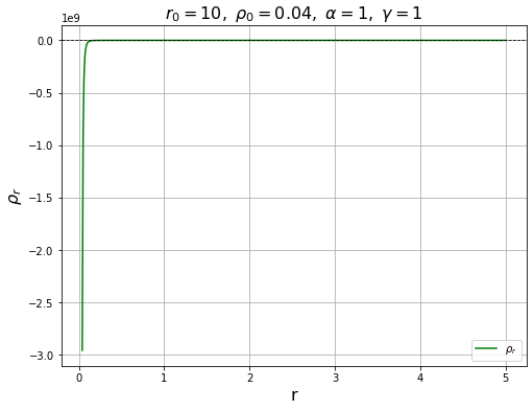

Figure 4.2: $\rho(r)$ versus r plot

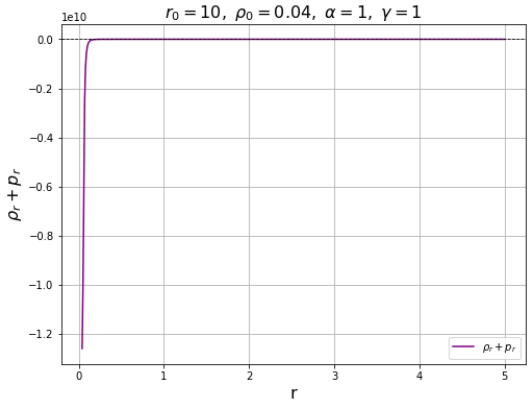

Figure 4.3: NEC Violation

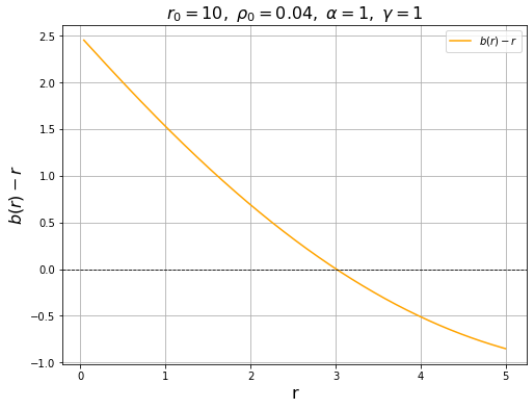

Figure 4.4: ($b(r) - r$) versus r plot

CASE-2: $\gamma = 2$

$$\rho(r) = \frac{\rho_0}{r^2\left(1+\frac{r}{r_0}\right)} \tag{4.31}$$

Now, we know,

$$b'(r) = \left(\frac{r^2}{2}\right)\sqrt{\frac{\rho}{\alpha}}$$

$$\Rightarrow b'(r) = \left(\frac{1}{2\sqrt{\alpha}}\right) r^2 \sqrt{\frac{\rho_0}{r^2\left(1+\frac{r}{r_0}\right)}}$$

$$\Rightarrow b(r) = \frac{1}{2}\sqrt{\frac{\rho_0}{\alpha}} \quad \int r\sqrt{\frac{1}{r\left(1+\frac{r}{r_0}\right)}}\ dr$$

$$\text{Let, } \ u = \left(1+\frac{r}{r_0}\right)$$

By differentiating both sides with respect to r, we get,

$$du = \left(\frac{1}{r_0}\right) dr$$

Also, using the substitution, we can write,

$$u = \left(\frac{r+r_0}{r_0}\right) \ \Rightarrow \ u\ r_0 = r + r_0 \ \Rightarrow \ r = r_0(u-1)$$

Therefore,

$$b(r) = \frac{1}{2}\sqrt{\frac{\rho_0}{\alpha}} \quad \int \left[r_0^2(u-1)\ \sqrt{\frac{1}{u}}\right] du$$

$$= \frac{r_0^2}{2}\sqrt{\frac{\rho_0}{\alpha}} \quad \int \left(\frac{u-1}{\sqrt{u}} \right) \quad du$$

$$= \frac{r_0^2}{2}\sqrt{\frac{\rho_0}{\alpha}} \quad \left[\int \sqrt{u}\, du - \int \frac{du}{\sqrt{u}} \right]$$

$$= \frac{r_0^2}{2}\sqrt{\frac{\rho_0}{\alpha}} \quad \left[\frac{2}{3}u^{(\frac{3}{2})} \; - \; 2\sqrt{u} \; + \; C \right]$$

Hence,

$$\boldsymbol{b(r) = \frac{r_0^2}{2}\sqrt{\frac{\rho_0}{\alpha}} \quad \left[\frac{2}{3}\left(1 + \frac{r}{r_0} \right)^{\frac{3}{2}} \; - \; 2\left(1 + \frac{r}{r_0} \right)^{\frac{1}{2}} \; + \; C \right]} \tag{4.32}$$

Using the boundary condition: $b(r_0) = r_0$, we obtain

$$r_0 = \frac{r_0^2}{2}\sqrt{\frac{\rho_0}{\alpha}} \quad \left[\frac{2}{3}(2)^{\frac{3}{2}} \; - \; 2\sqrt{2} \; + C \right]$$

$$\boldsymbol{\Rightarrow C = \frac{2}{r_0}\sqrt{\frac{\alpha}{\rho_0}} \; + \; 0.942} \tag{4.33}$$

In Figure: 4.5, the flare-out condition $b'(r) < 1$ is satisfied. Figure: 4.6 and Figure: 4.7 show similar behaviour as in CASE- 1, the graphs are just a little steeper than the previous ones. The NEC is violated,i.e., $\rho + p_r < 1$. In Figure: 4.8 the curve monotonically decreasing. It approaches a negative asymptote satisfying $b(r) < r$.

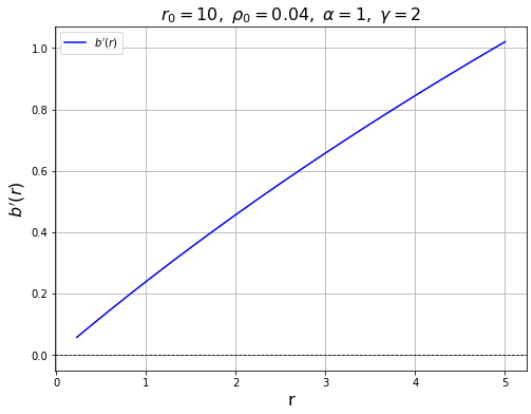

Figure 4.5: $b'(r)$ versus r plot

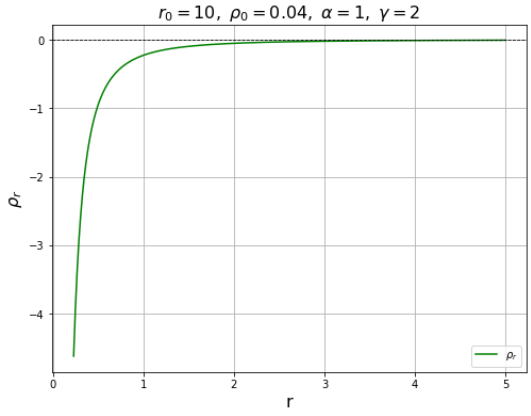

Figure 4.6: $\rho(r)$ versus r plot

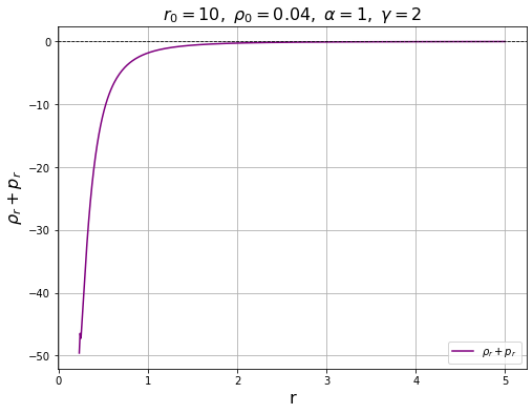

Figure 4.7: NEC Violation

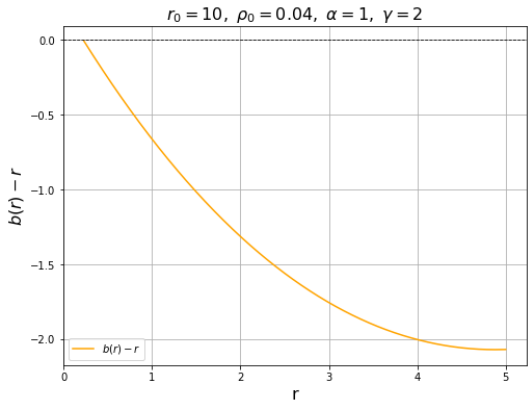

Figure 4.8: ($b(r) - r$) versus r plot

CASE-3: $\boldsymbol{\gamma = 3}$

$$\rho(r) = \frac{\rho_0}{r^2\left(1+\frac{r}{r_0}\right)} \tag{4.34}$$

Now, we know,

$$b'(r) = \left(\frac{r^2}{2}\right)\sqrt{\frac{\rho}{\alpha}}$$

$$\Rightarrow b'(r) = \left(\frac{1}{2\sqrt{\alpha}}\right) r^2 \sqrt{\frac{\rho_0}{r^3}}$$

$$\Rightarrow b(r) = \frac{1}{2}\sqrt{\frac{\rho_0}{\alpha}} \quad \int \sqrt{r} \;\; dr$$

Therefore,

$$\boldsymbol{b(r) = \frac{r}{3}\sqrt{\frac{\rho_0 r}{\alpha}} + C} \tag{4.35}$$

Using the boundary condition: $b(r_0) = r_0$, we get

$$r_0 = \frac{r_0}{3}\sqrt{\frac{\rho_0 r_0}{\alpha}} + C$$

$$\boldsymbol{\Rightarrow C = r_0\left(\,1 - \frac{1}{3}\sqrt{\frac{\rho_0 r_0}{\alpha}}\,\right)} \tag{4.36}$$

Figure: 4.9 shows a monotically increasing behaviour along with decreasing slope and approaches zero as $r \to \infty$. Figure: 4.10 and Figure: 4.11 show similar nature as previous cases, thus violating the NEC, i.e. $\rho + p_r < 1$. In Figure: 4.12, as $r \to 0$, $b(r) - r \approx 0$. The curve is non-monotonic, it initially decreases and then increases as we move away from the throat. Throughout the curve $b(r) < r$.

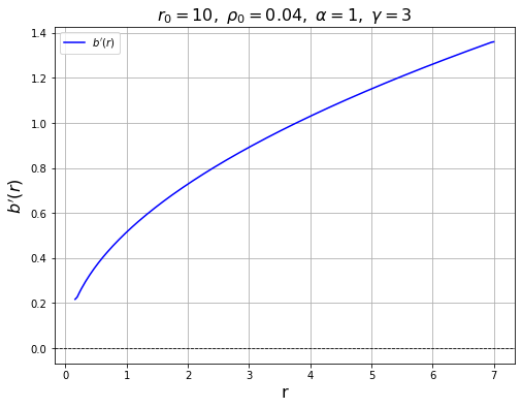

Figure 4.9: $b'(r)$ versus r plot

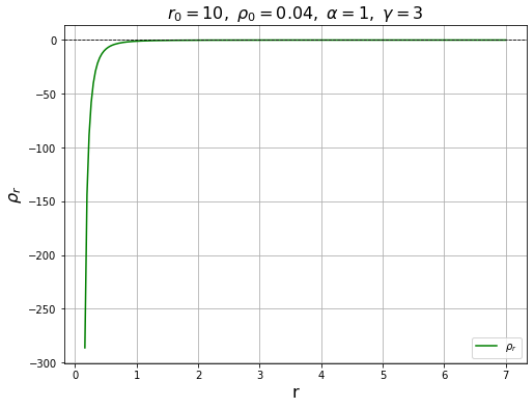

Figure 4.10: $\rho(r)$ versus r plot

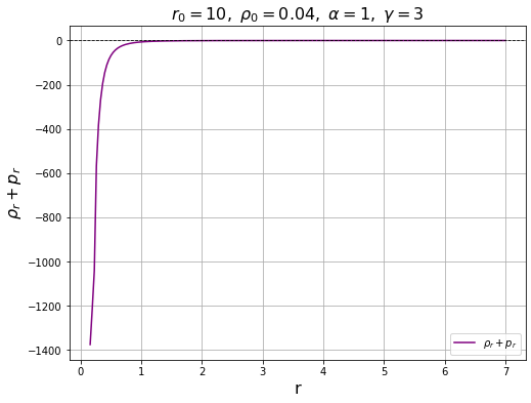

Figure 4.11: NEC Violation

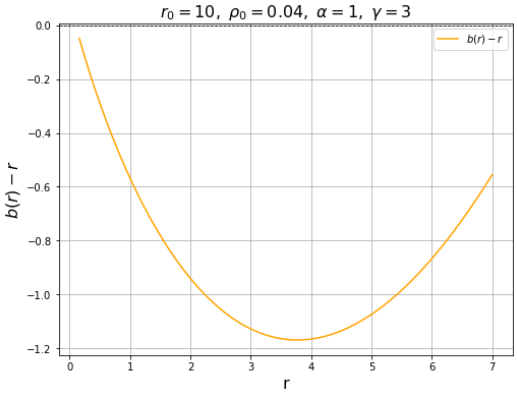

Figure 4.12: ($b(r) - r$) versus r plot

4.2 UDG King's Model

This model is tailored to describe the dark matter distribution in Ultra Diffuse Galaxies (UDGs). It uses a modified King density profile for dark matter distribution as follows: [14, 32]

$$\rho(r) = \kappa \left[\left(\frac{r}{r_0} \right)^2 + \lambda \right]^{\eta} \tag{4.37}$$

where, η, κ and λ are parameters

CASE-1 : $\boldsymbol{\kappa = 1,\ \lambda = 1}$ and $\boldsymbol{\eta = -\frac{1}{2}}$

$$\rho(r) = \left[\left(\frac{r}{r_0} \right)^2 + 1 \right]^{-\frac{1}{2}} \tag{4.38}$$

We know,

$$b'(r) = \left(\frac{r^2}{2} \right) \sqrt{\frac{\rho}{\alpha}}$$

$$\Rightarrow b(r) = \left(\frac{1}{2\sqrt{\alpha}} \right) r^2 \sqrt{\frac{1}{1 + \left(\frac{r}{r_0} \right)^2}} \ dr$$

$$\text{Let,} \quad u^2 = 1 + \left(\frac{r}{r_0} \right)^2$$

$$\Rightarrow 2u \ du = \left(\frac{2r}{r_0^2} \right) \ dr$$

$$\Rightarrow r_0^2 u \ du = r \ dr$$

Thus,

$$b(r) = \left(\frac{1}{2\sqrt{\alpha}}\right) \int (r_0\sqrt{u^2-1}) \left(\frac{1}{\sqrt{u}}\right) (r_0^2 u)\ du$$

$$= \left(\frac{r_0^3}{2\sqrt{\alpha}}\right) \int \sqrt{u(u^2-1)}\ \ du \qquad \text{[A standard class of elliptic integrals]}$$

$$= \left(\frac{r_0^3}{2\sqrt{\alpha}}\right) \left[\ \frac{1}{3}(2u^2-1)\sqrt{u(u^2-1)}\ +\ C\ \right] \qquad (\text{for } u > 1)$$

Hence,

$$b(r) = \left(\frac{r_0^3}{2\sqrt{\alpha}}\right) \left[\ \left(\frac{r}{r_0}\sqrt{1+\left(\frac{r}{r_0}\right)^2}\right) \left(\frac{2}{3}\left(1+\left(\frac{r}{r_0}\right)^2\right) - \frac{1}{3}\right) + C\ \right]$$

$$\boldsymbol{b(r) = \left(\frac{r_0^3}{2\sqrt{\alpha}}\right) \left[\frac{r}{r_0}\left(\frac{2}{3}\left[1+\left(\frac{r}{r_0}\right)^2\right]^{\frac{3}{2}} - \frac{1}{3}\sqrt{(1+\left(\frac{r}{r_0}\right)^2}\right) + C\right]} \tag{4.39}$$

By using the boundary condition: $b(r_0) = r_0$, we have,

$$r_0 = \left(\frac{r_0^3}{2\sqrt{\alpha}}\right) \left(\ \sqrt{2}\ +\ C\ \right)$$

$$\boldsymbol{\Rightarrow C = \frac{2}{r_0^2}\ -\ \sqrt{2}} \tag{4.40}$$

In Figure: 4.13 $b'(r)$ increases as r increases but here $b'(r) > 1$ thus the flare-out condition isn't satisfied. Figure: 4.14 shows that the energy density is negative everywhere, which indicates the presence of exotic matter. Figure: 4.15 shows the violation of NEC. Figure: 4.16 shows that $b(r) - r < 0$ and $b(r)$ increases as r increases.

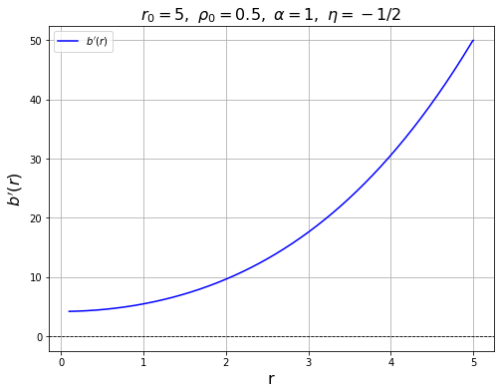

Figure 4.13: $b'(r)$ versus r plot

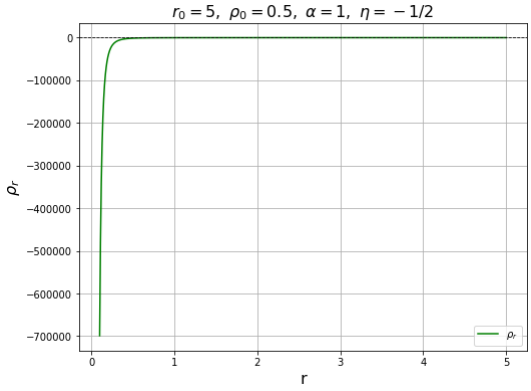

Figure 4.14: $\rho(r)$ versus r plot

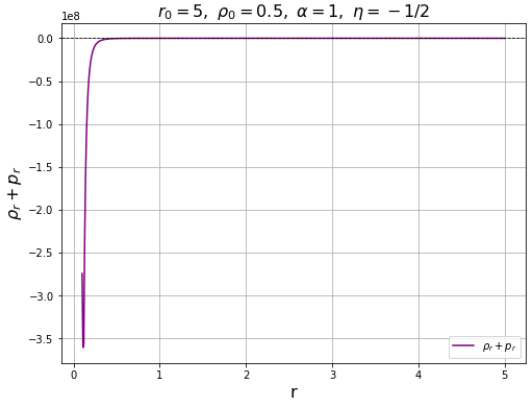

Figure 4.15: NEC Violation

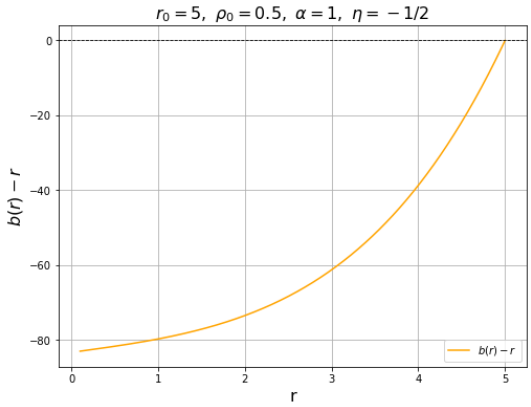

Figure 4.16: ($b(r) - r$) versus r plot

CASE-2 : $\kappa = 1,\ \lambda = 1$ and $\eta = -1$

$$\rho(r) = \frac{1}{1 + \left(\frac{r}{r_0}\right)^2} \tag{4.41}$$

We know,

$$b'(r) = \left(\frac{r^2}{2}\right)\sqrt{\frac{\rho}{\alpha}}$$

$$\Rightarrow b(r) = \left(\frac{1}{2\sqrt{\alpha}}\right) \int \left(\frac{r^2}{\sqrt{1 + \left(\frac{r}{r_0}\right)^2}}\right) dr$$

$$\text{Let, } u = \frac{r}{r_0}$$

By differentiating both sides with respect to r, we get,

$$du = \frac{1}{r_0} dr$$

Also, using the substitution, we can write,

$$u = \frac{r}{r_0} \quad \Rightarrow \quad r = u\, r_0$$

Thus, we have,

$$b(r) = \left(\frac{1}{2\sqrt{\alpha}}\right) \int u^2\ r_0^2\ (u^2+1)^{-\frac{1}{2}}\ \ r_0\ du$$

$$= r_0^3 \left(\frac{1}{2\sqrt{\alpha}}\right) \int \frac{u^2}{\sqrt{(u^2+1)}}\ du$$

$$= r_0^3 \left(\frac{1}{2\sqrt{\alpha}}\right) \int \frac{(u^2+1)-1}{\sqrt{(u^2+1)}}\ du$$

$$\Rightarrow \boldsymbol{b(r) = r_0^3 \left(\frac{1}{2\sqrt{\alpha}}\right) \left[\int \sqrt{(u^2+1)}\, du - \int \frac{du}{\sqrt{(u^2+1)}}\right]} \tag{4.42}$$

Now, we will solve the two integral terms in the expression $b(r)$ separately.

First term:

$$\int \sqrt{(u^2+1)}\, du$$

$$\text{Let, } u = sinh(t)$$

Now, by applying the sine inverse on both sides, we get,

$$t = sinh^{-1}(u)$$

$$\text{Also let, } \; du = cosh(t)\, dt$$

Therefore,

$$\int \sqrt{(u^2+1)}\, du = \int \sqrt{(sinh(t)^2+1)}\, cosh(t)\, dt$$

$$= \int \sqrt{(cosh(t))^2}\, cosh(t)\, dt \qquad [\text{ Since, } cosh^2(t) - sinh^2(t) = 1\ ]$$

$$= \int cosh^2(t) dt$$

$$= \frac{1}{2} \int [\ 1 + cosh(2t)\ ]\ dt$$

$$= \frac{1}{2} \left[\ \int dt + \int cosh(2t)\ dt\ \right]$$

$$= \frac{1}{2}\left[\ t + \frac{sinh(2t)}{2}\ \right]$$

$$= \frac{1}{2}\left[\ t + \frac{1}{2}(2\ sinh(t)\ cosh(t))\ \right] \quad [\ \text{Since,}\ \ sinh(2t) = 2\ sinh(t)\ cosh(t)\ ]$$

$$= \frac{1}{2}[\ t + sinh(t)\ cosh(t)\ ]$$

$$= \frac{1}{2}\left[\ sinh^{-1}(u) + u\sqrt{u^2+1})\ \right] \qquad \left[\ \text{Since, } cosh(t) = \sqrt{1 + sinh^2(t)}\ )\ \right]$$

$$= \frac{1}{2}ln(u+\sqrt{u^2+1}) + \frac{1}{2}(u\sqrt{u^2+1}) \quad \left[\ \text{Since,}\ \ sinh^{-1}(x) = ln(x + \sqrt{x^2+1})\right] \tag{4.43}$$

Second term:

$$\int \frac{du}{\sqrt{u^2+1}}$$

$$\text{Let, } u = tan\theta$$

By differentiating both sides with respect to θ, we get,

$$du\ =\ sec^2\theta\ d\theta$$

Also, we know that, $\quad (1 + tan^2\theta) =\ sec^2\theta \quad \Rightarrow \quad sec\theta =\ \sqrt{u^2+1}$

Thus,

$$\int \frac{du}{\sqrt{u^2+1}} = \int \frac{sec^2\theta}{\sqrt{tan^2\theta+1}}\ \ d\theta$$

$$= \int sec\theta\ \ d\theta \qquad [\text{Since, } (1 + tan^2\theta) =\ sec^2\theta]$$

$$=\ ln(\ sec\theta + tan\theta\ )$$

Hence,

$$\int \frac{du}{\sqrt{u^2+1}} \;=\; ln(\sqrt{1+u^2}+u) \qquad (4.44)$$

Now, by putting equations (4.43) and (4.44) in (4.42), we obtain,

$$b(r) = r_0^3\left(\frac{1}{2\sqrt{\alpha}}\right)\left[\;\frac{ln(u+\sqrt{u^2+1})}{2} \;+\frac{u\sqrt{u^2+1}}{2} -\; ln(\sqrt{1+u^2})+C_1\;\right]$$

$$= \left(\frac{r_0^3}{2}\right)\left(\frac{1}{2\sqrt{\alpha}}\right)\left[\;u\sqrt{u^2+1} -\; ln(u+\sqrt{1+u^2}) +\; C\;\right]$$

Thus, we finally get,

$$\boldsymbol{b(r) = \frac{r_0^3}{4\sqrt{\alpha}}\left[\left(\frac{r}{r_0}\right)\sqrt{1+\left(\frac{r}{r_0}\right)^2} - ln\left(\left(\frac{r}{r_0}\right)+\sqrt{1+\left(\frac{r}{r_0}\right)^2}\right)+C\right]} \qquad (4.45)$$

Using the boundary condition: $b(r_0) = r_0$,we have,

$$r_0 = \left(\frac{r_0^3}{4\sqrt{\alpha}}\right)\left[\;\sqrt{2}\;-\;ln\left(1+\sqrt{2}\right)\;+\;C\;\right]$$

$$\Rightarrow \boldsymbol{C = \frac{4\sqrt{\alpha}}{r_0^2}\;-\;\sqrt{2}\;+\;ln\left(1+\sqrt{2}\right)} \qquad (4.46)$$

Figure: 4.17 shows violation of the flare-out condition $b'(r) < 1$. In Figure: 4.18 we can see that ρ is negative everywhere. In Figure: 4.19, we observe that $\rho + p_r$ is initially positive and then becomes zero for $r = 7$ to $r = 12$ and then falls drastically, becoming negative. Figure: 4.20 doesn't satisfy the condition $b(r) - r < 0$.

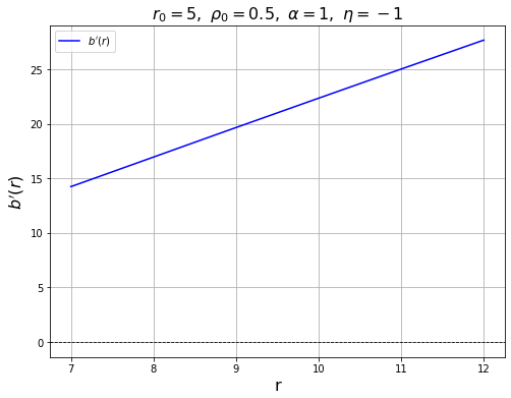

Figure 4.17: $b'(r)$ versus r plot

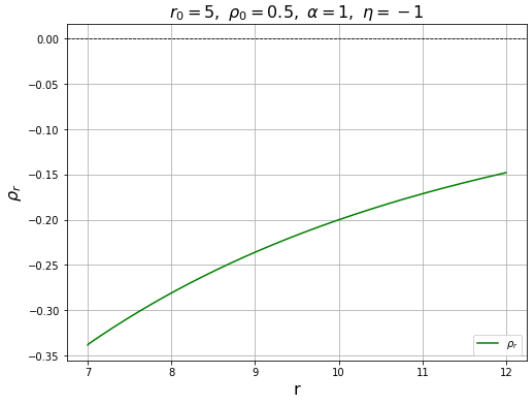

Figure 4.18: $\rho(r)$ versus r plot

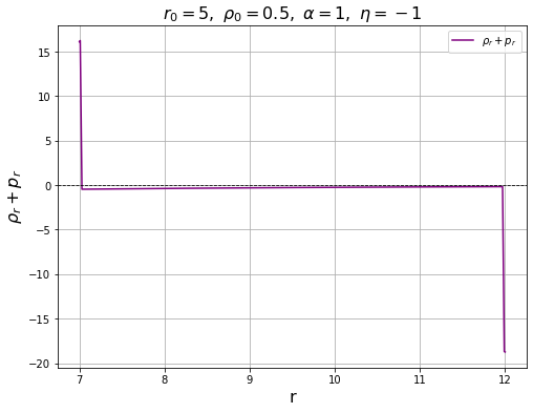

Figure 4.19: NEC Violation

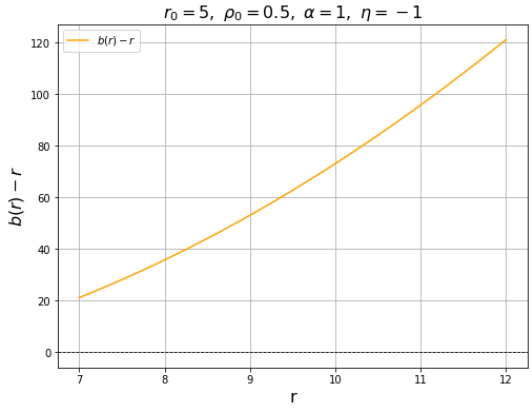

Figure 4.20: ($b(r) - r$) versus r plot

4.3 Universal Rotation Curve Density Profile

The density profile for the dark matter distribution is as follows:

$$\rho(r) = \frac{\rho_0 r^3}{(r + r_0)(r^2 + r_0^2)} \tag{4.47}$$

We know that,

$$b'(r) = \left(\frac{r^2}{2}\right)\sqrt{\frac{\rho}{\alpha}}$$

$$\Rightarrow b(r) = \left(\frac{1}{2\sqrt{\alpha}}\right) \int r^2 \sqrt{\frac{\rho_0 r^3}{(r + r_0)(r^2 + r_0^2)}}\ dr$$

$$\Rightarrow b(r) = \frac{r_0}{2}\sqrt{\frac{\rho_0 r_0}{\alpha}} \int \frac{r^2}{\sqrt{(r + r_0)(r^2 + r_0^2)}}\ dr$$

$$\text{Let, } u = r^2 + r_0^2$$

By differentiating both sides with respect to r, we get,

$$du = 2r\ dr$$

Also, using the substitution, we can write,

$$u = r^2 + r_0^2 \quad \Rightarrow \quad r = \sqrt{u - r_0}$$

Thus, we have,

$$\boldsymbol{b(r) = \frac{r_0}{4}\sqrt{\frac{\rho_0 r_0}{\alpha}} \int \frac{u - r_0}{\sqrt{u(\sqrt{u - r_0} + r_0)}}} + \text{constant} \tag{4.48}$$

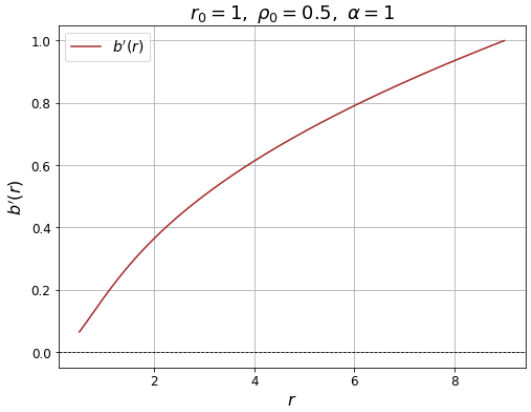

Figure 4.21: $b'(r)$ versus r plot

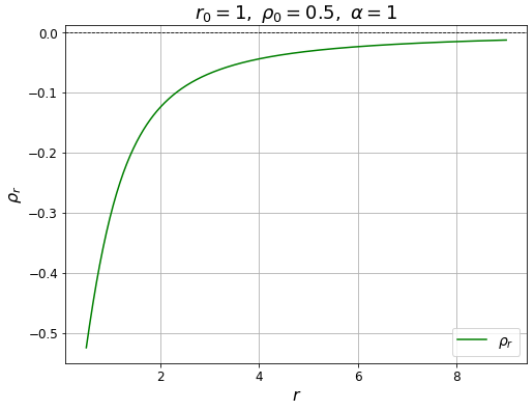

Figure 4.22: Energy density

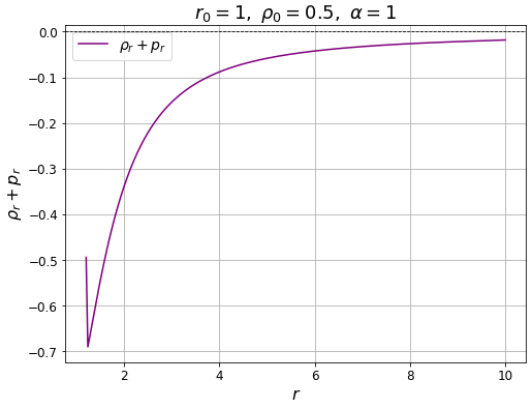

Figure 4.23: NEC Violation

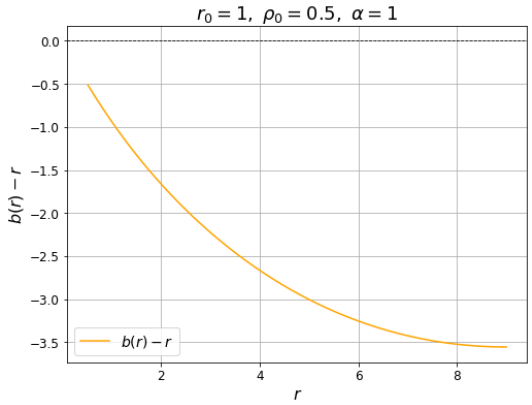

Figure 4.24: $(b(r) - r)$ versus r plot

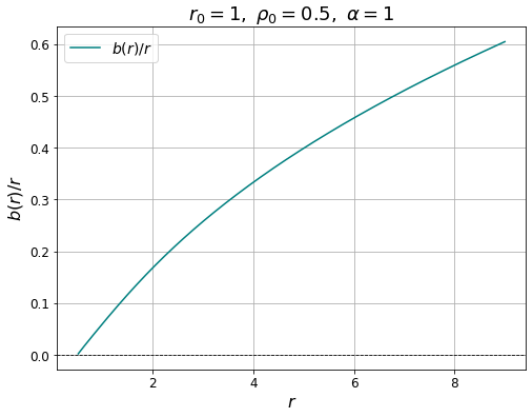

Figure 4.25: $\frac{b(r)}{r}$ versus r plot

In Figure: 4.21 the flare-out condition $b'(r) < 1$ at $r = r_0$. Figure: 4.22 implies the presence of exotic matter as ρ is negative everywhere. In Figure: 4.23 we observe that there is an initial decrease, $\rho + p_r$, and then it increases monotonically and then appears to approach zero. The curve violates NEC,i.e., $\rho + p_r < 0$ throughout the plot. Figure: 4.24 shows the decrease $b(r)$ as r increases satisfying the shape function condition. Figure: 4.25 satisfies the condition $\frac{b(r)}{r} < 1$.

4.4 Stability Analysis

For the f(R) gravity calculation, we have assumed that

$$f(R) = \alpha R^2 \quad , \qquad \text{where} \quad R = \frac{2b'(r)}{r^2} \tag{4.49}$$

Now, we have,

$$\rho = F\left(\frac{b'(r)}{r^2}\right) \tag{4.50}$$

$$p_r = -F\left(\frac{b(r)}{r^3}\right) + F'\left(\frac{b'(r) - b(r)}{2r^2}\right) - F''\left(1 - \frac{b(r)}{r}\right) \tag{4.51}$$

$$p_t = -\frac{F'}{r}\left(1 - \frac{b(r)}{r}\right) + F\left(\frac{b(r) - b'(r)}{2r^3}\right) \tag{4.52}$$

We know,

$$F = \frac{df(R)}{dR} = \frac{d}{dR}(\alpha R^2) = 2\alpha R \tag{4.53}$$

Thus,

$$F = 2\alpha R = 4\alpha\left(\frac{b'(r)}{r^2}\right) \tag{4.54}$$

By differentiating on both sides with respect to R, we get,

$$F' \;=\; 2\alpha \;=\; \text{constant} \tag{4.55}$$

Again, by differentiating on both sides with respect to R, we obtain,

$$F'' \;=\; 0 \tag{4.56}$$

Hence, the expressions of ρ , p_r and p_t reduce to:

$$\rho = -F\left(\frac{b'(r)}{r^2}\right) \tag{4.57}$$

$$p_r = -F\left(\frac{b(r)}{r^3}\right) \tag{4.58}$$

$$p_t = F\left(\frac{b(r) - b'(r)}{2r^3}\right) \tag{4.59}$$

We consider that, α is approximately close to zero, thus, $F' \approx 0$

As we have already learned, the redshift function $\Phi(r)$ should be finite everywhere for a wormhole to exist. In order to make the analysis manageable, we assume that $\Phi(r) \equiv$ constant. This implies that $\Phi'(r) \equiv 0$ [33]. Hence,

$$\boldsymbol{F_g = -(\rho + p_r)\Phi'(r) = 0} \tag{4.60}$$

Then,

$$F_h = -\frac{dp_r}{dr}$$

$$= -\frac{d}{dr}\left[-F\left(\frac{b(r)}{r^3}\right)\right]$$

$$= F\left(\frac{r^3 b'(r) - 3r^2 b(r)}{(r^3)^2}\right)$$

$$= F\left(\frac{rb'(r) - 3b(r)}{r^4}\right)$$

$$\Rightarrow \quad \boldsymbol{F_h = F\left(\frac{rb'(r) - 3b(r)}{r^4}\right)} \tag{4.61}$$

And,

$$F_a = \frac{2}{r}(p_t - p_r)$$

$$= \frac{2}{r}\left[F\left(\frac{b(r)}{r^3}\right) - F\left(\frac{rb'(r) - b(r)}{2r^3}\right)\right]$$

$$\Rightarrow \quad \boldsymbol{F_a = -F\left(\frac{rb'(r) - 3b(r)}{r^4}\right) = -F_h} \tag{4.62}$$

Therefore, we get,

$$F_g + F_h + F_a \;=\; (\; 0 + F_h - F_h \;) \;=\; 0$$

Hence, the equilibrium condition is satisfied; thus, the wormhole is stable.

In the Figure: 4.26, the hydrostatic force F_h (represented by the green line) begins with a large positive value for small r (near the throat of the wormhole)and then rapidly decreases as the value of r increases. F_h decreases and eventually diminishes (approaching zero) as we move away from the throat.

In contrast to the nature of F_h, the anisotropic force F_a (represented by the blue line) begins at a large negative value at small r, and then increases with an increase in r, eventually approaching zero. From this behaviour, we can observe that F_a, it initially contracts at the throat and then becomes less significant as we move away from the throat.

We had considered while solving the TOV equations that $f'(r) \sim \frac{1}{r}$, i.e., $f'(r) \to 0$ as $r \to \infty$. Therefore, the value of the gravitational force F_g (represented by the red dotted line) is too small, as shown in the graph.

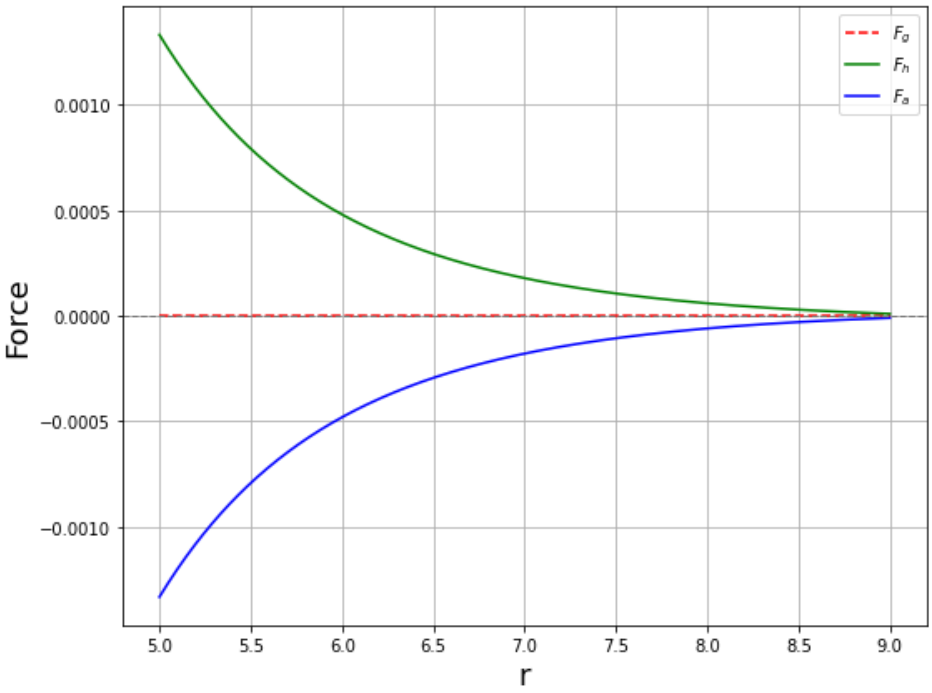

Figure 4.26: A plot showing the behaviour of the three forces in the TOV equilibrium condition against r in $f(R)$ gravity

Concluding remarks

The primary objective of this study was to investigate the possibility of traversable wormhole formation in the ultra-diffuse galaxy Dragonfly 44, utilizing three distinct dark matter density profiles: the Navarro-Frenk-White (NFW) profile, the Universal Rotation Curve (URC) profile, and the Ultra-Diffuse Galaxy (UDG) King model. To achieve this, we employed the Morris-Thorne wormhole metric to calculate the shape function $b(r)$ corresponding to each profile and examined the satisfaction of key wormhole conditions: the shape function condition $\frac{b(r)}{r} < 1$, the flare-out condition $b'(r) < 1$ at the throat, and the violation of the null energy condition (NEC) $\rho + p_r < 0$, which indicates the presence of exotic matter.

In the context of Einstein gravity, both the NFW and URC density profiles were found to satisfy all the necessary geometric and energy conditions for traversable wormholes. These results indicate that these two profiles can potentially support stable wormhole structures in the Dragonfly 44 galaxy. However, the UDG King's model failed to satisfy the shape function condition across all cases considered. While the UDG profile does satisfy the NEC violation in Einstein gravity, implying the presence of exotic matter, it does not meet the geometric criteria (specifically the shape function and flare-out conditions), which are crucial for maintaining a traversable wormhole structure. As a result, wormhole solutions cannot be sustained within this profile despite the NEC violation.

Under the framework of modified $f(R)$ gravity, the NFW and URC profiles once again fulfilled all the wormhole requirements, reinforcing their suitability for wormhole formation in both classical and modified gravity theories. In contrast, the UDG King's model performs even more poorly under $f(R)$ gravity. It fails not only to meet the geometric conditions but also does not exhibit consistent NEC violation. Specifically, for the case where $\eta = -1$, the quantity $\rho + p_r$ remains positive in the beginning, becomes zero in the range $r = 7$ to $r = 12$, and only later turns negative, making the NEC violation neither strong nor sustained enough to support a wormhole structure.

In summary, this study concludes that both the NFW and URC density profiles are favorable candidates for supporting traversable wormholes in the ultra-diffuse galaxy Dragonfly 44, under both Einstein and $f(R)$ theories of gravity. The UDG King's profile, despite indicating the presence of exotic matter in Einstein gravity, fails to satisfy the full set of necessary conditions in either gravitational framework, and therefore cannot support the existence of traversable wormholes.

Future Scope

The study of wormhole physics offers many promising avenues for future investigations:

1. **In-Depth Analysis of Wormhole Dynamics:**
   There is a critical need for more research regarding the dynamic processes of wormholes under different circumstances, such as interactions with exotic and normal matter, and the exact mechanisms behind transitions among wormholes, black holes, and cosmological environments. Defining and investigating explicit exotic matter models continues to be important in evaluating the physical possibility of wormholes.

2. **Stability within Modified Gravity:**
   A more extensive examination of the stability of wormholes in bigger classes of modified gravity theories beyond linear stability is required to evaluate dynamic stability. This involves analyzing the contribution from higher-order terms in curvature as well as from non-minimal couplings for the existence of stable traversable wormholes with no exotic matter that violates energy conditions.

3. **Observational Signatures and Detection:**
   Further work should aim to make more specific predictions for the observational signatures of wormholes in astrophysical settings. These involve quantitative investigations of gravitational lensing effects, the dynamics of test particles or waves passing through wormholes, and possible relations with unidentified astronomical phenomena such as the dynamics of dark matter in

galactic centers or halos. It has also been proposed that wormholes might be detectable through the scattering of scalar waves.

4. **Quantum Aspects of Wormholes:**
   Quantum field theory interactions with wormhole geometries also require further study. This would involve exploring quantum vacuum energy contributions to wormhole stability (e.g., Casimir wormholes) and exploring ways to correlate traversable wormholes with quantum field theory and possible constraints due to quantum gravity.

5. **Extra Dimensions and Higher-Dimensional Wormholes:**
   Investigating wormhole solutions to higher-dimensional theories and their possible influence on the existence and detection of extra spatial dimensions is a promising direction.

6. **Theoretical Foundations and Energy Conditions:**
   Further research regarding the basic requirements of traversable wormholes, with a focus on the violation of energy conditions. Investigating situations where violations can be localized or evaded in physically reasonable manners, particularly in models of modified gravity, will prove to be critical. Generalizing definitions of wormhole throats and investigating energy conditions in dynamically evolving wormholes are also current areas of concern.

In summary, although the theoretical framework for wormholes has progressed extensively, future research holds the potential of further clarifying their inherent properties, possible existence, and implications for our understanding of the universe and the laws of physics.

Bibliography

[1] Miguel Alcubierre and Francisco SN Lobo. Warp drive basics. *Wormholes, Warp Drives and Energy Conditions*, pages 257–279, 2017.

[2] Atharv Ambade. Worm whole — time travel, 2023. Accessed: 2025-04-22.

[3] Atlearner. 2-d space-time diagram, 2020. Accessed: 2025-04-22.

[4] Anton N Baushev. Galaxy collisions as a mechanism of ultra diffuse galaxy (udg) formation. *New Astronomy*, 60:69–73, 2018.

[5] José A Benavides, Laura V Sales, Mario G Abadi, Federico Marinacci, Mark Vogelsberger, and Lars Hernquist. Origin and evolution of ultradiffuse galaxies in different environments. *Monthly Notices of the Royal Astronomical Society*, 522(1):1033–1048, 2023.

[6] Steven K Blau. A large galaxy made almost entirely of dark matter. *Physics Today*, 69(11):24–25, 2016.

[7] KA Bronnikov. Scalar-tensor theory and scalar charge. *Acta. Phys. Pol*, page B4, 1973.

[8] KA Bronnikov, PA Korolyov, A Makhmudov, and MV Skvortsova. Wormholes and black universes communicated with extra dimensions. In *Journal of Physics: Conference Series*, volume 798, page 012090. IOP Publishing, 2017.

[9] KA Bronnikov, LN Lipatova, ID Novikov, and AA Shatskiy. Example of a stable wormhole in general relativity. *Gravitation and Cosmology*, 19(4):269–274, 2013.

[10] Adam R Brown and Leonard Susskind. A holographic wormhole traversed in a quantum computer, 2022.

[11] Rainer Burghardt et al. Linking conditions for models with geometrical basis. *Journal of Modern Physics*, 11(03):355, 2020.

[12] S Capozziello, G Lambiase, M Sakellariadou, An Stabile, and Ar Stabile. Probing models of extended gravity using gravity probe b and lares experiments. *arXiv preprint arXiv:1410.8316*, 2014.

[13] Sean M Carroll. An introduction to general relativity: spacetime and geometry. *Addison Wesley*, 101:102, 2004.

[14] Mauricio Cataldo and Fabian Orellana. Static phantom wormholes of finite size. *Physical Review D*, 96(6):064022, 2017.

[15] Ta-Pei Cheng. *Relativity, gravitation and cosmology: a basic introduction*, volume 11. Oxford University Press, 2009.

[16] Peter Collier. *A most incomprehensible thing: notes towards a very gentle introduction to the mathematics of relativity.* Incomprehensible Books, 2017.

[17] MSR Delgaty and Robert B Mann. Traversable wormholes in (2+ 1) and (3+ 1) dimensions with a cosmological constant. *International Journal of Modern Physics D*, 4(02):231–245, 1995.

[18] Albert Einstein. Die grundlagen der allgemeinen. *Relativitatstheorie, Annale der Physic*, 49:769, 1916.

[19] Albert Einstein. Relativity: The special and general theory, trans. *Robert W. Lawson (New York: Crown, 1961)*, 26, 1920.

[20] Albert Einstein. Time, space, and gravitation. *Science*, 51(1305):8–10, 1920.

[21] Albert Einstein and Nathan Rosen. The particle problem in the general theory of relativity. *Physical Review*, 48(1):73, 1935.

[22] Homer G Ellis. Ether flow through a drainhole: A particle model in general relativity. *Journal of Mathematical Physics*, 14(1):104–118, 1973.

[23] Homer G Ellis. The evolving, flowless drainhole: A nongravitating-particle model in general relativity theory. *General Relativity and Gravitation*, 10:105–123, 1979.

[24] Jonathan L Feng. Dark matter candidates from particle physics and methods of detection. *Annual Review of Astronomy and Astrophysics*, 48(1):495–545, 2010.

[25] Brian Greene. The theory of relativity, then and now. Technical report, Retrieved 2015-09-26, 2015.

[26] Mustafa Halilsoy, A Ovgun, and S Habib Mazharimousavi. Thin-shell wormholes from the regular hayward black hole. *The European Physical Journal C*, 74(3):1–7, 2014.

[27] Sean A Hayward. Dynamic wormholes. *International Journal of Modern Physics D*, 8(03):373–382, 1999.

[28] Sean A Hayward. Recent progress in wormhole dynamics. *arXiv preprint gr-qc/0306051*, 2003.

[29] David Hochberg and Matt Visser. Geometric structure of the generic static traversable wormhole throat. *Physical Review D*, 56(8):4745, 1997.

[30] David Hochberg and Matt Visser. Null energy condition in dynamic wormholes. *Physical review letters*, 81(4):746, 1998.

[31] Sayeedul Islam, Farook Rahaman, Ali Övgün, and Mustafa Halilsoy. Formation of wormholes by dark matter in the galaxy dragonfly 44. *Canadian Journal of Physics*, 97(3):241–247, 2019.

[32] Sayan Kar, Sayantani Lahiri, and Soumitra SenGupta. Can extra dimensional effects allow wormholes without exotic matter? *Physics Letters B*, 750:319–324, 2015.

[33] Peter KF Kuhfittig. A note on the stability of morris-thorne wormholes. *arXiv preprint arXiv:2009.11179*, 2020.

[34] Francisco SN Lobo. From the flamm–einstein–rosen bridge to the modern renaissance of traversable wormholes. *International Journal of Modern Physics D*, 25(07):1630017, 2016.

[35] Francisco SN Lobo and Miguel A Oliveira. Wormhole geometries in f (r) modified theories of gravity. *Physical Review D—Particles, Fields, Gravitation, and Cosmology*, 80(10):104012, 2009.

[36] Charles W Misner, Kip S Thorne, John Archibald Wheeler, and WH Gravitation. Freeman and company. *San Francisco*, 891, 1973.

[37] Charles W Misner and John A Wheeler. Classical physics as geometry. *Annals of physics*, 2(6):525–603, 1957.

[38] Julio F Navarro. The structure of cold dark matter halos. In *Symposium-international astronomical union*, volume 171, pages 255–258. Cambridge University Press, 1996.

[39] Ali Ovgün, Izzet Sakallı, and Halil Mutuk. Quasinormal modes of schwarzschild black hole and damour-solodukhin wormhole via feedforward neural network method. *arXiv preprint arXiv:1904.09509*.

[40] Nataša Pavlov and Ana Mitrašinović. Puzzling ultra-diffuse galaxy evolution (pudge). i. the existence of a nube-like galaxy in illustristng. *arXiv preprint arXiv:2502.04833*, 2025.

[41] GP Perry and Robert B Mann. Traversible wormholes in (2+ 1) dimensions. *General relativity and gravitation*, 24:305–321, 1992.

[42] Ramesh Radhakrishnan, Patrick Brown, Jacob Matulevich, Eric Davis, Delaram Mirfendereski, and Gerald Cleaver. A review of stable, traversable wormholes in f (r) gravity theories. *Symmetry*, 16(8):1007, 2024.

[43] F Rahaman, M Kalam, and S Chakraborty. Thin shell wormholes in higher dimensional einstein–maxwell theory. *General Relativity and Gravitation*, 38:1687–1695, 2006.

[44] Farook Rahaman. *The general theory of relativity: A mathematical approach*. Cambridge University Press, 2021.

[45] Farook Rahaman, PKF Kuhfittig, Saibal Ray, and Nasarul Islam. Possible existence of wormholes in the galactic halo region. *The European Physical Journal C*, 74(2):2750, 2014.

[46] K Srinivasa Rao. *The rotation and Lorentz groups and their representations for physicists*. John Wiley & Sons, 1988.

[47] Martin G Richarte and Claudio Simeone. Wormholes in einstein-born-infeld theory. *Physical Review D—Particles, Fields, Gravitation, and Cosmology*, 80(10):104033, 2009.

[48] Fritz Rohrlich. *From paradox to reality: Our basic concepts of the physical world*. Cambridge University Press, 1989.

[49] Thomas A Roman. Inflating lorentzian wormholes. *Physical Review D*, 47(4):1370, 1993.

[50] Bernard Schutz. *Gravity from the ground up: An introductory guide to gravity and general relativity*. Cambridge university press, 2003.

[51] Alex Simpson. Traversable wormholes, regular black holes, and black-bounces. *arXiv preprint arXiv:2104.14055*, 2021.

[52] Takashi Torii and Hisa-aki Shinkai. Wormholes in higher dimensional space-time: Exact solutions and their linear stability analysis. *Physical Review D—Particles, Fields, Gravitation, and Cosmology*, 88(6):064027, 2013.

[53] Matt Visser. Traversable wormholes: Some simple examples. *Physical Review D*, 39(10):3182, 1989.

[54] Matt Visser. Lorentzian wormholes. from einstein to hawking. *Woodbury*, 1995.

Appendix A

Appendix: Python programs for generating graphs

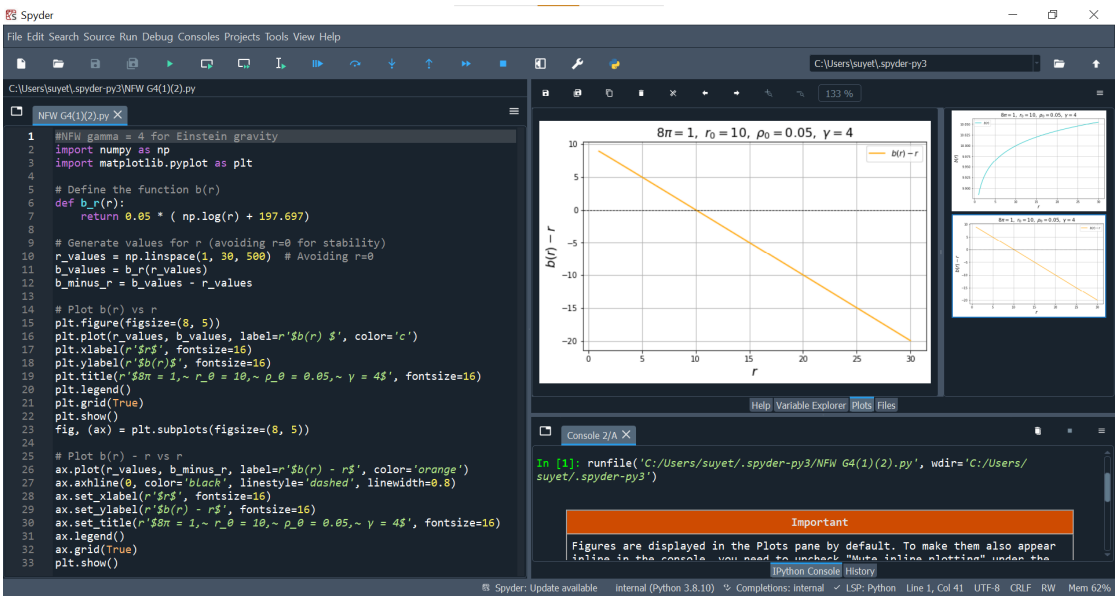
Spyder
File Edit Search Source Run Debug Consoles Projects Tools View Help
C:\Users\suyet\.spyder-py3\NFW G4(1)(2).py
NFW G4(1)(2).py
#NFW gamma = 4 for Einstein gravity
import numpy as np
import matplotlib.pyplot as plt
# Define the function b(r)
def b_r(r):
return 0.05 * (np.log(r) + 197.697)
# Generate values for r (avoiding r=0 for stability)
r_values = np.linspace(1, 30, 500) # Avoiding r=0
b_values = b_r(r_values)
b_minus_r = b_values - r_values
# Plot b(r) vs r
plt.figure(figsize=(8, 5))
plt.plot(r_values, b_values, label=r'$b(r) $', color='c')
plt.xlabel(r'r', fontsize=16)
plt.ylabel(r'$b(r)$', fontsize=16)
plt.title(r'$8π = 1,~ r_0 = 10,~ ρ_0 = 0.05,~ γ = 4$', fontsize=16)
plt.legend()
plt.grid(True)
plt.show()
fig, (ax) = plt.subplots(figsize=(8, 5))
# Plot b(r) - r vs r
ax.plot(r_values, b_minus_r, label=r'$b(r) - r$', color='orange')
ax.axhline(0, color='black', linestyle='dashed', linewidth=0.8)
ax.set_xlabel(r'r', fontsize=16)
ax.set_ylabel(r'$b(r) - r$', fontsize=16)
ax.set_title(r'$8π = 1,~ r_0 = 10,~ ρ_0 = 0.05,~ γ = 4$', fontsize=16)
ax.legend()
ax.grid(True)
plt.show()
$8\pi = 1,\ r_0 = 10,\ \rho_0 = 0.05,\ \gamma = 4$
$b(r) - r$
r
Help Variable Explorer Plots Files
Console 2/A
In [1]: runfile('C:/Users/suyet/.spyder-py3/NFW G4(1)(2).py', wdir='C:/Users/suyet/.spyder-py3')
Important
Figures are displayed in the Plots pane by default. To make them also appear
IPython Console History
Spyder: Update available
internal (Python 3.8.10)
Completions: internal
LSP: Python
Line 1, Col 41
UTF-8
CRLF
RW
Mem 62%

Figure A.1: NFW CASE - 1: $\gamma = 1$ for Einstein Gravity

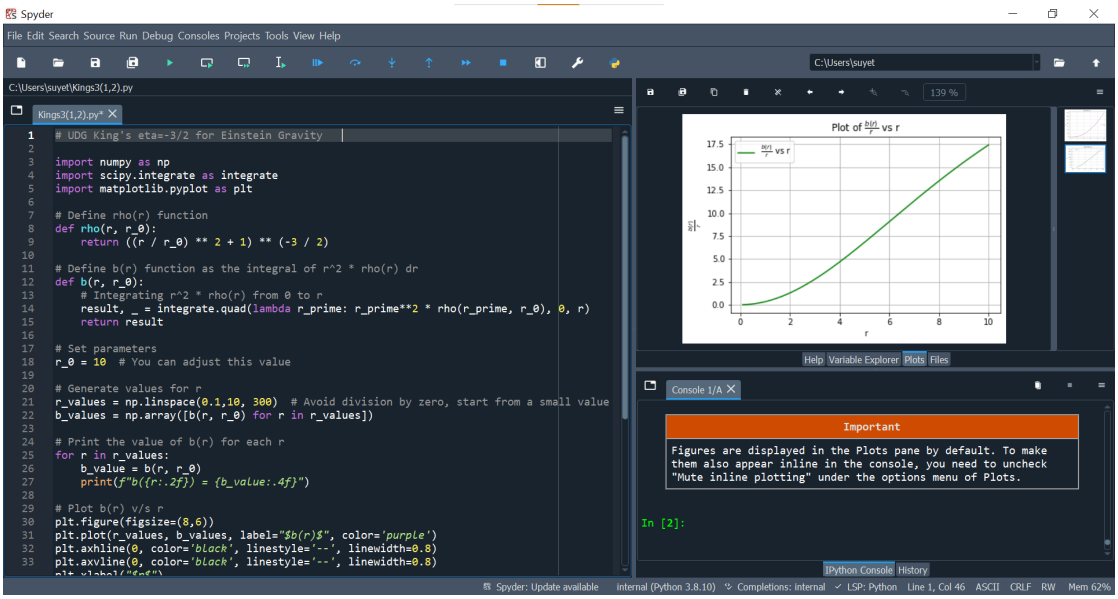
Spyder
File Edit Search Source Run Debug Consoles Projects Tools View Help
C:\Users\suyet\Kings3(1,2).py
Kings3(1,2).py*
# UDG King's eta=-3/2 for Einstein Gravity
import numpy as np
import scipy.integrate as integrate
import matplotlib.pyplot as plt
# Define rho(r) function
def rho(r, r_0):
return ((r / r_0) ** 2 + 1) ** (-3 / 2)
# Define b(r) function as the integral of r^2 * rho(r) dr
def b(r, r_0):
# Integrating r^2 * rho(r) from 0 to r
result, _ = integrate.quad(lambda r_prime: r_prime**2 * rho(r_prime, r_0), 0, r)
return result
# Set parameters
r_0 = 10 # You can adjust this value
# Generate values for r
r_values = np.linspace(0.1,10, 300) # Avoid division by zero, start from a small value
b_values = np.array([b(r, r_0) for r in r_values])
# Print the value of b(r) for each r
for r in r_values:
b_value = b(r, r_0)
print(f"b({r:.2f}) = {b_value:.4f}")
# Plot b(r) v/s r
plt.figure(figsize=(8,6))
plt.plot(r_values, b_values, label="$b(r)$", color='purple')
plt.axhline(0, color='black', linestyle='--', linewidth=0.8)
plt.axvline(0, color='black', linestyle='--', linewidth=0.8)
Plot of b(r)/r vs r
Help Variable Explorer Plots Files
Console 1/A
Important
Figures are displayed in the Plots pane by default. To make them also appear inline in the console, you need to uncheck "Mute inline plotting" under the options menu of Plots.
In [2]:
IPython Console History
Spyder: Update available
internal (Python 3.8.10)
Completions: internal
LSP: Python
Line 1, Col 46
ASCII
CRLF
RW
Mem 62%

Figure A.2: UDG King's CASE - 3: $\eta = -\frac{3}{2}$ for Einstein Gravity

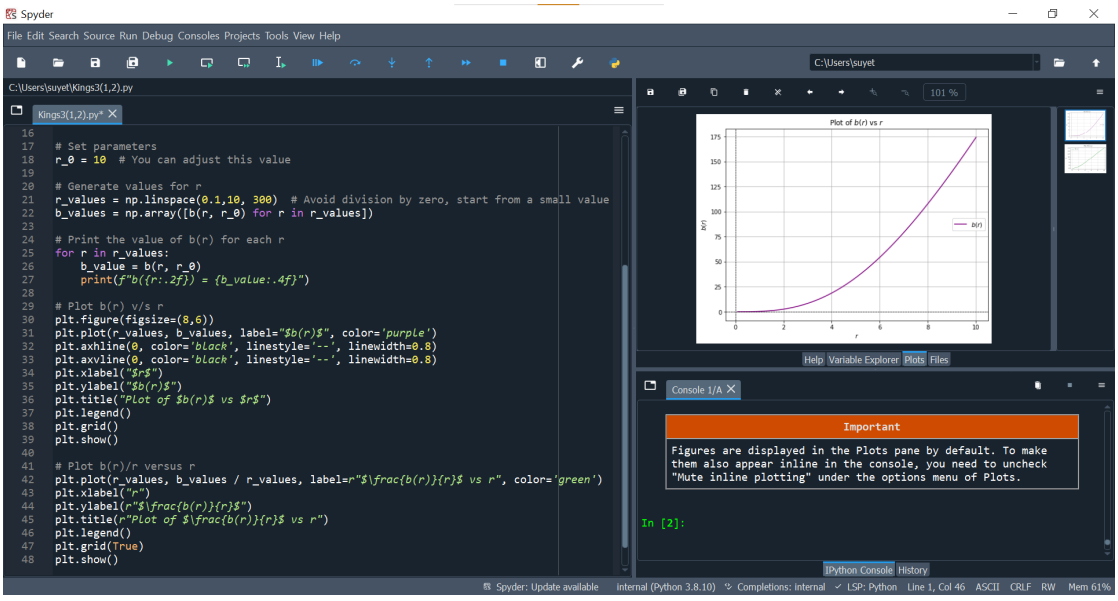

Figure A.3: UDG King's CASE - 3: $\eta = -\frac{3}{2}$ for Einstein Gravity

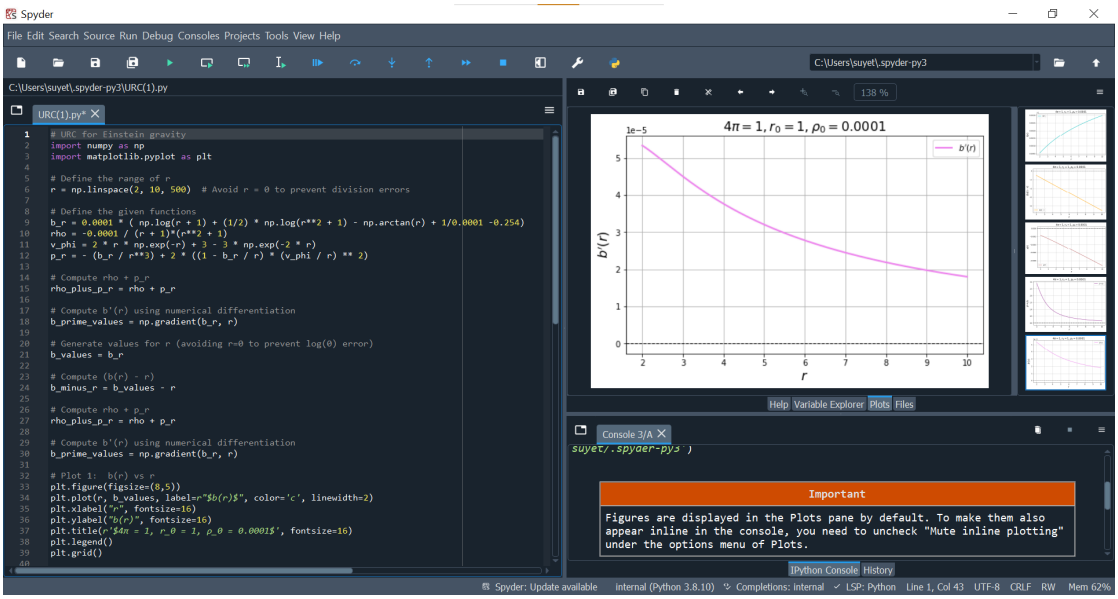
Spyder
File Edit Search Source Run Debug Consoles Projects Tools View Help
C:\Users\suyet\.spyder-py3\URC(1).py
URC(1).py*
# URC for Einstein gravity
import numpy as np
import matplotlib.pyplot as plt
# Define the range of r
r = np.linspace(2, 10, 500) # Avoid r = 0 to prevent division errors
# Define the given functions
b_r = 0.0001 * (np.log(r + 1) + (1/2) * np.log(r**2 + 1) - np.arctan(r) + 1/0.0001 -0.254)
rho = -0.0001 / (r + 1)*(r**2 + 1)
v_phi = 2 * r * np.exp(-r) + 3 - 3 * np.exp(-2 * r)
p_r = - (b_r / r**3) + 2 * ((1 - b_r / r) * (v_phi / r) ** 2)
# Compute rho + p_r
rho_plus_p_r = rho + p_r
# Compute b'(r) using numerical differentiation
b_prime_values = np.gradient(b_r, r)
# Generate values for r (avoiding r=0 to prevent log(0) error)
b_values = b_r
# Compute (b(r) - r)
b_minus_r = b_values - r
# Compute rho + p_r
rho_plus_p_r = rho + p_r
# Compute b'(r) using numerical differentiation
b_prime_values = np.gradient(b_r, r)
# Plot 1: b(r) vs r
plt.figure(figsize=(8,5))
plt.plot(r, b_values, label=r"$b(r)$", color='c', linewidth=2)
plt.xlabel("r", fontsize=16)
plt.ylabel("b(r)", fontsize=16)
plt.title(r'$4π = 1, r_0 = 1, ρ_0 = 0.0001$', fontsize=16)
plt.legend()
plt.grid()
$4\pi = 1, r_0 = 1, \rho_0 = 0.0001$
b'(r)
r
Help Variable Explorer Plots Files
Console 3/A
suyet/.spyder-py3')
Important
Figures are displayed in the Plots pane by default. To make them also appear inline in the console, you need to uncheck "Mute inline plotting" under the options menu of Plots.
IPython Console History
Spyder: Update available
internal (Python 3.8.10)
Completions: internal
LSP: Python
Line 1, Col 43
UTF-8
CRLF
RW
Mem 62%

Figure A.4: URC density profile for Einstein Gravity

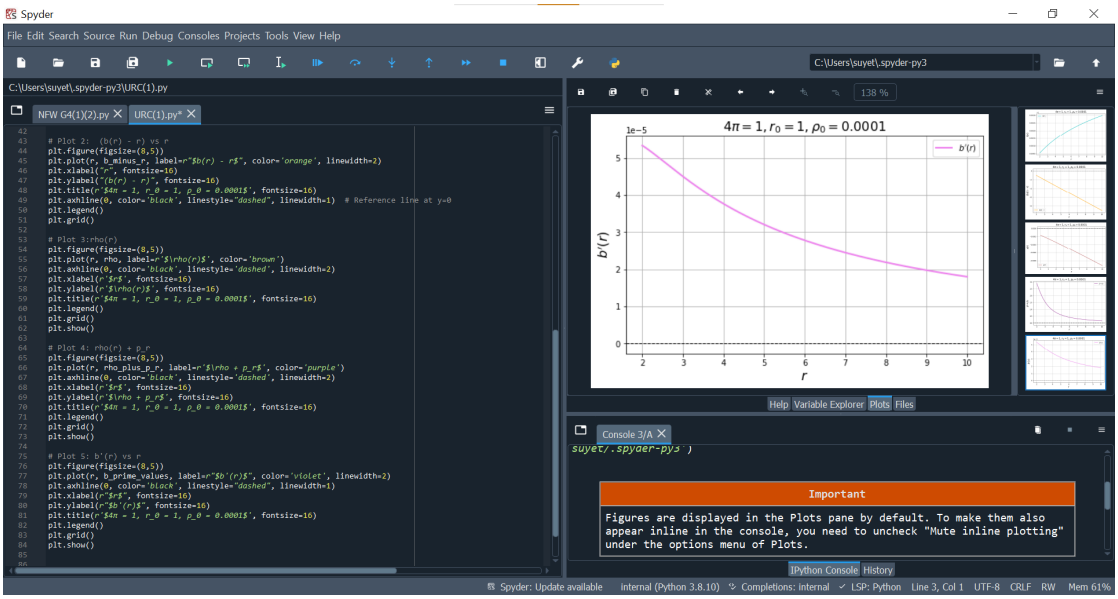

Figure A.5: URC density profile for Einstein Gravity

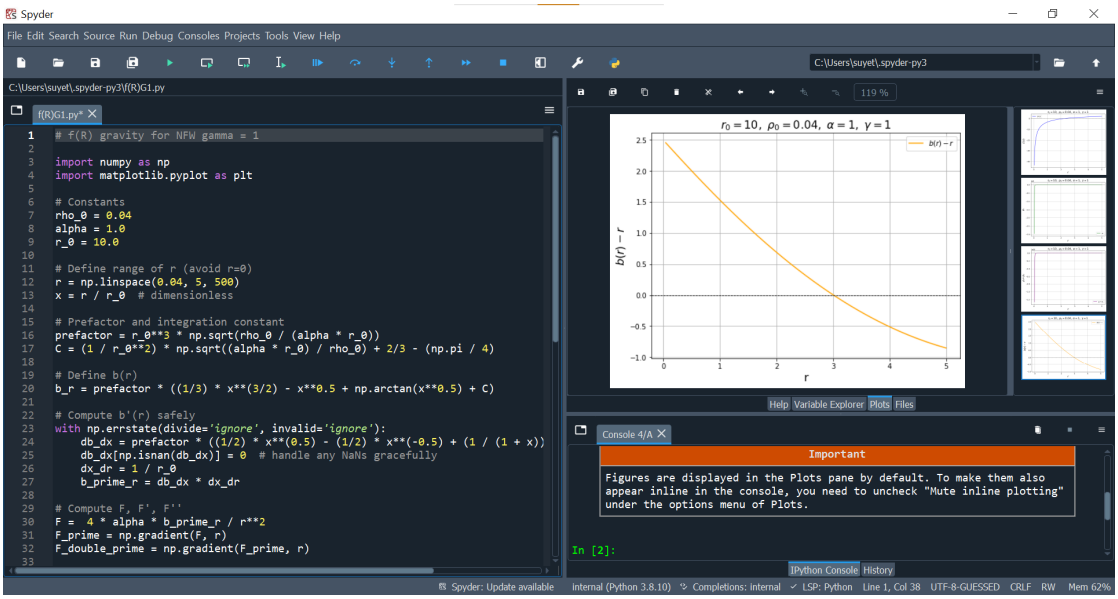
Spyder
File Edit Search Source Run Debug Consoles Projects Tools View Help
C:\Users\suyet\.spyder-py3\f(R)G1.py
f(R)G1.py*
# f(R) gravity for NFW gamma = 1
import numpy as np
import matplotlib.pyplot as plt
# Constants
rho_0 = 0.04
alpha = 1.0
r_0 = 10.0
# Define range of r (avoid r=0)
r = np.linspace(0.04, 5, 500)
x = r / r_0 # dimensionless
# Prefactor and integration constant
prefactor = r_0**3 * np.sqrt(rho_0 / (alpha * r_0))
C = (1 / r_0**2) * np.sqrt((alpha * r_0) / rho_0) + 2/3 - (np.pi / 4)
# Define b(r)
b_r = prefactor * ((1/3) * x**(3/2) - x**0.5 + np.arctan(x**0.5) + C)
# Compute b'(r) safely
with np.errstate(divide='ignore', invalid='ignore'):
db_dx = prefactor * ((1/2) * x**(0.5) - (1/2) * x**(-0.5) + (1 / (1 + x)))
db_dx[np.isnan(db_dx)] = 0 # handle any NaNs gracefully
dx_dr = 1 / r_0
b_prime_r = db_dx * dx_dr
# Compute F, F', F''
F = 4 * alpha * b_prime_r / r**2
F_prime = np.gradient(F, r)
F_double_prime = np.gradient(F_prime, r)
$r_0 = 10,\ \rho_0 = 0.04,\ \alpha = 1,\ \gamma = 1$
$b(r) - r$
r
Help Variable Explorer Plots Files
Console 4/A
Important
Figures are displayed in the Plots pane by default. To make them also appear inline in the console, you need to uncheck "Mute inline plotting" under the options menu of Plots.
In [2]:
IPython Console History
Spyder: Update available
internal (Python 3.8.10)
Completions: internal
LSP: Python
Line 1, Col 38
UTF-8-GUESSED
CRLF
RW
Mem 62%

Figure A.6: NFW CASE - 1: $\gamma = 1$ for $f(R)$ Gravity

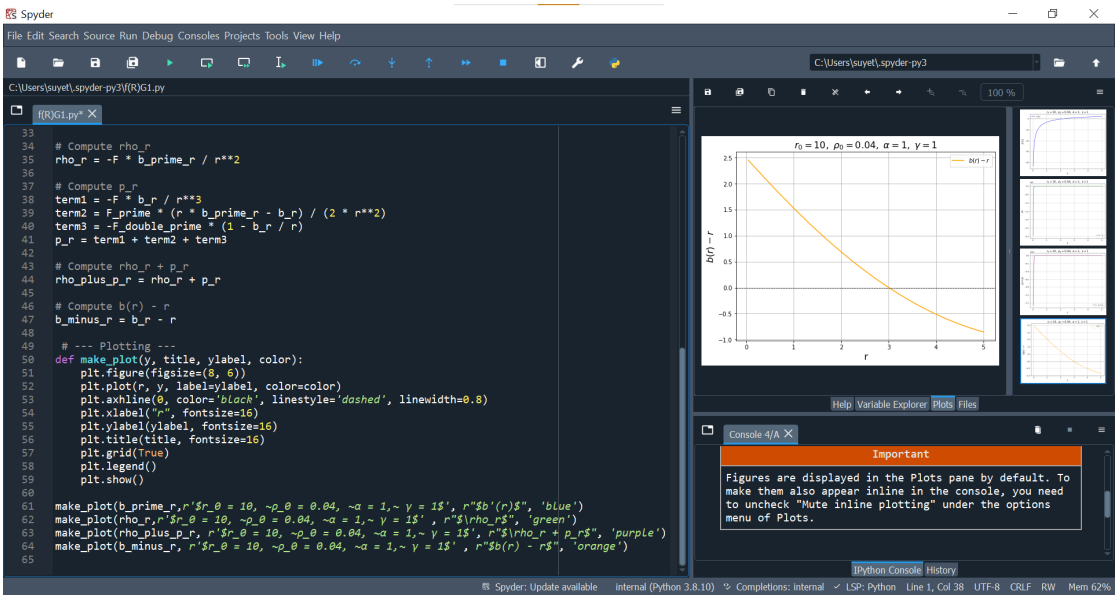
Spyder
File Edit Search Source Run Debug Consoles Projects Tools View Help
C:\Users\suyet\.spyder-py3\f(R)G1.py
f(R)G1.py*
# Compute rho_r
rho_r = -F * b_prime_r / r**2
# Compute p_r
term1 = -F * b_r / r**3
term2 = F_prime * (r * b_prime_r - b_r) / (2 * r**2)
term3 = -F_double_prime * (1 - b_r / r)
p_r = term1 + term2 + term3
# Compute rho_r + p_r
rho_plus_p_r = rho_r + p_r
# Compute b(r) - r
b_minus_r = b_r - r
# --- Plotting ---
def make_plot(y, title, ylabel, color):
plt.figure(figsize=(8, 6))
plt.plot(r, y, label=ylabel, color=color)
plt.axhline(0, color='black', linestyle='dashed', linewidth=0.8)
plt.xlabel("r", fontsize=16)
plt.ylabel(ylabel, fontsize=16)
plt.title(title, fontsize=16)
plt.grid(True)
plt.legend()
plt.show()
make_plot(b_prime_r,r'$r_0 = 10, ~\rho_0 = 0.04, ~\alpha = 1,~ \gamma = 1$', r"$b'(r)$", 'blue')
make_plot(rho_r,r'$r_0 = 10, ~\rho_0 = 0.04, ~\alpha = 1,~ \gamma = 1$' , r"$\rho_r$", 'green')
make_plot(rho_plus_p_r, r'$r_0 = 10, ~\rho_0 = 0.04, ~\alpha = 1,~ \gamma = 1$', r"$\rho_r + p_r$", 'purple')
make_plot(b_minus_r, r'$r_0 = 10, ~\rho_0 = 0.04, ~\alpha = 1,~ \gamma = 1$' , r"$b(r) - r$", 'orange')
$r_0 = 10,\ \rho_0 = 0.04,\ \alpha = 1,\ \gamma = 1$
$b(r) - r$
r
Help Variable Explorer Plots Files
Console 4/A
Important
Figures are displayed in the Plots pane by default. To make them also appear inline in the console, you need to uncheck "Mute inline plotting" under the options menu of Plots.
IPython Console History
Spyder: Update available
internal (Python 3.8.10)
Completions: internal
LSP: Python
Line 1, Col 38
UTF-8
CRLF
RW
Mem 62%

Figure A.7: NFW CASE - 1: $\gamma = 1$ for $f(R)$ Gravity

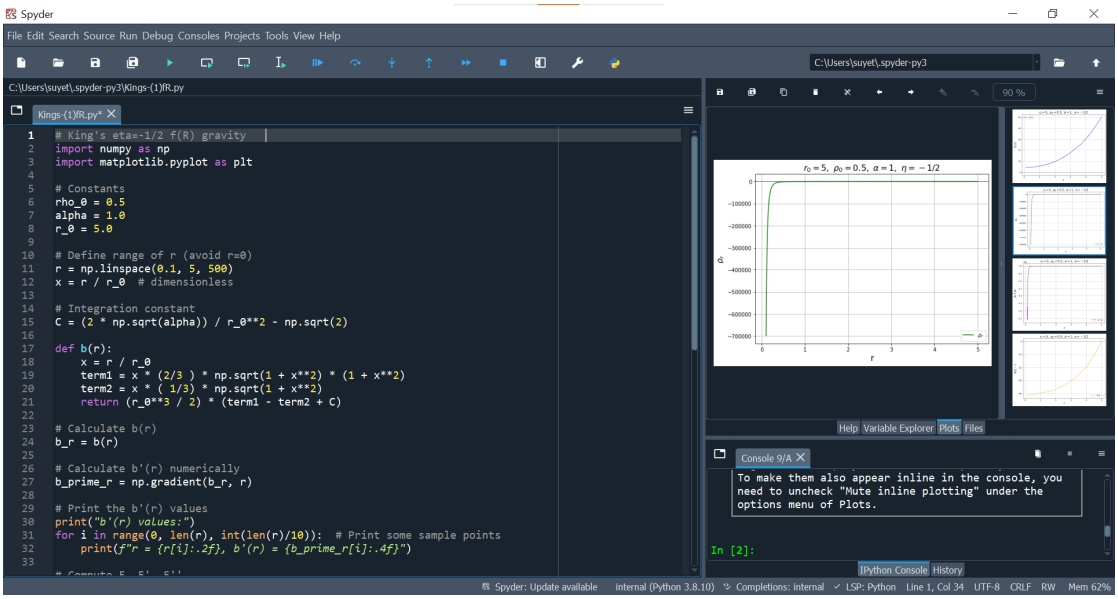
Spyder
File Edit Search Source Run Debug Consoles Projects Tools View Help
C:\Users\suyet\.spyder-py3\Kings-(1)fR.py
Kings-(1)fR.py*
# King's eta=-1/2 f(R) gravity
import numpy as np
import matplotlib.pyplot as plt
# Constants
rho_0 = 0.5
alpha = 1.0
r_0 = 5.0
# Define range of r (avoid r=0)
r = np.linspace(0.1, 5, 500)
x = r / r_0 # dimensionless
# Integration constant
C = (2 * np.sqrt(alpha)) / r_0**2 - np.sqrt(2)
def b(r):
x = r / r_0
term1 = x * (2/3) * np.sqrt(1 + x**2) * (1 + x**2)
term2 = x * (1/3) * np.sqrt(1 + x**2)
return (r_0**3 / 2) * (term1 - term2 + C)
# Calculate b(r)
b_r = b(r)
# Calculate b'(r) numerically
b_prime_r = np.gradient(b_r, r)
# Print the b'(r) values
print("b'(r) values:")
for i in range(0, len(r), int(len(r)/10)): # Print some sample points
print(f"r = {r[i]:.2f}, b'(r) = {b_prime_r[i]:.4f}")
Help Variable Explorer Plots Files
Console 9/A
To make them also appear inline in the console, you need to uncheck "Mute inline plotting" under the options menu of Plots.
In [2]:
IPython Console History
Spyder: Update available
internal (Python 3.8.10)
Completions: internal
LSP: Python
Line 1, Col 34
UTF-8
CRLF
RW
Mem 62%

Figure A.8: UDG King's CASE - 1: $\eta = -\frac{1}{2}$ for $f(R)$ Gravity

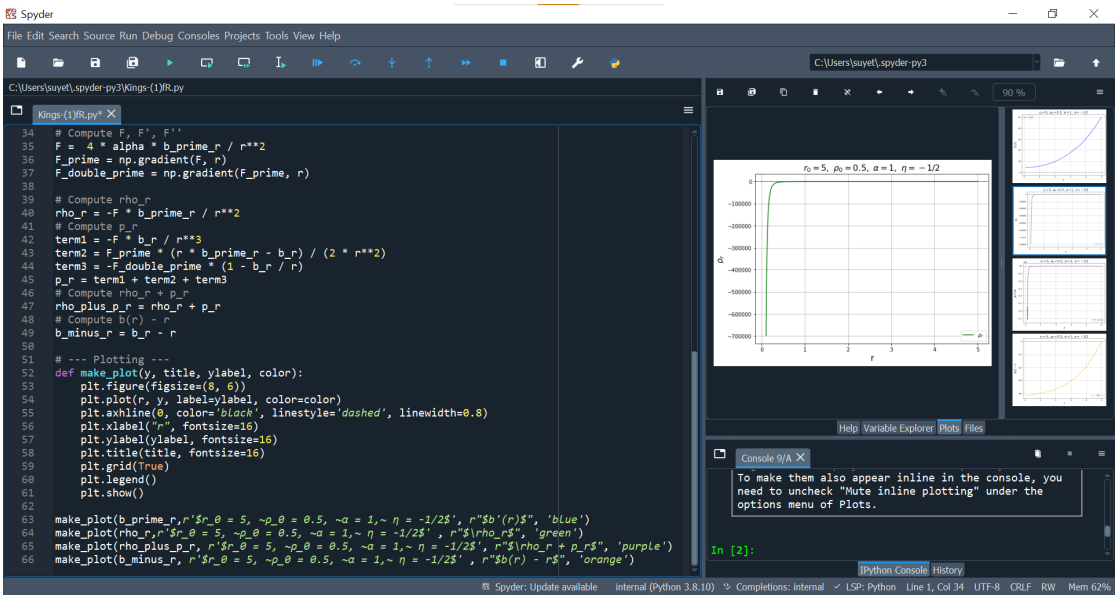
Spyder
File Edit Search Source Run Debug Consoles Projects Tools View Help
C:\Users\suyet\.spyder-py3\Kings-(1)fR.py
Kings-(1)fR.py*
# Compute F, F', F''
F = 4 * alpha * b_prime_r / r**2
F_prime = np.gradient(F, r)
F_double_prime = np.gradient(F_prime, r)
# Compute rho_r
rho_r = -F * b_prime_r / r**2
# Compute p_r
term1 = -F * b_r / r**3
term2 = F_prime * (r * b_prime_r - b_r) / (2 * r**2)
term3 = -F_double_prime * (1 - b_r / r)
p_r = term1 + term2 + term3
# Compute rho_r + p_r
rho_plus_p_r = rho_r + p_r
# Compute b(r) - r
b_minus_r = b_r - r
# --- Plotting ---
def make_plot(y, title, ylabel, color):
plt.figure(figsize=(8, 6))
plt.plot(r, y, label=ylabel, color=color)
plt.axhline(0, color='black', linestyle='dashed', linewidth=0.8)
plt.xlabel("r", fontsize=16)
plt.ylabel(ylabel, fontsize=16)
plt.title(title, fontsize=16)
plt.grid(True)
plt.legend()
plt.show()
make_plot(b_prime_r,r'$r_0 = 5, ~\rho_0 = 0.5, ~\alpha = 1,~ \eta = -1/2$', r"$b'(r)$", 'blue')
make_plot(rho_r,r'$r_0 = 5, ~\rho_0 = 0.5, ~\alpha = 1,~ \eta = -1/2$' , r"$\rho_r$", 'green')
make_plot(rho_plus_p_r, r'$r_0 = 5, ~\rho_0 = 0.5, ~\alpha = 1,~ \eta = -1/2$', r"$\rho_r + p_r$", 'purple')
make_plot(b_minus_r, r'$r_0 = 5, ~\rho_0 = 0.5, ~\alpha = 1,~ \eta = -1/2$' , r"$b(r) - r$", 'orange')
Help Variable Explorer Plots Files
Console 9/A
To make them also appear inline in the console, you need to uncheck "Mute inline plotting" under the options menu of Plots.
In [2]:
IPython Console History
Spyder: Update available
internal (Python 3.8.10)
Completions: internal
LSP: Python
Line 1, Col 34
UTF-8
CRLF
RW
Mem 62%

Figure A.9: UDG King's CASE - 1: $\eta = -\frac{1}{2}$ for $f(R)$ Gravity

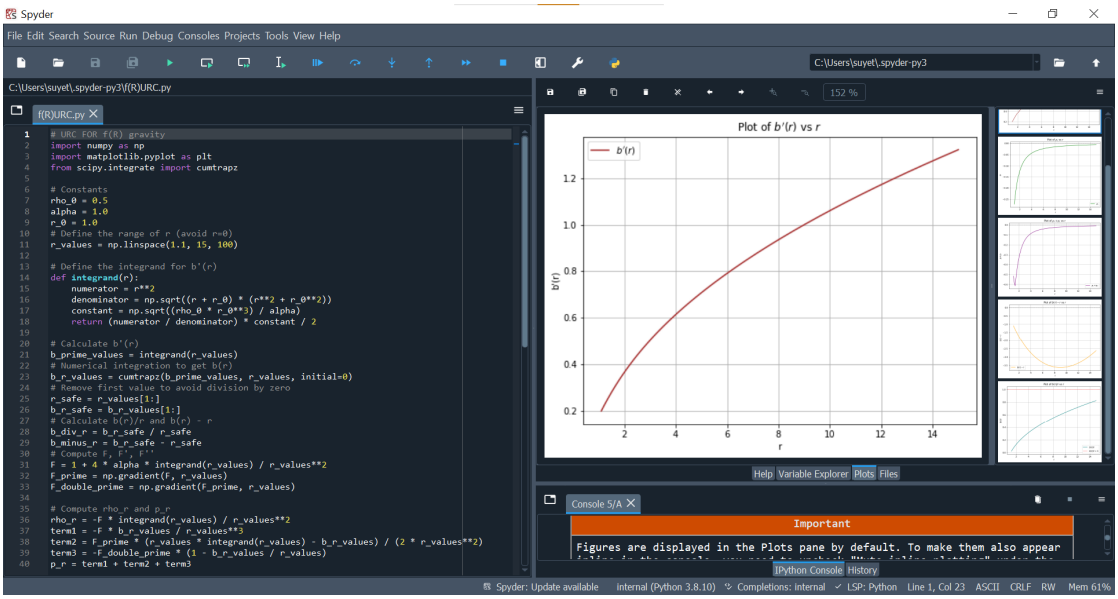
Spyder
File Edit Search Source Run Debug Consoles Projects Tools View Help
C:\Users\suyet\.spyder-py3\f(R)URC.py
f(R)URC.py
# URC FOR f(R) gravity
import numpy as np
import matplotlib.pyplot as plt
from scipy.integrate import cumtrapz
# Constants
rho_0 = 0.5
alpha = 1.0
r_0 = 1.0
# Define the range of r (avoid r=0)
r_values = np.linspace(1.1, 15, 100)
# Define the integrand for b'(r)
def integrand(r):
numerator = r**2
denominator = np.sqrt((r + r_0) * (r**2 + r_0**2))
constant = np.sqrt((rho_0 * r_0**3) / alpha)
return (numerator / denominator) * constant / 2
# Calculate b'(r)
b_prime_values = integrand(r_values)
# Numerical integration to get b(r)
b_r_values = cumtrapz(b_prime_values, r_values, initial=0)
# Remove first value to avoid division by zero
r_safe = r_values[1:]
b_r_safe = b_r_values[1:]
# Calculate b(r)/r and b(r) - r
b_div_r = b_r_safe / r_safe
b_minus_r = b_r_safe - r_safe
# Compute F, F', F''
F = 1 + 4 * alpha * integrand(r_values) / r_values**2
F_prime = np.gradient(F, r_values)
F_double_prime = np.gradient(F_prime, r_values)
# Compute rho_r and p_r
rho_r = -F * integrand(r_values) / r_values**2
term1 = -F * b_r_values / r_values**3
term2 = F_prime * (r_values * integrand(r_values) - b_r_values) / (2 * r_values**2)
term3 = -F_double_prime * (1 - b_r_values / r_values)
p_r = term1 + term2 + term3
Plot of b'(r) vs r
b'(r)
b'(r)
r
Help Variable Explorer Plots Files
Console 5/A
Important
Figures are displayed in the Plots pane by default. To make them also appear
IPython Console History
Spyder: Update available
internal (Python 3.8.10)
Completions: internal
LSP: Python
Line 1, Col 23
ASCII
CRLF
RW
Mem 61%

Figure A.10: URC density profile for $f(R)$ Gravity

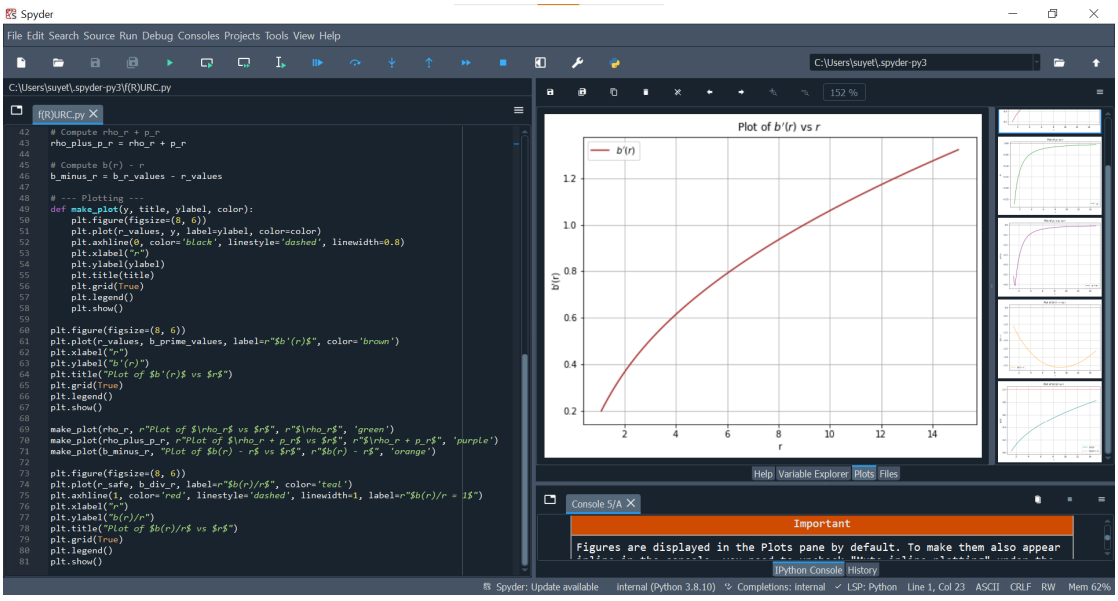

Figure A.11: URC density profile for $f(R)$ Gravity

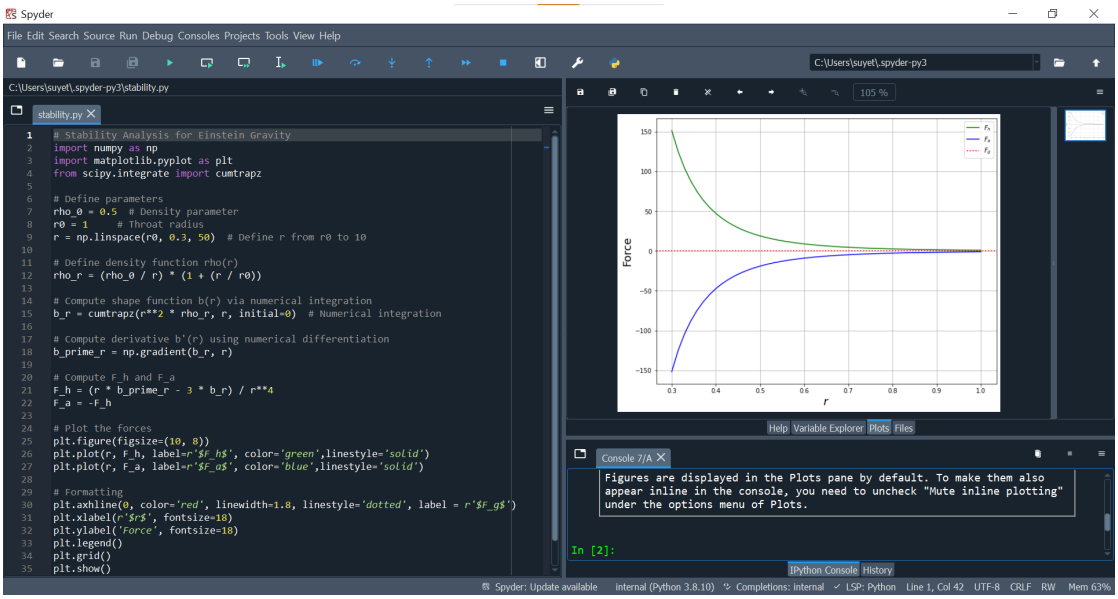
Spyder
File Edit Search Source Run Debug Consoles Projects Tools View Help
C:\Users\suyet\.spyder-py3\stability.py
stability.py
# Stability Analysis for Einstein Gravity
import numpy as np
import matplotlib.pyplot as plt
from scipy.integrate import cumtrapz
# Define parameters
rho_0 = 0.5 # Density parameter
r0 = 1 # Throat radius
r = np.linspace(r0, 0.3, 50) # Define r from r0 to 10
# Define density function rho(r)
rho_r = (rho_0 / r) * (1 + (r / r0))
# Compute shape function b(r) via numerical integration
b_r = cumtrapz(r**2 * rho_r, r, initial=0) # Numerical integration
# Compute derivative b'(r) using numerical differentiation
b_prime_r = np.gradient(b_r, r)
# Compute F_h and F_a
F_h = (r * b_prime_r - 3 * b_r) / r**4
F_a = -F_h
# Plot the forces
plt.figure(figsize=(10, 8))
plt.plot(r, F_h, label=r'F_h', color='green',linestyle='solid')
plt.plot(r, F_a, label=r'F_a', color='blue',linestyle='solid')
# Formatting
plt.axhline(0, color='red', linewidth=1.8, linestyle='dotted', label = r'F_g')
plt.xlabel(r'r', fontsize=18)
plt.ylabel('Force', fontsize=18)
plt.legend()
plt.grid()
plt.show()
Force
r
Help Variable Explorer Plots Files
Console 7/A
Figures are displayed in the Plots pane by default. To make them also appear inline in the console, you need to uncheck "Mute inline plotting" under the options menu of Plots.
In [2]:
IPython Console History
Spyder: Update available internal (Python 3.8.10) Completions: internal LSP: Python Line 1, Col 42 UTF-8 CRLF RW Mem 63%

Figure A.12: Stability Analysis of Einstein Gravity

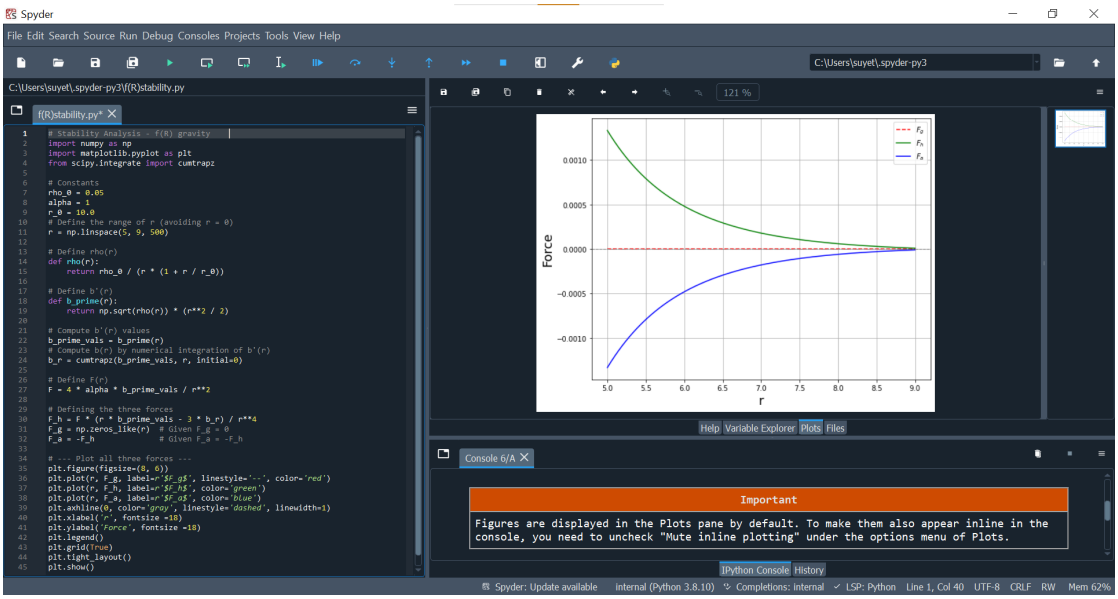
Spyder
File Edit Search Source Run Debug Consoles Projects Tools View Help
C:\Users\suyet\.spyder-py3\f(R)stability.py
f(R)stability.py*
# Stability Analysis - f(R) gravity
import numpy as np
import matplotlib.pyplot as plt
from scipy.integrate import cumtrapz
# Constants
rho_0 = 0.05
alpha = 1
r_0 = 10.0
# Define the range of r (avoiding r = 0)
r = np.linspace(5, 9, 500)
# Define rho(r)
def rho(r):
return rho_0 / (r * (1 + r / r_0))
# Define b'(r)
def b_prime(r):
return np.sqrt(rho(r)) * (r**2 / 2)
# Compute b'(r) values
b_prime_vals = b_prime(r)
# Compute b(r) by numerical integration of b'(r)
b_r = cumtrapz(b_prime_vals, r, initial=0)
# Define F(r)
F = 4 * alpha * b_prime_vals / r**2
# Defining the three forces
F_h = F * (r * b_prime_vals - 3 * b_r) / r**4
F_g = np.zeros_like(r) # Given F_g = 0
F_a = -F_h # Given F_a = -F_h
# --- Plot all three forces ---
plt.figure(figsize=(8, 6))
plt.plot(r, F_g, label=r'F_g', linestyle='--', color='red')
plt.plot(r, F_h, label=r'F_h', color='green')
plt.plot(r, F_a, label=r'F_a', color='blue')
plt.axhline(0, color='gray', linestyle='dashed', linewidth=1)
plt.xlabel('r', fontsize =18)
plt.ylabel('Force', fontsize =18)
plt.legend()
plt.grid(True)
plt.tight_layout()
plt.show()
Force
r
Help Variable Explorer Plots Files
Console 6/A
Important
Figures are displayed in the Plots pane by default. To make them also appear inline in the console, you need to uncheck "Mute inline plotting" under the options menu of Plots.
IPython Console History
Spyder: Update available internal (Python 3.8.10) Completions: internal LSP: Python Line 1, Col 40 UTF-8 CRLF RW Mem 62%

Figure A.13: Stability Analysis of $f(R)$ Gravity

Results

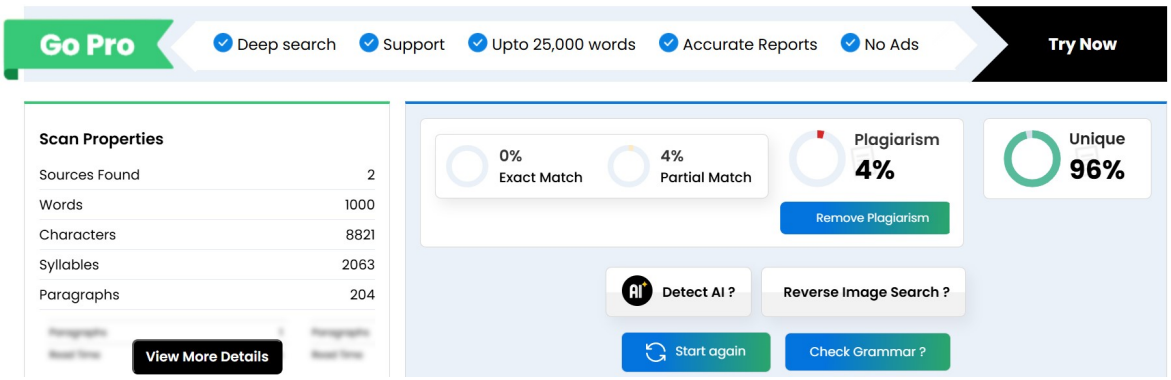
Go Pro
Deep search
Support
Upto 25,000 words
Accurate Reports
No Ads
Try Now
Scan Properties
Sources Found 2
Words 1000
Characters 8821
Syllables 2063
Paragraphs 204
View More Details
0%
Exact Match
4%
Partial Match
Plagiarism
4%
Remove Plagiarism
Unique
96%
Detect AI ?
Reverse Image Search ?
Start again
Check Grammar ?

Plagiarism Scan Report

4% Plagiarism	0% Exact Match
	4% Partial Match

96% Unique

Words	1000
Characters	8821
Sentences	12
Paragraphs	204
Read Time	5 minute(s)
Speak Time	7 minute(s)

Content Checked For Plagiarism

The study of wormhole physics offers many promising avenues for future investigations:

In-Depth Analysis of Wormhole Dynamics: There is critical need for more research regarding the dynamic processes of wormholes under different circumstances, such as interactions with exotic and normal matter, and Defining and investigating explicit exotic matter models continues to be important in evaluating the physical possibility of wormholes.
Stability within Modified Gravity A more extensive examination of the stability of wormholes in bigger classes of modified gravity theories beyond linear stability is required to evaluate dynamic stability. This involves analyzing the contribution from higher-order terms in curvature as well as from non-minimal couplings for the existence of stable traversable wormholes with no exotic matter that violates energy conditions.
\item\textbf{Observational Signatures and Detection:}\\ Further work should aim to make more specific predictions for the observational signatures of wormholes in astrophysical settings. These involve quantitative investigations of gravitational lensing effects, the dynamics of test particles or waves passing through wormholes, and possible relations with unidentified astronomical phenomena such as the dynamics of dark matter in galactic centers or halos. It has also been proposed that wormholes might be detectable through the scattering of scalar waves.

Christofell Symbols:}
The metric for wormhole geometry (traversable) in spherical co-ordinate (t,r,θ,ϕ) is given as\textsuperscript{\textbf{[30]}}:
$ f(r)\rightarrow$ Redshift function\\\\
$ b(r)\rightarrow$ Shape function \\\\
$r\rightarrow$ Radial coordinate \\\\
Writing the above equation in matrix form:

\begin{equation}
g_{ab} =
\left[
\begin{array}{cccc}
-e^{2f(r)} & 0 & 0 & 0 \\
0 & \left(1- \frac{b(r)}{r}\right)^{-1} & 0 & 0 \\
0 & 0 & r^2 & 0 \\
0 & 0 & 0 & r^2sin^2\theta
\end{array}
\right]
\end{equation}
The non-zero components of the metric tensor are: